SANDIA REPORT

RS-8232-2/ 67072   Cy1

Performance Evaluation of Molten Salt Thermal Storage Systems

G. J. Kolb, U. Nikolai

8232-2//067072

00000001   -

SF2900Q(8-81)

117 04 8 3

Performance Evaluation of Molten Salt Thermal Storage Systems

G. J. Kolb

Central Receiver Technology Division
Sandia National Laboratories
Albuquerque, New Mexico

U. Nikolai

Deutsche Forschungs-und Versuchsanstalt
Fuer Luft-und Raumfahrt
Cologne, West Germany

ABSTRACT

The thermal performance of the molten salt thermal storage
system located at the Central Receiver Test Facility (CRTF) was
measured. The 7-MWht system is composed of a hot storage tank
containing molten nitrate salt at a temperature of 1050 °F (566
°C) and a cold tank containing 550 °F (288 °C) salt with
associated valves and controls. The thermal performance of this
system was evaluated and compared with the CESA-1 and Themis
salt storage systems developed by the European solar community.
Results of the comparison indicate that the performance of the
three salt storage systems is similar. Test data were also used
to validate a simulation model of the CRTF system and a proposed
commercial-scale system (1200 MWht). The simulation model of
the 1200-MWht system predicted an annual system efficiency of
greater than 98%. The simulation also predicted that a
relatively small amount of parasitic energy would be required to
prevent the salt from freezing during a typical operating year.

ACKNOWLEDGMENTS

CONTENTS

FIGURES

FIGURES Continued -

vii

FIGURES Continued –

TABLES

FOREWORD

The research and development described in this document was conducted within the U.S. Department of Energy's (DOE) Solar Thermal Technology Program. The goal of the Solar Thermal Technology Program is to advance the engineering and scientific understanding of solar thermal technology, and to establish the technology base from which private industry can develop solar thermal power production options for introduction into the competitive energy market.

Solar thermal technology concentrates solar radiation by means of tracking mirrors or lenses onto a receiver where the solar energy is absorbed as heat and converted into electricity or incorporated into products as process heat. The two primary solar thermal technologies, central receivers and distributed receivers, employ various point and line-focus optics to concentrate sunlight. Current central receiver systems use fields of heliostats (two-axis tracking mirrors) to focus the sun's radiant energy onto a single tower-mounted receiver. Parabolic dishes up to 17 meters in diameter track the sun in two axes and use mirrors to focus radiant energy onto a receiver. Troughs and bowls are line-focus tracking reflectors that concentrate sunlight onto receiver tubes along their focal lines. Concentrating collector modules can be used alone or in a multi-module system. The concentrated radiant energy absorbed by the solar thermal receiver is transported to the conversion process by a circulating working fluid. Receiver temperatures range from 100C in low-temperature troughs to over 1500C in dish and central receiver systems.

The Solar Thermal Technology Program is directing efforts to advance and improve promising system concepts through the research and development of solar thermal materials, components, and subsystems, and the testing and performance evaluation of subsystems and systems. These efforts are carried out through the technical direction of DOE and its network of national laboratories who work with private industry. Together they have established a comprehensive, goal-directed program to improve performance and provide technically proven options for eventual incorporation into the nation's energy supply.

To be successful in contributing to an adequate national energy supply at reasonable cost, solar thermal energy must eventually be economically competitive with a variety of other energy sources. Components and system-level performance targets have been developed as quantitative program goals. The performance targets are used in planning research and development activities, measuring progress, assessing alternative technology options, and making optimal component developments. These targets will be pursued vigorously to insure a successful program.

Chapter 1

Introduction and Overview of Results

During the past several years a wide variety of thermal energy storage subsystems has been examined for use with solar central receiver power plants. One of the most attractive concepts was the use of molten nitrate salt (60% $NaNO_3$, 40% KNO_3 by weight) as a sensible heat storage medium. This salt has high heat capacity per unit volume, low vapor pressure, good heat transfer properties and is low in cost. Because the salt can also be used as the heat-transport fluid in the solar receiver, its use simplies the solar side of a plant; this enhances the plant's reliability and efficiency. The molten salt's working temperature limits of approximately 450 °F (freezing point) to 1100 °F (salt decomposition point) are ideally suited to the generation and use of high pressure, superheated steam for either electrical power generation or industrial process heat applications.

To demonstrate the advantages of molten salt thermal storage, Martin Marietta Corporation designed and built a storage system in the early 1980s (1). The system was installed at the Central Receiver Test Facility (CRTF) in Albuquerque, New Mexico, and has operated successfully since that time in conjunction with several molten salt receiver tests. This 7-MWht system is a prototype for a hypothetical 1200-MWht commercial-scale system. It is composed of a hot storage tank containing 1050 °F salt and a cold storage tank containing 550 °F salt with associated valves and controls. Martin Marietta subjected the system to several tests soon after installation. These tests indicated that commercial-scale molten salt thermal storage systems are both technically and economically feasible. The tests also indicated that a commercial system should have a daily charge/discharge cycle efficiency of greater than 99%.

The present report documents results from more recent tests that were performed during 1986 and 1987; i.e., five years after Martin Marietta's. The results and accompanying analysis provide input to future studies, which will be performed by Sandia Laboratories, and will investigate improving the performance and reducing the costs of thermal storage systems for central receiver plants. This is the goal of research described in the Department of Energy's National Solar Thermal Five Year Research and Development Plan (2).

Before the improvement studies mentioned above can be done, it is necessary to understand and compare the performance of current U. S. and European molten salt thermal storage systems and to construct performance models of future systems, the goal of the work described here. The work was divided into four tasks: 1) current thermal performance was compared with the CRTF's performance soon after the system was installed, 2) a dynamic computer model of the CRTF system was validated with

experimental data, 3) the validated computer model was extended and simulations were performed in order to estimate the annual system efficiency for a hypothetical commercial-scale 1200-MWht system, and 4) the performance of the CRTF system was compared with molten salt thermal storage systems developed by the European solar community. Each of these tasks is discussed, with a brief summary of the results obtained, in the paragraphs that follow.

Comparison of current CRTF storage system thermal performance with original performance

We were interested in knowing whether the hot and cold tanks thermal losses had changed over the past five years. The current tests indicate that the hot tank's thermal losses are similar to those previously measured by Martin Marietta. The cold tank, however, appears to have considerably fewer losses today than were measured in 1982. During the previous tests the cold tank's insulation was wet. The insulation is dry today and therefore performs much more effectively. The results of this comparison are presented in Chapter 4.

Validation of dynamic computer model

We constructed a dynamic computer model of the CRTF storage system, which can be used to predict the time-dependent temperature response of the system as well as the system's thermal losses during a variety of storage charging and discharging scenarios. Comparisons of simulation predictions with the recent experimental data indicate good agreement. A discussion of the model is presented in Chapter 3, and validation of the model with the experimental data is presented in Chapter 5. In Chapter 6 we use the validated model to calculate charge and discharge cycle efficiencies for the CRTF hot tank.

Annual efficiency estimate for a commercial-scale system

The 99% storage efficiency calculated by Martin Marietta for the hypothetical 1200-MWht system was based upon a daily charge and discharge cycle. This value may not be representative for the system on an annual basis. Factors that could make the annual efficiency lower than the daily efficiency are the effects weather outages at the central receiver plant, equipment outages, and parasitic power required to prevent the salt from freezing.

The validated computer model was extended so that annual simulations of a hypothetical 1200-MWht commercial-scale system could be made. The simulations employed Solar One's experience with weather and equipment availability and accounted for the parasitic power needs of the storage system. The analysis showed that a relatively small amount of parasitic energy is required to prevent the salt from freezing during a typical operating year. An annual efficiency of greater than 98% was calculated for the system. These calculations are discussed in Chapter 8.

Comparison of CRTF storage system with European systems

The CRTF storage system was compared with the CESA-1 and Themis molten salt storage systems developed by the European solar community. A physical description of the CRTF system is presented in Chapter 2. Descriptions of the European systems are presented in Chapter 7, where the thermal performance comparison is also presented. The thermal performance of the three systems appears to be similar.

Chapter 2

Description of the Thermal Storage System Located at the Central Receiver Test Facility

2.1 Overview of the CRTF Storage System

Figure 2-1 is a simplified process diagram of the CRTF. Salt at a temperature of 550 °F flows from the cold salt tank to the cold sump. The cold pump carries the salt either through the propane-fired heater or to the receiver. To use the receiver, the boost pump must also be used. After the salt is heated to 1050 °F (either by the receiver or propane heater), it flows into the hot storage tank. The hot salt is pumped back to the cold storage tank after it is cooled when it produces steam in the steam generator. A detailed system description can be found in Tracey (1).

2.2 Design of the CRTF Cold Storage Tank

The dimensions and principal elements of the cold tank are shown in Figure 2-2. The design uses a common carbon-steel (e.g., SA516 grade 70) shell. The shell is covered with fibrous and block-type insulation. The tank sits upon a concrete foundation, and a layer of castable insulation separates the tank shell and the foundation. The tank vents to the atmosphere. Molten salt enters and exits the tank through the pipes indicated in the figure.

Listed in Table 2-1 are the materials and thicknesses of the cold tank.

2.3 Design of the CRTF Hot Storage Tank

The dimensions and principal elements of the hot tank are shown in Figure 2-3. The design employs thin layers of stainless steel and corrugated Incoloy to contain the salt. These layers line the inside of an insulating brick wall and floor (see Figure 2-4). A carbon steel shell bears the tank load and is located on the outer surface of the brick wall. The shell is covered with fibrous insulation. The tank sits upon a concrete foundation. A layer of castable insulation separates the tank shell and the foundation. The tank vents to the atmosphere. Molten salt enters and exits the tank via the pipes indicated in the figure.

Listed in Table 2-2 are the materials and thicknesses of the hot tank.

Table 2-3 shows the parameters for the hot tank that are important to the thermal performance calculations described in Chapters 3 and 5.

2.4 Description of Measurement Devices for the Storage System

The measurement devices described in this section provided the data that we used to estimate the thermal performance of the hot and cold tanks.

2.4.1 Equipment to Measure Temperature

The locations of the thermocouples used for temperature measurements in the hot tank are shown in Figure 2-5. The maximum salt level achieved during the tests was 128 inches. At this maximum level it can be noted that TE-292, TE-293 were used to measure the air temperature and HRW-15, HRW-17 were used to measure the liner temperature above the surface of the salt pool. Temperature measurements below the surface were performed using TE-291, HRW-3, and HRW-5. The temperature of the outer surface of the brick wall was measured with HT-2, 6, 12, and 16. The temperature of the outer surface of the sheathing was measured by HTS-1 and HTS-11.

The locations of the thermocouples used for temperature measurement in the cold tank are shown in Figure 2-6. The maximum salt level achieved during the cold tank test was 46 inches. At this level only TE-281 measured the salt temperature directly.

The inlet temperature to the hot tank was estimated by a thermocouple attached to the FCV-242 valve body. (This valve can be found on Figure 2-1). Measurement of inlet temperature by this means is only approximate because of the temperature gradient that exists across the valve body. This subject is discussed further in Section 5.3.1.

2.4.2 Equipment to Measure Mass Flow

The "sump depletion method" is the most accurate way of measuring mass flowrate at the CRTF. This is done by filling the cold sump to a high level, closing valve FCV-201, and recording level measurements as a function of time as the pump reduces the salt inventory in the sump. Since the volume of the sump is known, the time required to deplete the sump between two known sump levels can be equated to a mass flowrate. Level measurements are performed by a bubbling device.

2.2.3 Equipment to Measure Level

Bubbling devices are used to measure levels in the pump sumps and in the storage tanks.
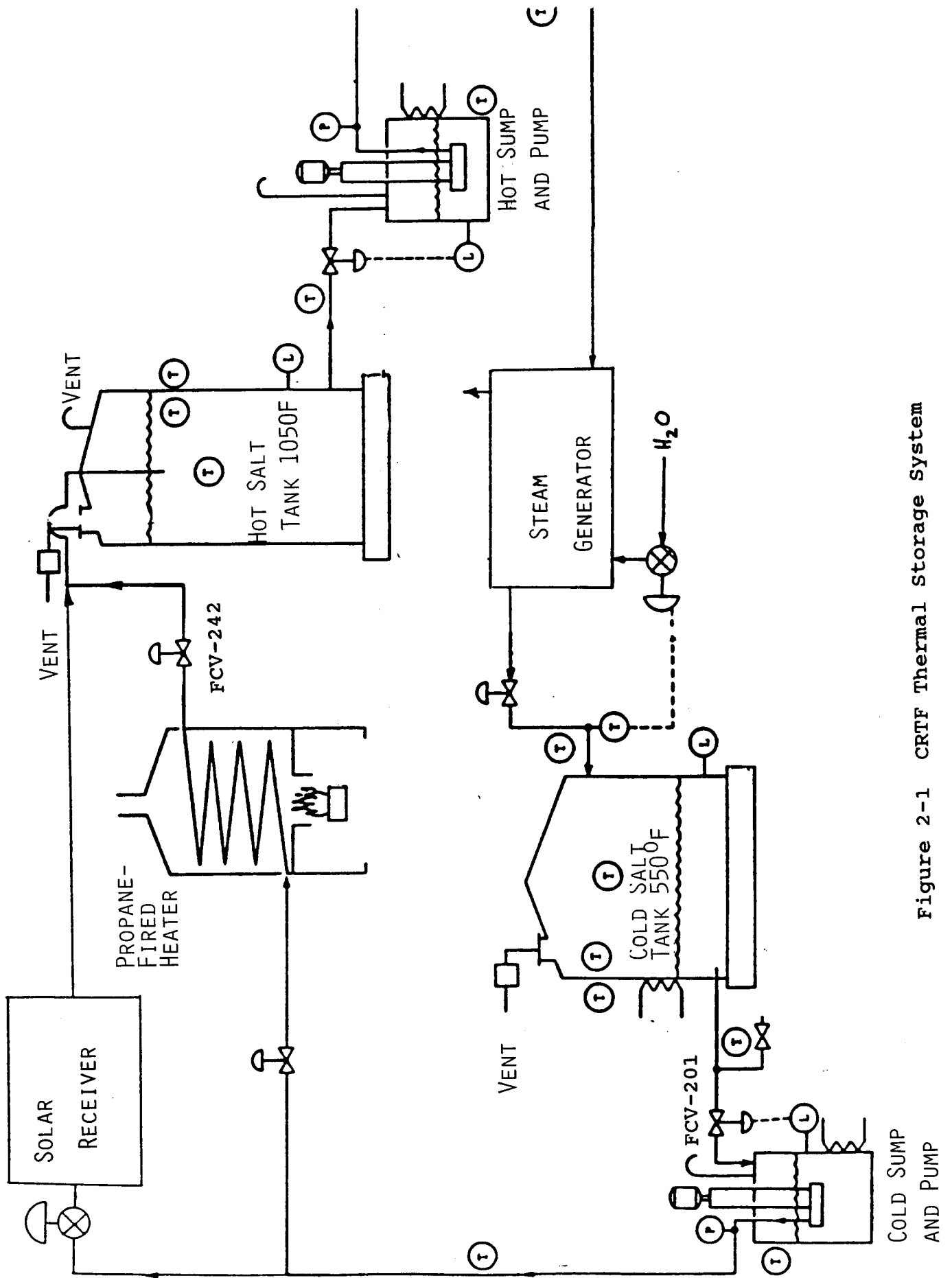
Figure 2-1 CRTF Thermal Storage System

7
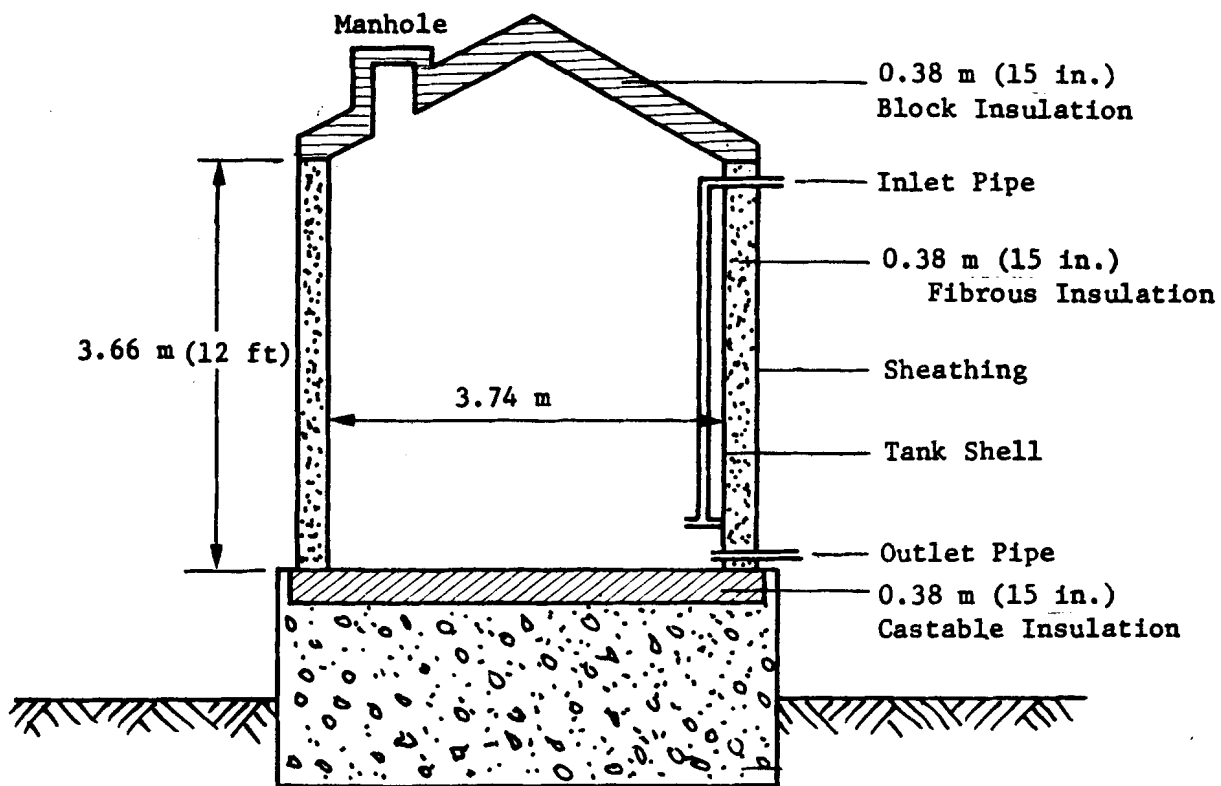
Figure 2-2 CRTF Cold Thermal Storage Tank
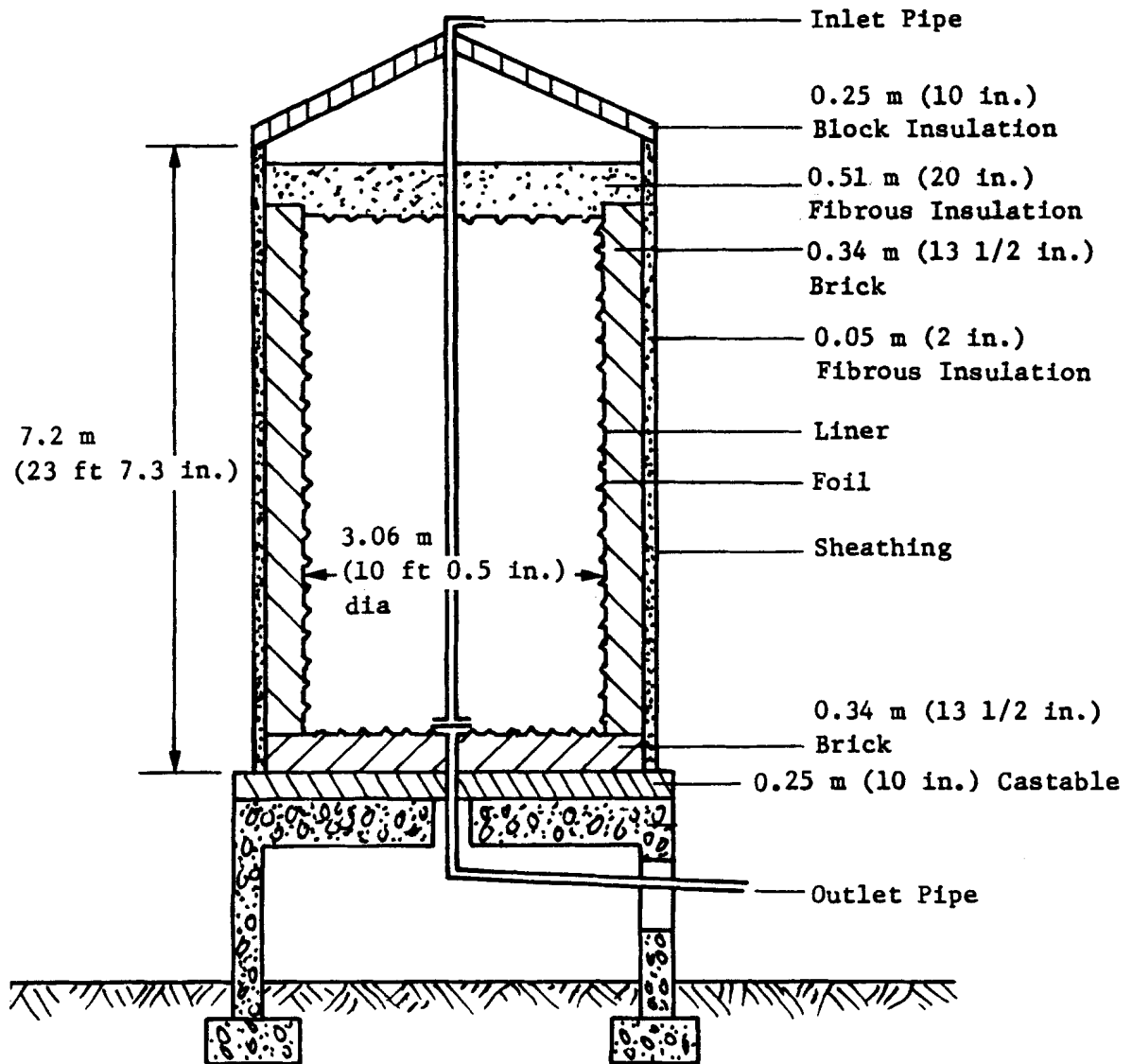
Figure 2-3   CRTF Hot Thermal Storage Tank
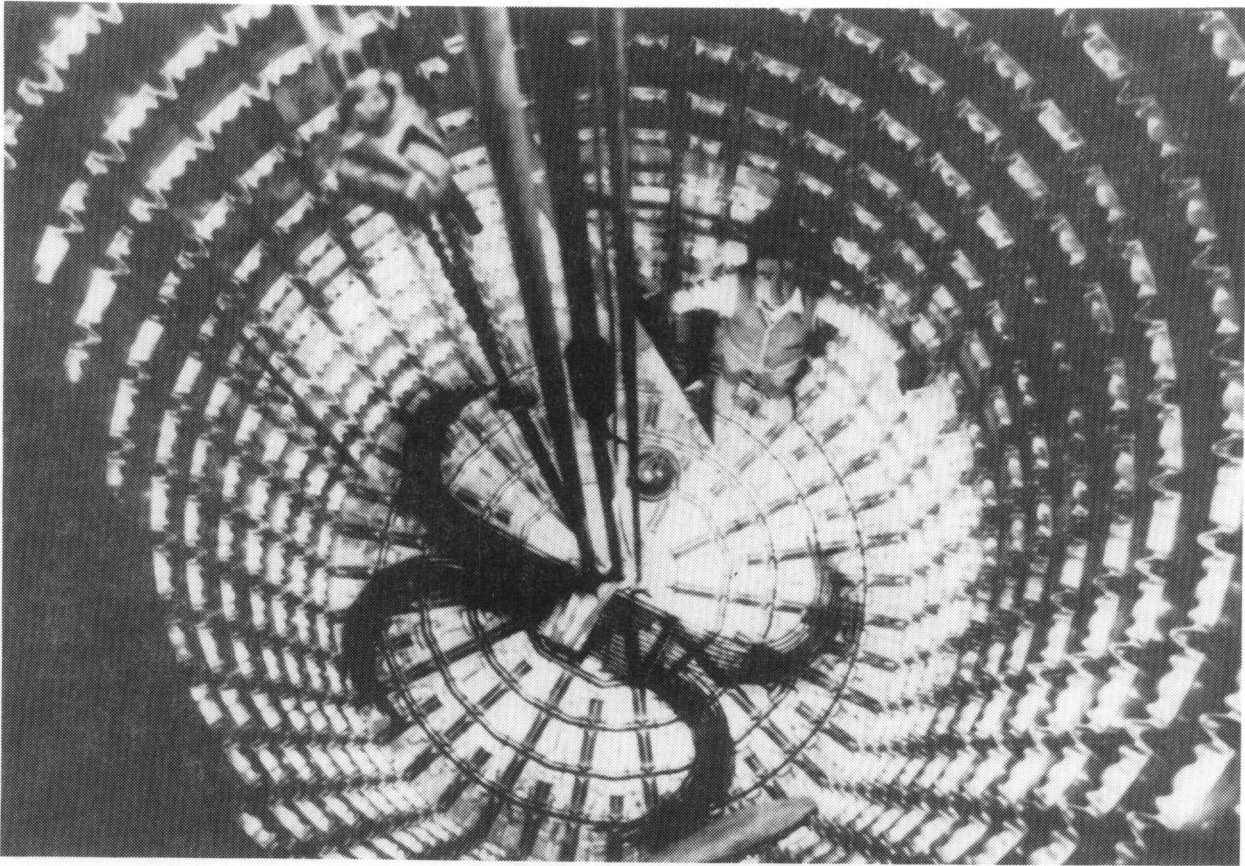
Figure 2-4   View of Inside the Hot Tank

TE-291	12 inches
TE-292	132 inches
TE-293	156 inches
HRW-3	36 inches
HRW-5	60 inches
HRW-15	180 inches
HRW-17	204 inches
HT-2	43 inches
HT-6	6 inches
HT-12	43 inches
HT-16	6 inches
HTS-1	6 inches
HTS-11	6 inches

Figure 2-5   Locations of Thermocouples in the Hot Tank

<u>Elevation from Inside Bottom of Tank</u>

TE-281   12 inches
TE-282   84 inches
TE-283   132 inches
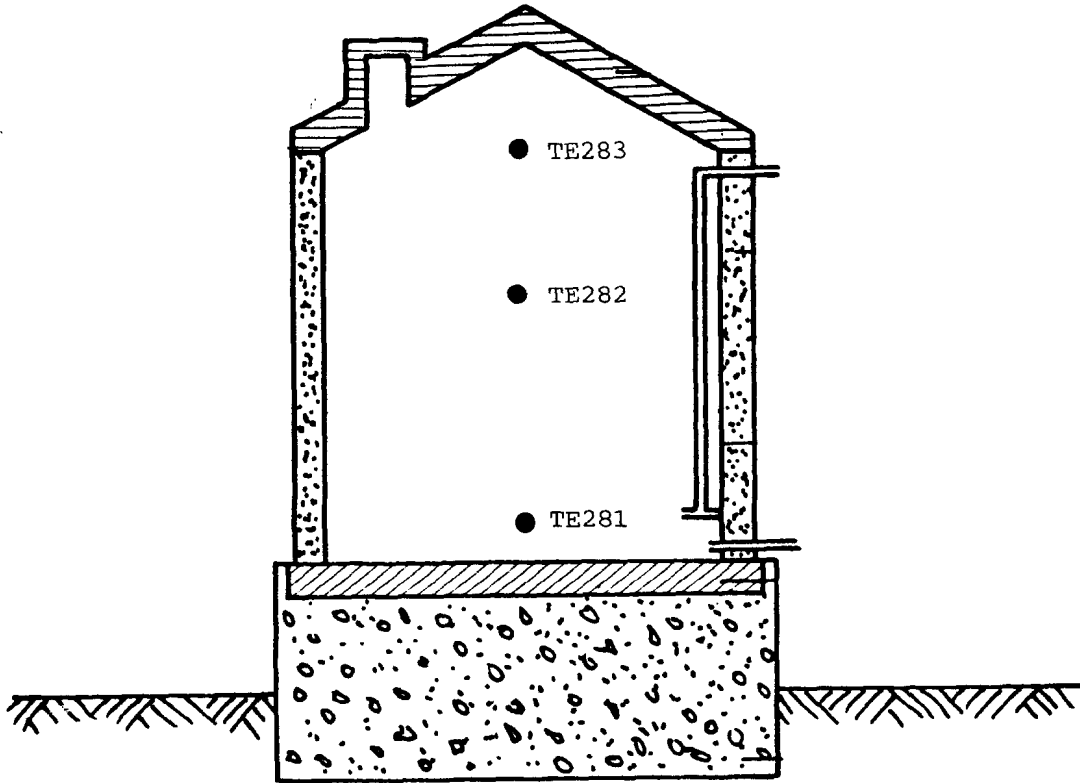
Figure 2-6 Locations of Thermocouples in the Cold Tank

Table 2-1 Materials and Thicknesses of the Cold Tank

Component	Tank Side	Tank Top	Tank Bottom
Shell	A516 Grade 70 Carbon Steel	A516 Grade 70 Carbon Steel	A516 Grade 70 Carbon Steel
External Insulation	Holmes Flexwhite 1260 (15 in.)	Holmes 1212 Block (15 in.)	Manville 2100 Castable (15 in.)
Sheathing	Aluminum with White Coating	Aluminum with White Coating	N/A

Table 2-2 Materials and Thicknesses of the Hot Tank

Component	Tank Side	Tank Top	Tank Bottom
Liner	Incoloy 800 (0.050 in.)	304 Stainless (0.050 in.)	Incoloy 800 (0.050 in.)
Foil	304 Stainless (0.010 in.)	N/A	304 Stainless (0.010 in.)
Internal Insulation	Manville C22ZSL Brick (13-1/2 in.) with Zelie Mortar (10 in.)	Holmes Flexwhite 1260 (10 in.)	Manville C22ZSL Brick (13 1/2 in.)
Shell	A516 Grade 70 Carbon Steel	A516 Grade 70 Carbon Steel	A516 Grade 70 Carbon Steel
External Insulation	Holmes Flexwhite 1260 (2 in.)	Holmes 1212 Block (6 in.)	Manville 2100 Castable (10 in.)
Sheathing Insulation	Aluminum with White Coating	Aluminum with White Coating	N/A

14

Table 2-3   Thermal Parameters of the Hot Tank

	Unit	Specifications
Heat Capacity of Brick	Btu/(lb °F)	0.24
Heat Capacity of Castable	Btu/(lb °F)	0.20
Density of Brick	lb/(ft^3)	47.0
Density of Castable	lb/(ft^3)	120.0
Heat Conductivity of Brick	Btu/(hr °F ft)	0.25
Heat Conductivity of Castable	Btu/(hr °F ft)	0.37
Heat Capacity of Salt	Btu/(lb °F)	0.365
Density of Salt	lb/(ft^3)	132 - 0.0232 T (T in °F)

Chapter 3

Analytical Model of the Thermal Storage System

3.1 Overview

This section describes the analytical model developed for the CRTF molten salt thermal storage system. The model was developed by writing several time-dependent mass and energy conservation equations for the hot and cold storage tanks. Sections 3.2 and 3.3 describe the governing equations for the hot and cold tank, respectively.

Several assumptions were incorporated into the analytical models to facilitate the analysis. They were:

1) Temperature stratification within the tanks was assumed not to be significant.
2) The specific heats and thermal conductivities of the tank materials were assumed to be constant.
3) Weather conditions outside the tanks were assumed to be constant and were based on average values.
4) An adiabatic boundary condition was assumed at the interface between the castable insulator in the floor of a tank and the concrete foundation.

The definitions of the variables are listed below:

Ac - Cross-sectional area of the cold tank (ft**2)
Acf - Area of cold tank floor (ft**2)
Acwr - Area of the cold tank walls and roof (ft**2)
Ah - Cross-sectional area of the hot tank (ft**2)
Ahf - Area of hot tank floor (ft**2)
Ahins - Area of the hot tank wall's fibrous insulation (ft**2)
Ahr - Area of the hot tank roof (ft**2)
Ahw - Area of the hot tank brick wall (ft**2)
Cb - Specific heat of the brick walls or floor (Btu/(lbm °F))
Cc - Specific heat of the castable (Btu/(lbm °F))
Cs - Specific heat of salt (Btu/(lbm °F))
Kb - Thermal conductivity of brick wall (Btu/sec ft °F))
Kc - Thermal conductivity of castable (Btu/(sec ft °F))
Lc - Salt level in the cold tank (ft)
Lh - Salt level in the hot tank (ft)
Mc - Mass of salt in the cold tank (lbm)
Mcf - Mass of castable in the cold tank floor (lbm)
Mh - Mass of salt in the hot tank (lbm)
Qhf - Heat loss from hot salt to brick floor (Btu/sec)
Qhins - Heat loss from the hot tank brick wall to the
         environment (Btu/sec)
Qhr - Heat loss from hot salt through the roof (Btu/sec)
Qhw - Heat loss from hot salt to brick wall (Btu/sec)
t - Time (sec)
T - Temperature (°F)

Tamb - Ambient temperature (°F)
Tb - Temperature of brick (°F)
Tbf - Temperature of hot tank brick floor (°F)
Tbw - Temperature of the hot tank brick wall (°F)
Tc - Temperature of salt in the cold tank (°F)
Tcf - Temperature of castable in the cold tank floor (°F)
Th - Temperature of salt in the hot tank (°F)
Tcin - Temperature of salt flowing into the cold tank (°F)
Tcout - Temperature of salt flowing out of the cold tank (°F)
Thin - Temperature of salt flowing into the hot tank (°F)
Thout - Temperature of salt flowing out of the hot tank (°F)
Ucwr - Overall heat-transfer coefficient between the cold salt
       and the environment via the walls and roof (Btu/(sec
       ft**2 °F))
Uhins - Overall heat-transfer coefficient between the outer
        surface of the hot tank brick wall and the environment
        (Btu/(sec ft**2 °F))
Uhr - Overall heat-transfer coefficient between the hot salt and
      the environment via the roof (Btu/(sec ft**2 °F))
Wcin - Mass flow into the cold tank (lbm/sec)
Wcout - Mass flow out of the cold tank (lbm/sec)
Whin - Mass flow into the hot tank (lbm/sec)
Whout - Mass flow out of the hot tank (lbm/sec)
x,r - Distance into the brick or castable measured from inside
      the tank (ft)
rhob - Density of the brick in the hot tank walls and floor
       (lbm/(ft**3))
rhoc - Density of the salt in the cold tank (lbm/(ft**3))
rhoh - Density of the salt in the hot tank (lbm/(ft**3))

Figures 2-2 and 2-3 display the principal system elements
modeled in this chapter. The reader should refer to these
figures to help clarify the definitions presented above and the
discussion that follows.

3.2   Analytic Model of the Hot Tank

3.2.1 Conservation of Mass Within the Hot Tank

The time dependent conservation of mass equation for the salt in
the tank is:

$$\frac{d(Mh)}{d(t)} = Whin - Whout ; \qquad (3-1)$$

also,

$$Mh = rhoh * Ah * Lh . \qquad (3-2)$$

Substitution of Equation (3-2) into (3-1) and rearranging terms
yield an expression for the tank level as a function of time:

$$\frac{d(Lh)}{d(t)} = \frac{(Whin - Whout)}{rhoh * Ah} - \frac{Lh}{rhoh} * \frac{d(rhoh)}{d(Th)} * \frac{d(Th)}{d(t)} . \qquad (3-3)$$

The salt density as a function of temperature is (3):

$$rhoh = 132 - 0.0232 * Th \; ; \tag{3-4}$$

therefore,

$$\frac{d(rhoh)}{d(Th)} = -0.0232 \; \frac{lbm}{ft\,F} \; .$$

3.2.2 Conservation of Energy Within the Hot Tank

The time-dependent conservation of energy equation for the salt in the tank is

$$Cs * \frac{d(Mh * Th)}{d(t)} = (Whin * Cs * Thin) - (Whout * Cs * Thout)$$

$$- Qhf - Qhw - Qhr \; . \tag{3-5}$$

The heat exchange from the salt to the brick floor and brick wall are respectively:

$$Qhf = Kb * Ahf * \left. \frac{d(Tbf)}{d(x)} \right|_{x=0} \tag{3-6}$$

$$Qhw = Kb * Ahw * \left. \frac{d(Tbw)}{d(r)} \right|_{r=0} \; . \tag{3-7}$$

The derivatives $d(Tbf)/d(x)$ and $d(Tbw)/d(r)$ are evaluated at the salt/brick interface, i.e., at x and r equal to zero.

Since the thermal resistance of the brick is much greater than the convective resistance between the salt and brick, it is a good approximation to ignore the latter.

The heat loss from the salt to the environment through the roof can be approximated as

$$Qhr = Uhr * Ahr * (Th - Tamb) \; . \tag{3-8}$$

The overall heat-transfer coefficient (Uhr) is obtained from experimental results.

Substitution of Equations (3-1), (3-6), (3-7), and (3-8) into (3-5) and rearranging terms yield an expression for the average tank salt temperature as a function of time:

$$\frac{d(Th)}{d(t)} = \frac{1}{Mh * Cs} * [Whin * Cs * Thin - Whin * Cs * Th$$

$$- Kb * Ahw * \left. \frac{d(Tbw)}{d(r)} \right|_{r=0} - Kb * Ahf * \left. \frac{d(Tbf)}{d(x)} \right|_{x=0}$$

$$- Uhr * Ahr * (Th - Tamb)] \; . \tag{3-9}$$

The time-dependent conservation of energy equations for the brick/castable floor and for the brick wall are of the form:

$$K * \frac{\partial^2 (Tbf)}{\partial (x)^2} = rho * C * \frac{\partial (Tbf)}{\partial (t)} \qquad \text{(Floor)} \qquad (3-10)$$

$$Kb * \frac{\partial^2 (Tbw)}{\partial (r)^2} = rhob * Cb * \frac{\partial (Tbw)}{\partial (t)} \qquad \text{(Wall)} \qquad (3-11)$$

where, the thermal conductivity (K), density (rho), and specific heat (C) are evaluated for the brick and castable.

The boundary conditions for Equations (3-10) and (3-11) are listed as Equations (3-6) and (3-7) at the salt/brick boundaries. The boundary conditions are adiabatic at the castable/foundation boundary, and they are

$$Qhins = Uhins * Ahins * (Tbw\Big|_{x=xout} - Tamb) \qquad (3-12)$$

at the interface between the brick and the fibrous insulation. The variable $Tbw\big|_{x=xout}$ is the temperature at the outer surface of the brick wall and Uhins is an experimentally determined overall heat-transfer coefficient between the outer surface of the brick wall, through the fibrous insulation, and to the environment.

3.2.3 Procedure Used to Solve the Analytical Model of the Hot Tank

The partial differential equations for heat conduction listed in Equation (3-10) were approximated by a set of first-order ordinary differential equations. This was done by writing time-dependent equations at several equally spaced locations across the thickness of the brick and castable. These heat-conduction equations along with Equations (3-3) and (3-8) formed a system of first-order, non-linear ordinary differential equations. This system of equations was numerically integrated on a personal computer with the System Simulation Language (SYSL) software package (4) to yield the tank salt level, the salt temperature, and several brick/castable temperatures as a function of time.

3.3 Analytical Model of the Cold Tank

The cold tank does not have insulating brick in the walls or in the floor. Rather, a lightweight fibrous insulation is used in the walls, and castable is used in the floor. Due to the lack of thermal mass in the cold tank walls, there is no need to write differential equations for the wall insulator. However, differential equations for conduction were written for the castable insulator in the floor since this material is capable of storing a significant amount of energy.

The mass and energy equations for the cold tank are similar to
the expressions for the hot tank except for the differences
noted in the above paragraph. The equations for the cold tank
are listed below:

$$\frac{d(Lc)}{d(t)} = \frac{(Wcin - Wcout)}{rhoc * Ac} - \frac{Lc}{rhoc} * \frac{d(rhoc)}{d(Tc)} * \frac{d(Tc)}{dt} , \tag{3-13}$$

$$\frac{d(Tc)}{d(t)} = \frac{1}{Mc * Cs} * [Wcin * Cs * Tcin - Wcin * Cs * Tc$$

$$- Kc * Acf * \left.\frac{d(Tcf)}{d(t)}\right|_{x=0} - Ucwr * Acwr * (Tc - Tamb)] , \tag{3-14}$$

and,

$$Kc * \frac{\partial^2 (Tcf)}{\partial (x)^2} = Mcf * Cc * \frac{\partial (Tcf)}{\partial (t)} . \tag{3-15}$$

The procedure for solving the model of the cold tank was also
similar to the procedure described for the hot tank in Section
3.2.3. The reader should refer to that section.

Chapter 4

Tests of the Thermal Storage System

4.1 Overview

In Sections 4.2 through 4.5 we present the data collected during
tests of the CRTF hot and cold tanks. Two different types of
tests were performed, namely, charging and cooling.

During a charging test, the tank exit pipe was closed and salt
was pumped into the tank through the inlet pipe. During the
time the tank was being filled, the salt inlet temperature and
various other temperatures inside the tank and insulator
materials were recorded. The inlet flow rate and tank level
were also recorded. The tank was filled until the desired level
was reached. At that point the charging test was terminated by
turning the pump off and closing the inlet pipe. We performed
one charging test of the hot tank.

The cooling test was usually performed following the charging
test. With the tank inlet and exit pipes closed, the tank was
allowed to cool down over a period of one to several days.
During the cool down of the tank, various temperatures inside
the tank and insulator materials were recorded. We performed
one cooling test of the cold tank and two for the hot tank.

In Section 4.6 we compare the current thermal performance of the
CRTF hot and cold tanks with that measured by Martin Marietta
Corporation in 1982.

4.2 Cooling Test of the Hot Tank from May 28, 1987 to June 1, 1987

Three days before beginning a charging test of the hot tank, a
cooling test was performed. The intention of this test was to
ensure at the beginning of the subsequent charge test that all
temperatures in the tank were in equilibrium. Before this
cooling test, the tank was filled with 950 °F salt to a level of
30 inches (20% full).

Figures 4-1 and 4-2 show seven temperature curves versus time.
Thermocouples TE-291, TE-292, TE-293, HRW-3, and HRW-15 were
used to measure the temperature inside the tank. Thermocouple
TE-291 was in contact with the salt, and the others were above
the surface of the salt and measured either the temperature of
the air or the liner (refer to Figure 2-5 for thermocouple
locations). For that reason, a temperature difference between
the air and salt inside the tank was observed. Earlier tests
performed by Martin Marietta showed that the temperature
gradient within the hot salt itself was negligible (1). The
thermocouples labeled HT in Figure 4-2 measured the temperature
of the shell (equivalent to the temperature at the outer surface

of the brick insulator). One day after beginning this cooling test, all measured temperatures decreased with time, which indicated that the tank had reached thermal equilibrium.

4.3 Charging Test of the Hot Tank Conducted on June 1, 1987

The charging test started June 1, 1987, at 12:26 p.m. (time zero for all figures presented in Sections 4.2 and 4.3 is 10:05 a.m. on June 1, 1987). Figure 4-3 illustrates the temperature behavior inside the tank before, during, and shortly after the charging test. Before starting the charging test, the salt temperature was approximately 600 °F, i.e., the final temperature of the cooling test described in Section 4.1. During the charging test the salt temperature was raised to over 1100 °F.

The levels of the cold salt storage tank (LT-281), hot salt storage tank (LT-291), and the cold salt sump (LT-201) are shown in Figure 4-4. The steps shown in the figure are due to several cold sump depletions that were performed before and during the charging test (see Section 2.4.2). This was done before the test to assure the tank was completely empty at the start of the test and to calibrate the level instrument. Sump depletions were performed during the test to obtain an accurate measurement of the mass flow rate into the hot tank (see discussion of "sump depletion method" in Section 2.4.2). These sump depletions did not affect the flow rate into the tank. During the charging test the level increased in a linear fashion indicating that a constant inlet flow rate had been achieved.

The temperature of the hot salt entering the tank was estimated using a thermocouple located on the outside surface of the flow control valve FCV-242. This valve is installed at the outlet of the propane heater (see Figure 2-1). Figure 4-5 shows the measured temperature of FCV-242 versus time. A comparison of the FCV-242 temperature and the tank temperatures located nearest the inlet line (see HRW-3 and TE-291 in Figures 4-3 and 4-6) shows a difference of approximately 70 °F. If it is assumed that HRW-3 and TE-291 gave a more accurate representation of salt inlet temperature, this implies the existence of a temperature gradient across the FCV-242 valve body of approximately 70 °F. The temperature peak in Figure 4-5 was due to the lowering of the heat input to the propane heater when the salt temperature became too high.

Figures 4-3 and 4-6 show the salt temperature inside the tank during the charging test. The TE-Thermocouples, located in the middle of the tank, follow the salt inlet temperature faster than the HRW thermocouples, located on the tank wall. Due to material restrictions of the propane heater, the charging test could not be stopped abruptly; cold salt was pumped through the unheated propane heater into the hot tank for several minutes toward the end of the charging phase (this occurred at time t=15200 seconds), causing a rapid drop in the hot salt temperature.

During charging, the salt at the bottom of the tank exhibited the highest temperature because it was near the hot inlet stream (Figure 2-3 shows the inlet pipe near the bottom). The salt in the higher elevations was at a lower temperature because relatively cool salt was pumped into the tank at the start of the charging phase, and this cooler salt had not yet mixed with the hotter salt at the bottom. This temperature stratification phenomenon can be seen in Figure 4-6. After the charging pump was turned off at 15,600 seconds, the salt in the tank became mixed, and the salt temperature throughout the tank approached a single value. The mixing phenomenon can also be observed in Figure 4-6.

4.4 Cooling Test of the Hot Tank from June 1 to 15, 1987

Upon termination of the charging test, a cooling test was performed. At the start of the test, the tank level was 127 inches. Salt, shell, and sheathing temperatures were recorded every hour. Figure 4-7 displays the salt temperature versus time. It can be seen that the salt temperature declined more rapidly on the first day. During this interval, the brick wall and floor were being heated by the salt. The salt temperature declined more slowly in this test than during the cooling test of May 28th. This was due to the higher salt content in the storage tank during the June 1 - 15 test. On June 12 at 9:15 a.m. (930710 sec) the tank was depleted. The temperature in the tank decreased much faster due to the reduced salt mass in the tank.

The shell temperatures (outer surface of the brick wall) are shown in Figure 4-8. The brick's temperature increased initially in response to the elevation of the salt temperature during the charging test. An equilibrium heat-transfer condition was reached approximately 50 hours (180000 seconds) after beginning the cooling test. After this time, all salt and brick temperatures declined together. The brick's temperature fell more rapidly toward the end of the cooling test in response to the lowering of the salt in the tank.

Figure 4-9 illustrates the surface temperatures of the sheathing (outer surface of fibrous insulation) and the ambient temperature versus time. The surface temperature was mainly influenced by the ambient temperature.

4.5 Cooling Test of the Cold Tank from September 27 to 29, 1986

On September 27, 1986, the cold tank was filled to a level of 46 inches with 570 °F salt. The tank was isolated and allowed to cool for a period of 50 hours (180000 seconds). Three thermocouples measured the inside temperature of the tank during this period. The temperature measurements are displayed in Figure 4-10. Thermocouple TE-281 was in contact with the salt, and the others were above the surface of the salt and measured

the air's temperature (refer to Figure 2-6 for thermocouple locations). For that reason a temperature difference inside the tank was observed. Earlier tests performed by Martin Marietta showed that the temperature gradient within the cold salt itself was negligible (1).

4.6 Comparison of Current Equilibrium Heat Loss Results with Original Results

After the CRTF thermal storage system was installed in 1982 it was subjected to several thermal performance tests by Martin Marietta Corporation (1). In this section we compare the hot and cold tank equilibrium heat loss estimates provided by Martin with the current estimates.

Equilibrium heat loss occurs in the hot tank when all temperatures in the salt and brick insulator trend downward together. As discussed in Sections 4.2 and 4.4, equilibrium heat transfer occurs approximately one to two days after the hot tank is charged with hot salt. The time delay is due to the poor thermal conductivity of the brick and the large amount of brick thermal mass. The cold tank, on the other hand, reaches equilibrium conditions much more quickly because of the lack of thermal mass in the tank wall. The comparison presented here was performed when both tanks were in equilibrium.

The original Martin results are compared with the current results in Table 4-1. The comparison indicates that the current heat loss in the hot tank is similar to the original. The cold tank, however, has considerably less heat loss today than was measured in 1982. The most likely reason for the difference is that during the Martin tests the cold tank's fibrous insulation was observed wet. The insulation is dry today and therefore performs much more effectively.

The heat loss was estimated from the following conservation of energy equation:

$$\text{Loss} = M_s * C_p * (dT_s/dt), \tag{4-1}$$

where,

M_s = mass of salt in the tank,
C_p = specific heat of salt, and
dT_s/dt = time rate of change of salt temperature.

The mass of the salt was estimated using the density and level of salt in the tank. The rate of change of salt temperature was estimated by drawing a tangent line on the salt's temperature-history curves (e.g., Figure 4-7 for hot tank and Figure 4-10 for cold tank) at the salt temperatures given in the table.

26

The Martin cold tank test was performed at a salt temperature of 660 °F and an ambient temperature of 38 °F. The current cold tank test was performed at salt temperatures ranging from 570 to 535 °F and an ambient temperature of approximately 70 °F. Since the heat loss is a function of the temperature difference between the salt and ambient, for purposes of comparison it was necessary to extrapolate the Martin test results to the conditions of the current test. If it is assumed that the overall cold tank heat-transfer coefficient remained constant during the Martin test, the following equation can be used to estimate a heat loss of 8.5 KW at a salt temperature of 550 °F and an ambient temperature of 70 °F:

$$Q2 = \frac{T2 * Q1}{T1}$$

where,

Q1 = heat loss measured during Martin test (11 KW),
Q2 = heat loss estimate at 550 °F salt temperature and 70 °F ambient temperature (8.5 KW),
T1 = salt/ambient temperature difference during Martin test (622 °F),
T2 = salt/ambient temperature difference at 550 °F salt temperature and 70° ambient temperature (480 °F).

Finally, it should be noted that comparisons at other salt temperatures reveal similar trends, i.e., heat losses in the hot tank are nearly identical, while cold tank losses are currently much fewer.
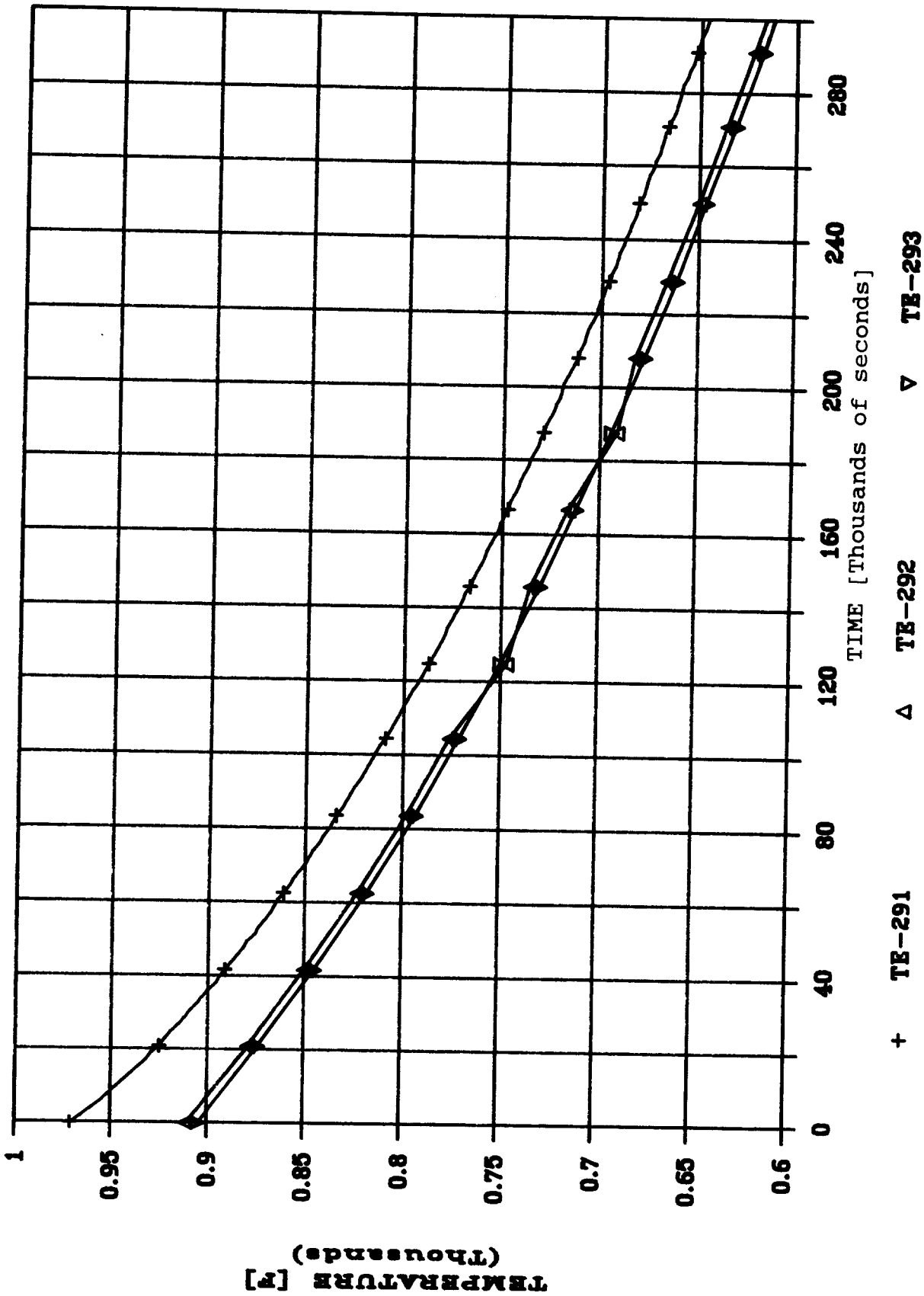
Figure 4-1 Hot Tank Inside Temperatures During Cooling Test
Conducted from May 28, 1987 to June 1, 1987
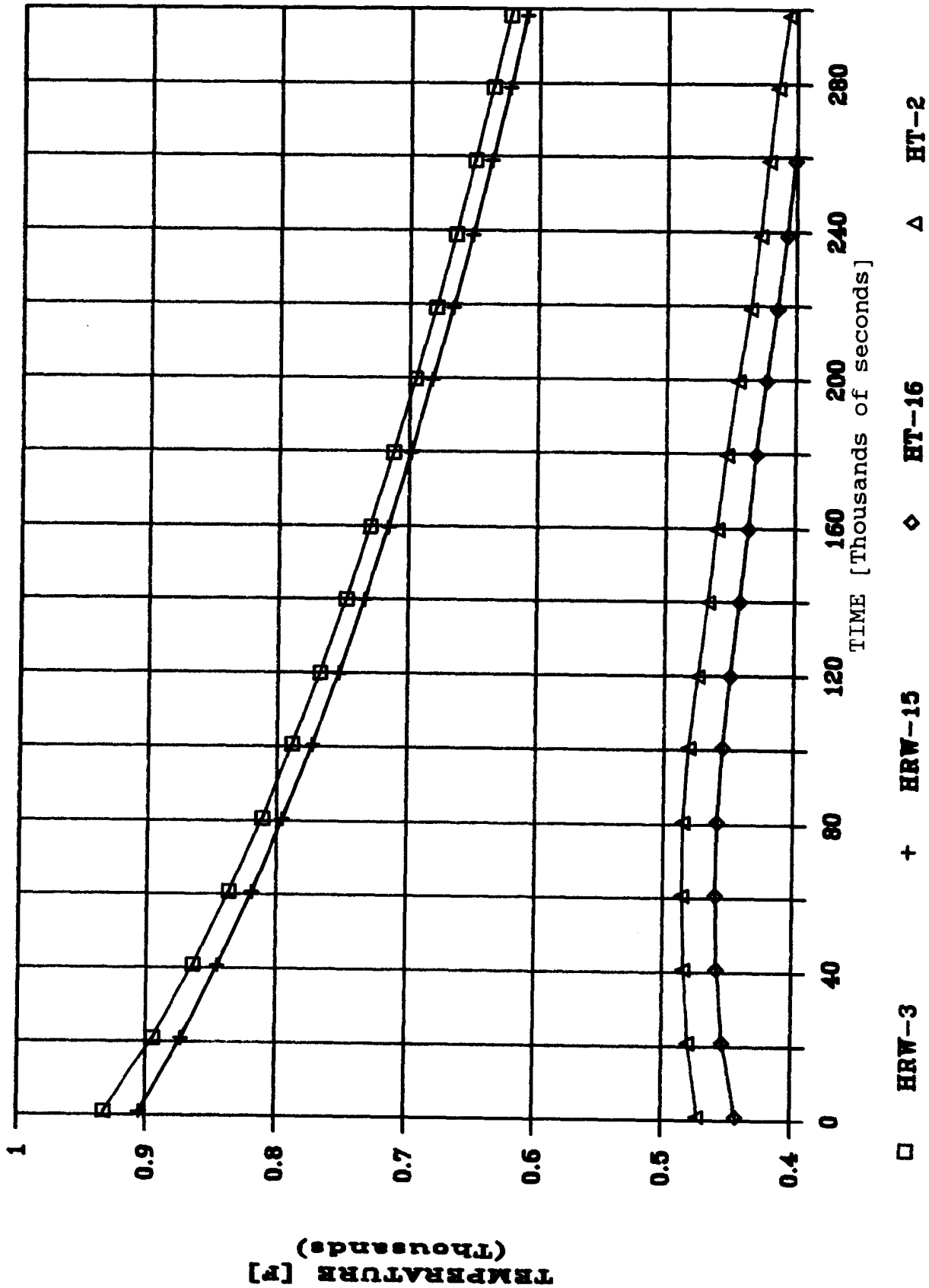
Figure 4-2 Hot Tank Inside and Brick Temperatures During Cooling Test
Conducted from May 28, 1987 to June 1, 1987
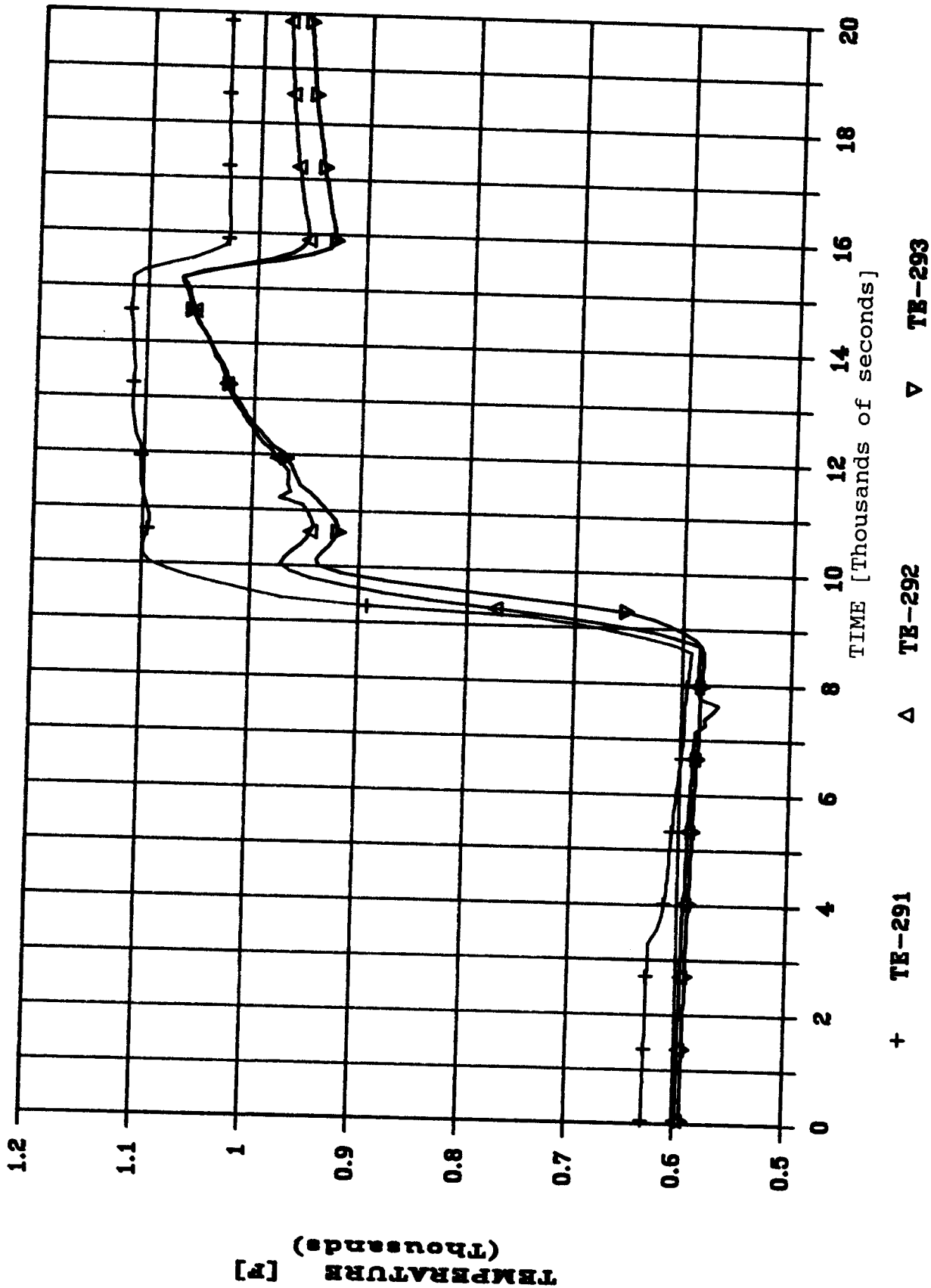
Figure 4-3   Hot Tank Inside Temperatures During Charging Test
              Conducted on June 1, 1987
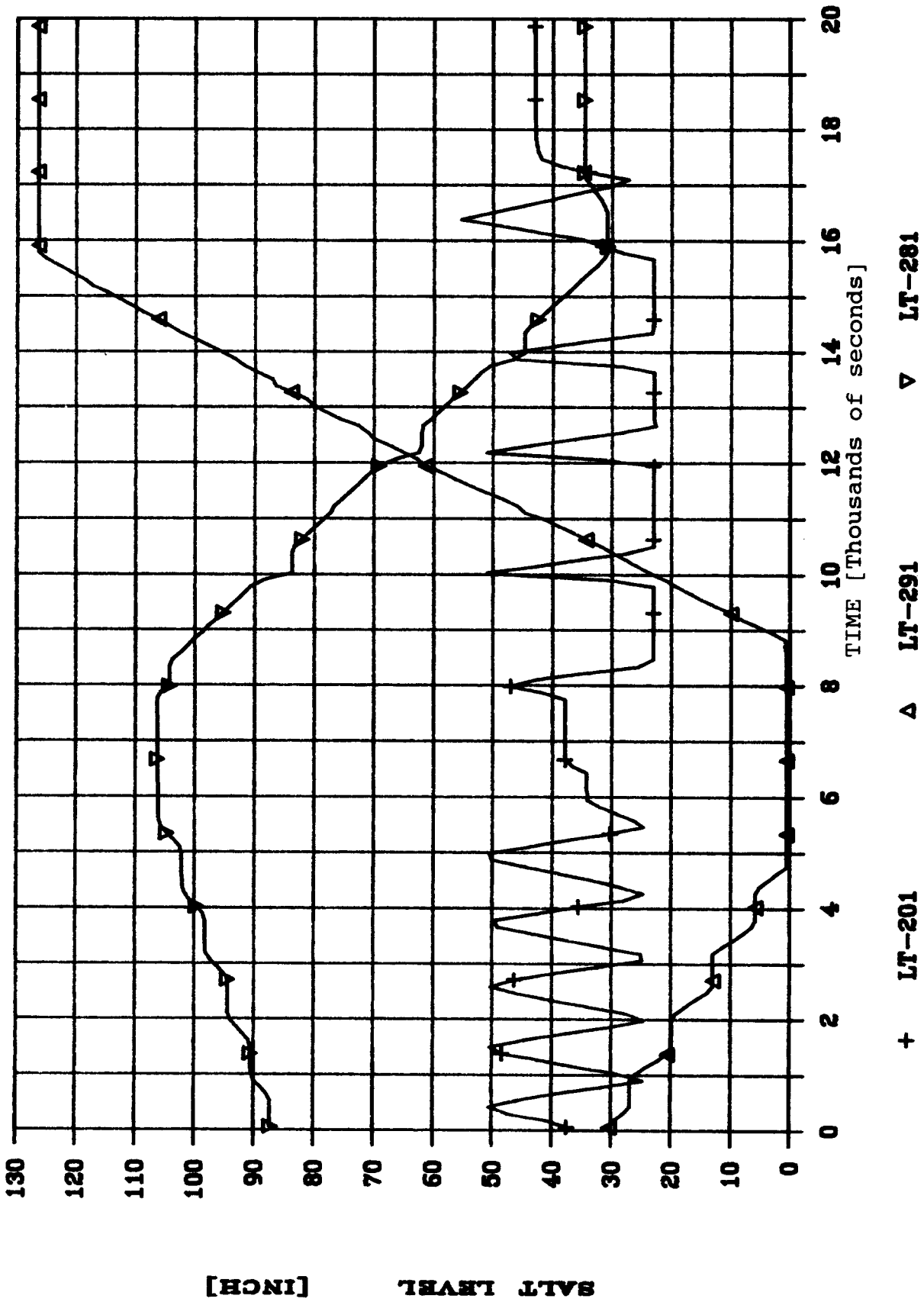
Figure 4-4 Salt Levels in the Cold Tank, Hot Tank, and Cold Sump
During the Charging Test Conducted on June 1, 1987

31
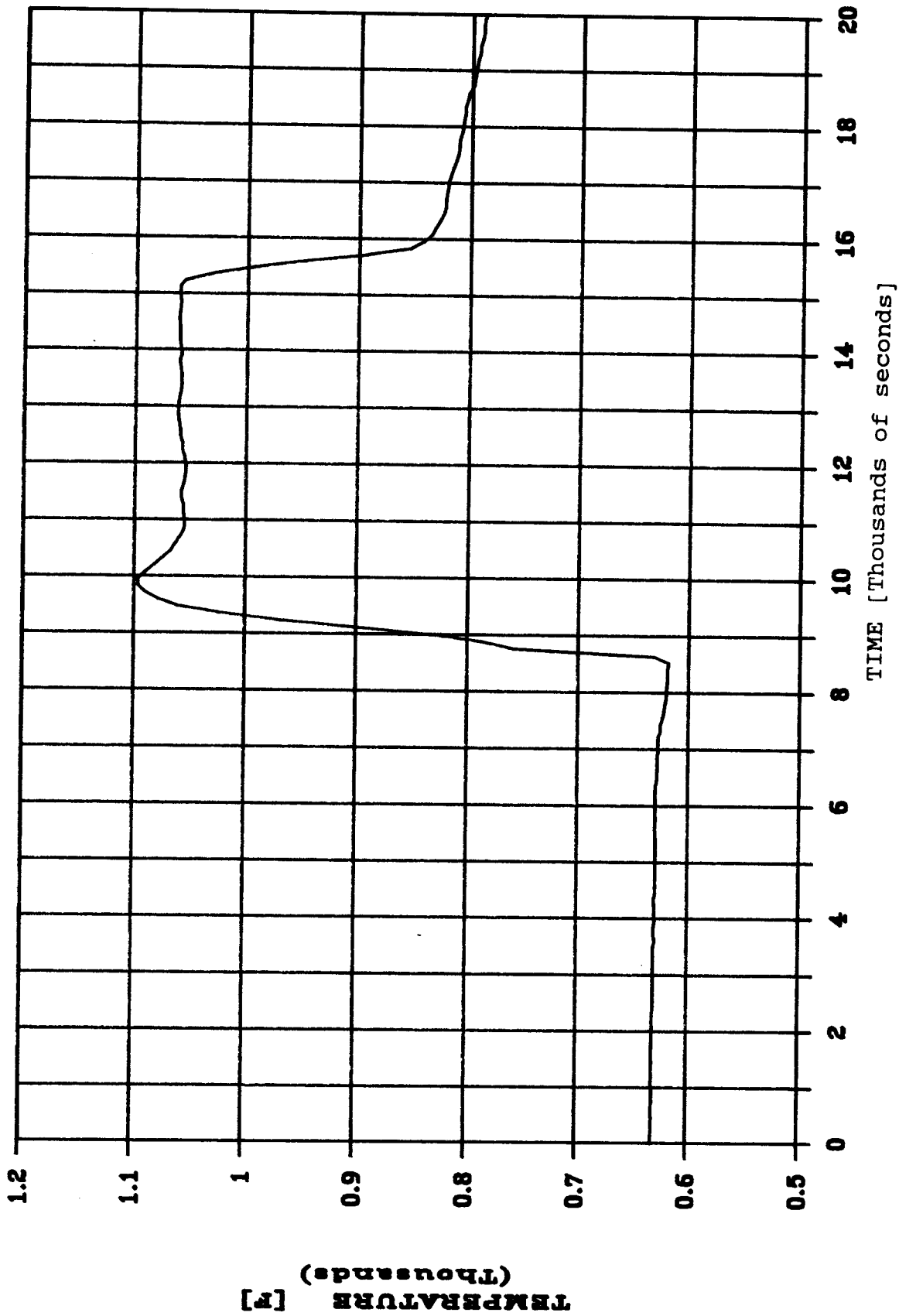
Figure 4-5   Temperature of Valve FCV-242 During the Charging Test
Conducted on June 1, 1987
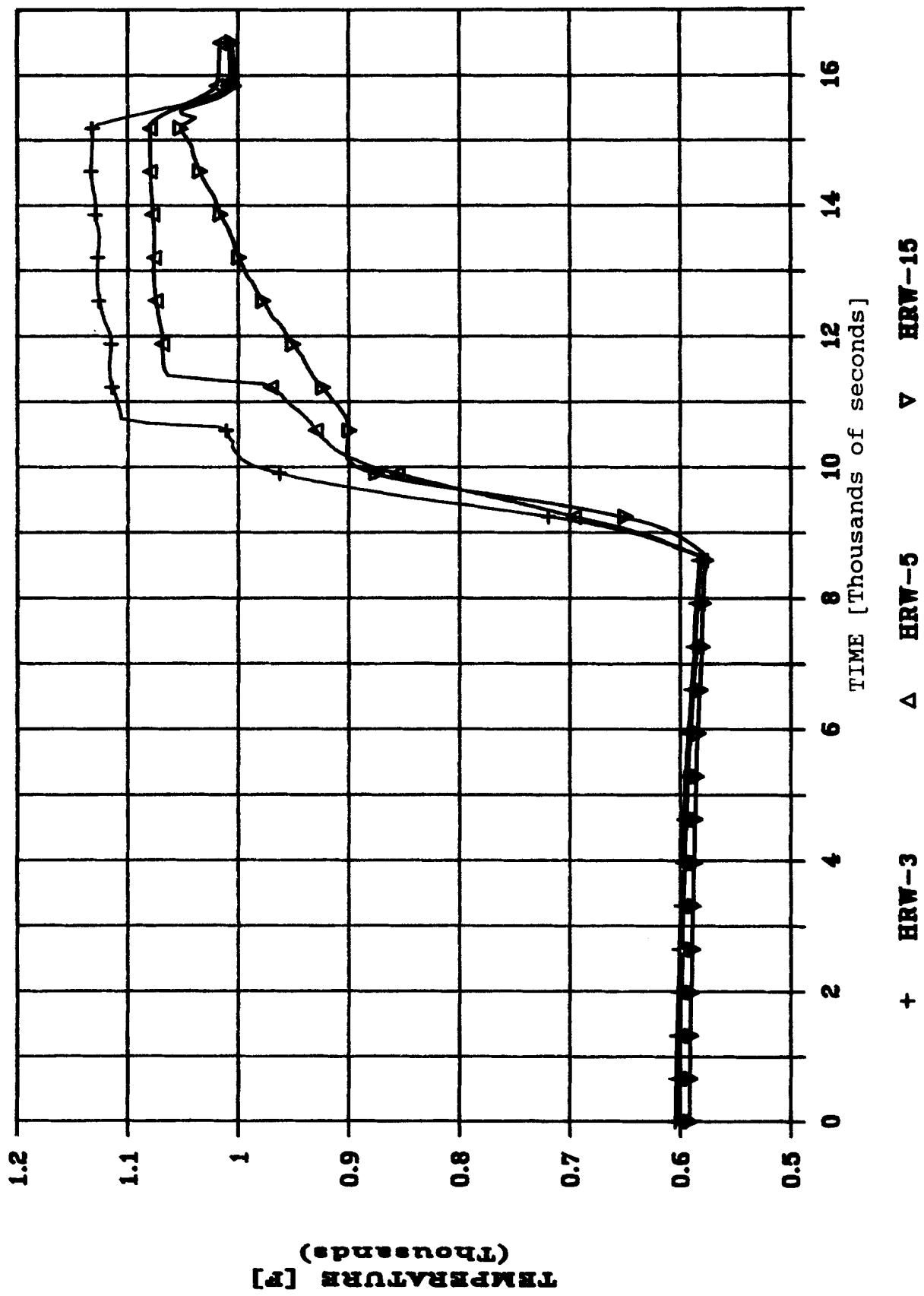
Figure 4-6 Hot Tank Liner Temperatures During the Charging Test
Conducted on June 1, 1987
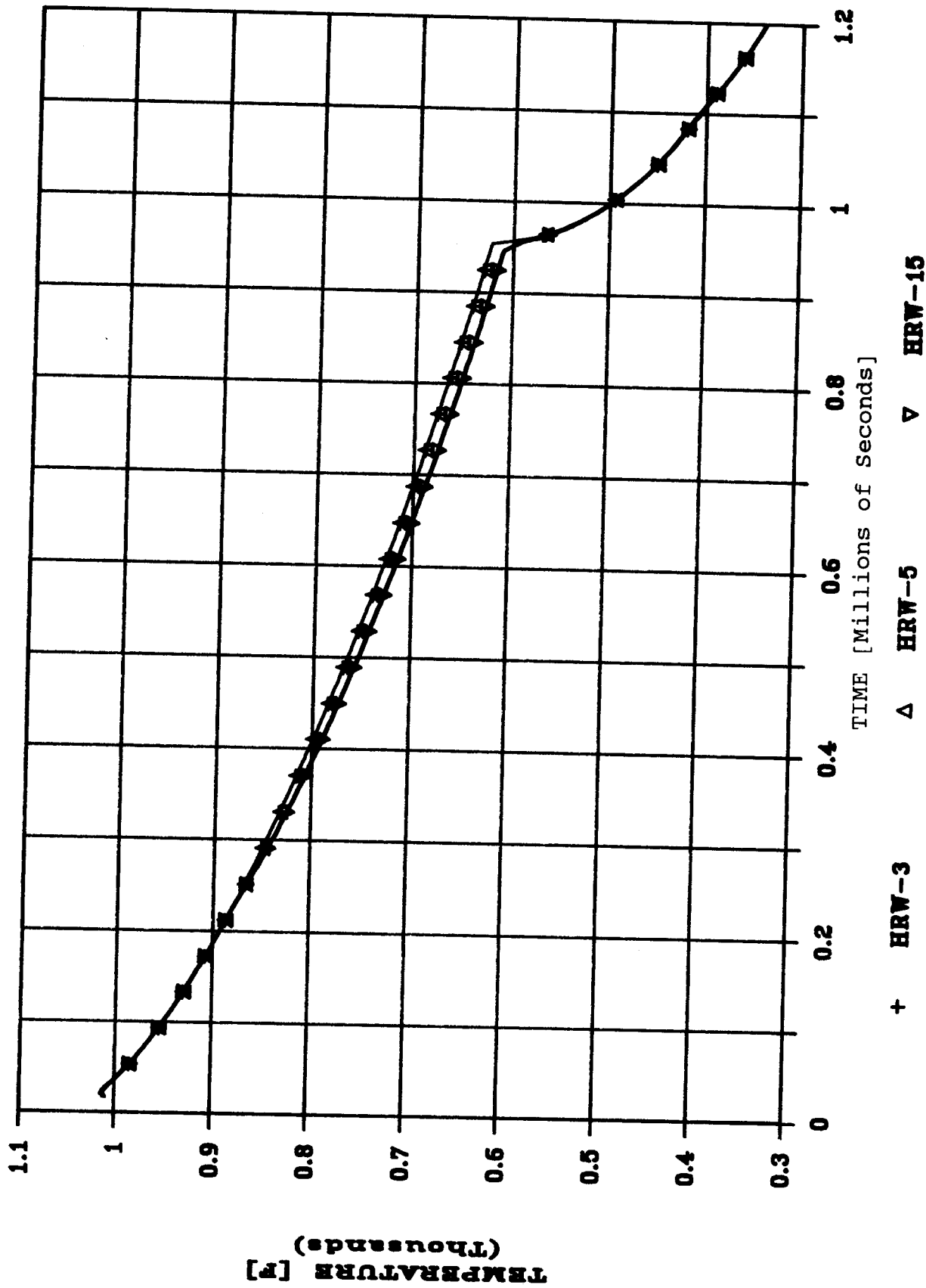
Figure 4-7   Hot Tank Liner Temperatures During the Cooling Test
Conducted from June 1, 1987 to June 15, 1987
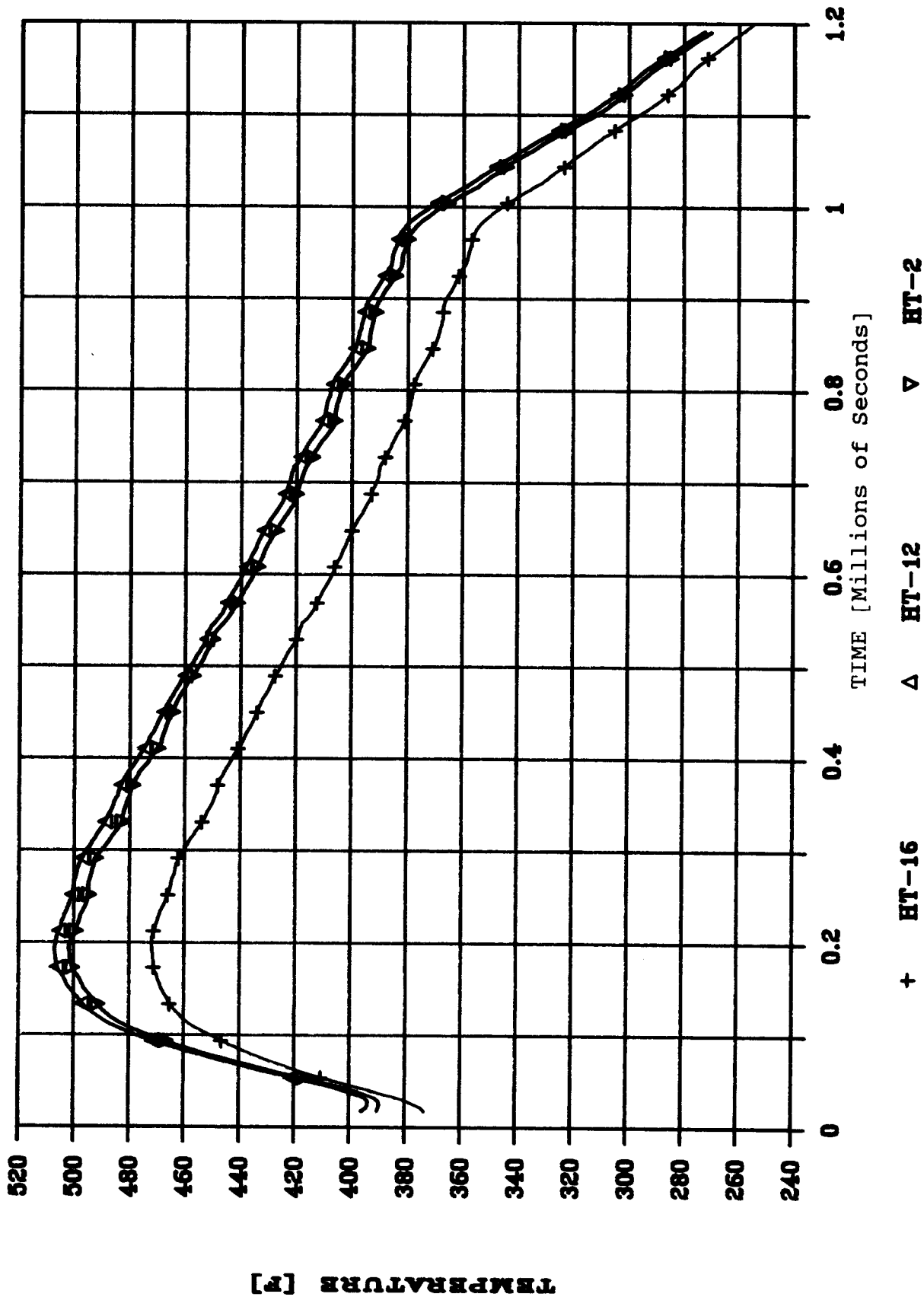
Figure 4-8   Temperatures at the Outer Surface of the Hot Tank
Brick Insulator During the Cooling Test Conducted
from June 1, 1987 to June 15, 1987

TEMPERATURE [F]

200 190 180 170 160 150 140 130 120 110 100 90 80 70 60 50 40 30 20 10 0

0   0.2   0.4   0.6   0.8   1   1.2

TIME [Millions of Seconds]

+   AMB. TEMP.   △   HTS-11   ▽   HTS-1
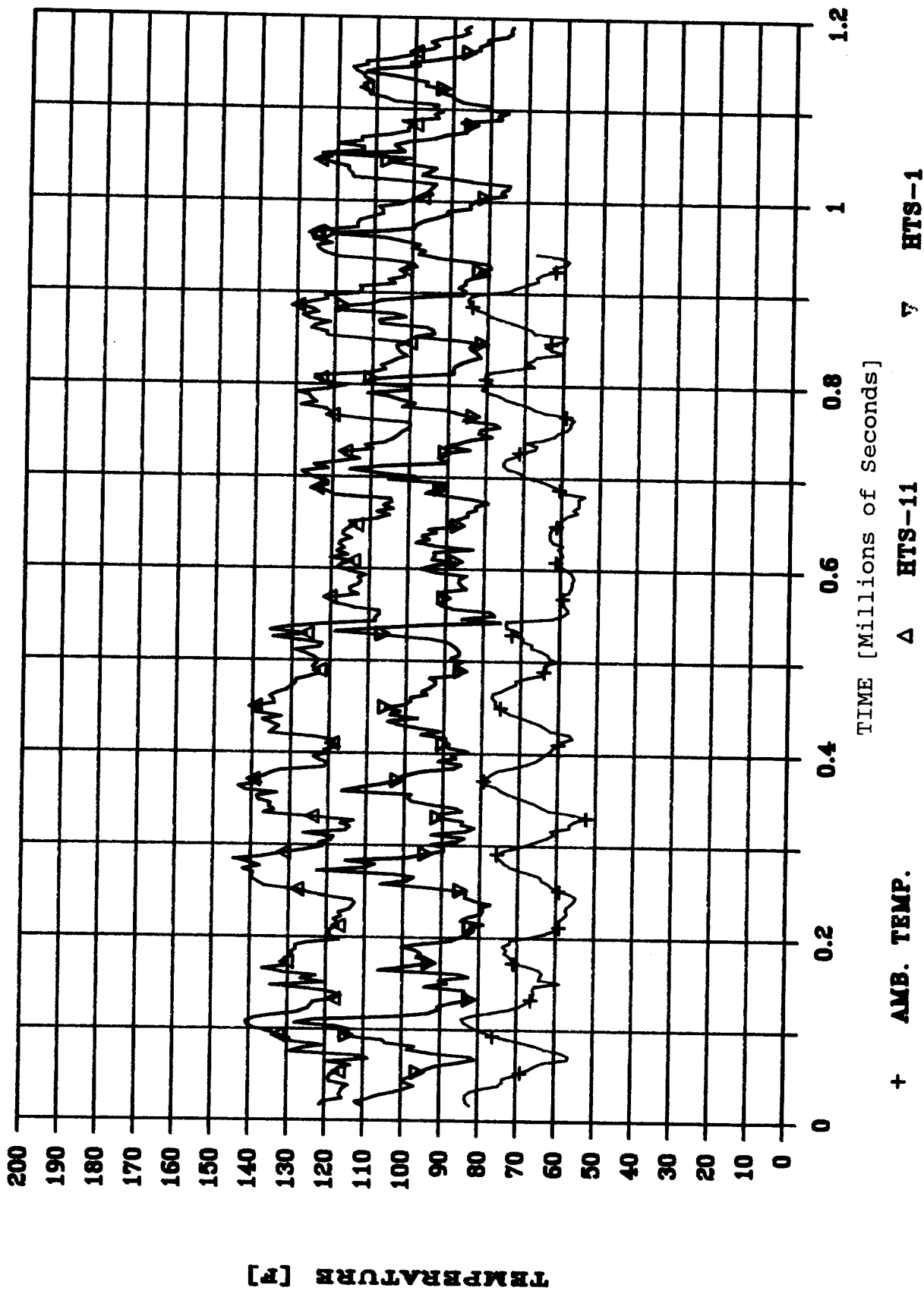
Figure 4-9   Ambient Temperature and Temperatures at the Outer
Surface of Sheathing During the Cooling Test Conducted
from June 1, 1987 to June 15, 1987
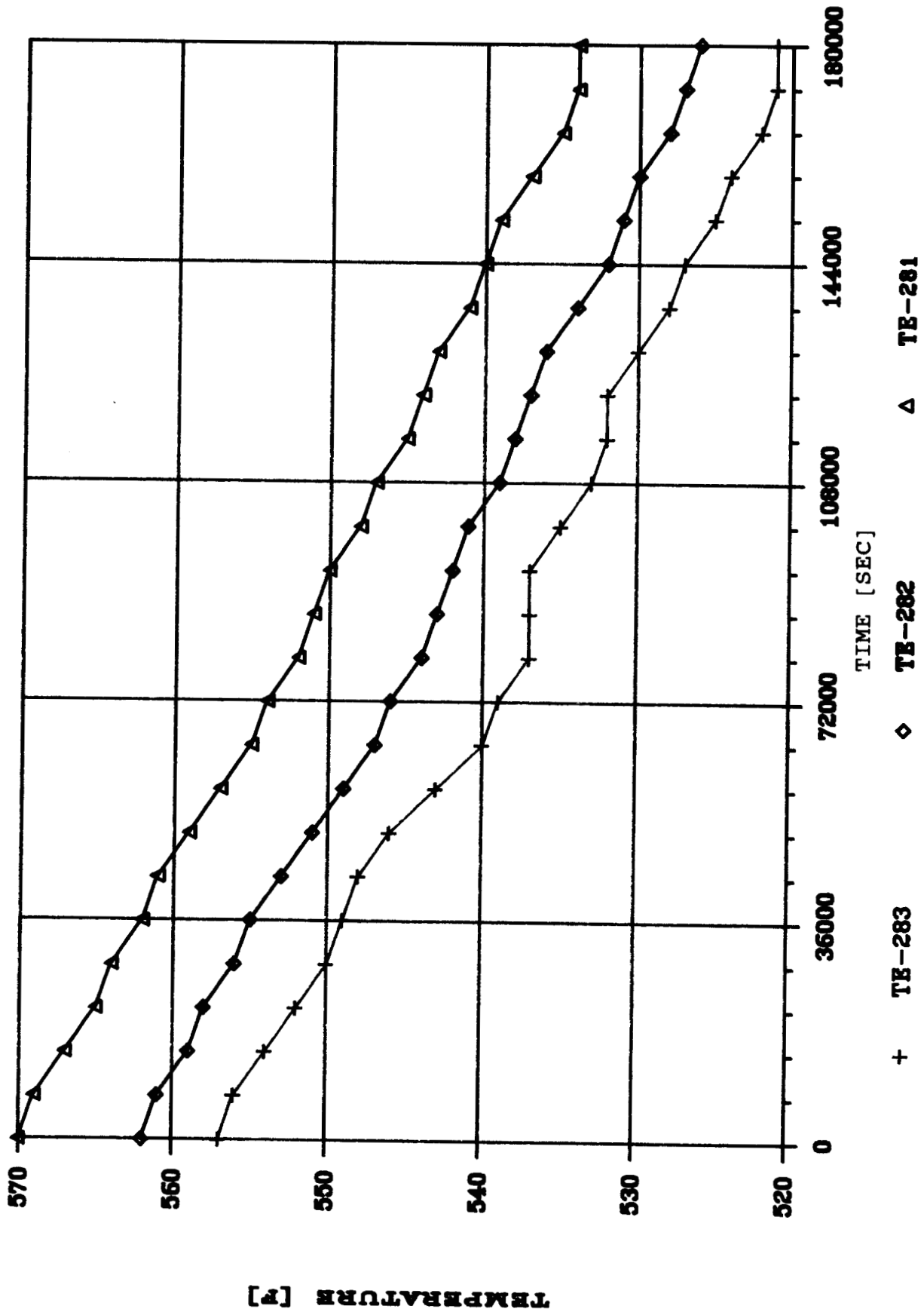
Figure 4-10   Cold Tank Inside Temperatures During the Cooling Test
Conducted from September 27, 1987 to September 29, 1987

Table 4-1
Comparison of Equilibrium Heat Loss Test Results

HOT TANK

Test Date	Salt Temperature (°F)	Salt Level (ft)	Heat Loss (KW)
1982	860	13.5	17
1987	860	10.6	17

COLD TANK

Test Date	Salt Temperature (°F)	Salt Level (ft)	Heat Loss (KW)
1982	550	0.46	8.5 *
1986	550	3.8	4.0

*   The heat loss at a salt temperature of 550 °F was extrapolated from test data obtained at 640 °F. See discussion in Section 4.3.

Chapter 5

Validation of Analytical Model

5.1 Overview

In this chapter we will compare the predictions of the
analytical model described in Chapter 3 with the experimental
data presented in Chapter 4 and with the original experimental
data collected by Martin Marietta Corporation in 1982. The
model is shown to give a good estimate of the time-dependent
thermal performance of the actual system.

In order to obtain agreement between the model and the
experimental data, it was first necessary to obtain reasonable
estimates for the various thermal parameters. This topic is
discussed in Section 5.2. In the sections following 5.2, a
comparison of the model and the experimental data is presented.

5.2 Estimation of Model Thermal Parameters

The analytical model described in Chapter 3 contained several
thermal parameters. These parameters and their values are
listed in Table 5-1. All of the parameter values listed are
handbook values from the material manufacturer except for those
that are underlined. The underlined values were obtained from
the CRTF storage system's experimental results. The estimation
of the underlined parameters is discussed in the paragraphs that
follow.

The average thermal conductivity of the brick wall, Kb, was
determined from the original Martin Marietta hot tank test data
(Reference 1) and the heat conduction equation for the brick
wall. The equation and experimental values are

$$Kb = \frac{Qhw*[ln(Do/Di)]}{2*PI*L*(Ti - To)} \quad , \tag{5-1}$$

where,

Do = the outer diameter of the brick wall (12.3 ft),
Di = the inner diameter of the brick wall (10.04 ft),
L = the length of the wall (15.95 ft),
Qhw = equilibrium heat transfer through the wall (52318 Btu/hr),
Ti = inside brick temperature (950 °F), and
To = outside brick temperature (527 °F).

Substitution of these values into Equation 5-1 yields a value
for Kb of 0.25 Btu/(hr ft °F). This approach was taken rather
than using the handbook value for brick because the wall is
actually composed of brick and mortar. The average thermal
conductivity of the brick wall must therefore include the mortar
as well. If one uses only the handbook value for brick, the
predicted outside brick temperature is much lower than that
observed in the Martin Marietta experiment.

The other hot tank parameters, Uhins and Uhr, were also estimated from results of the Martin hot tank test and from an equilibrium heat-transfer equation. The equations and the experimental values are

$$Uhins = \frac{Qhins}{Ahins*(To - Tamb)} \quad \text{and} \quad (5\text{-}2)$$

$$Uhr = \frac{Qhr}{Ahr*(Th - Tamb)} \quad , \quad (5\text{-}3)$$

where,

Ahins = approximate area of the hot tank wall's fibrous insulation (633 ft**2),
Ahr = approximate area of the hot tank's ceiling (119 ft**2),
Qhins = equilibrium heat transfer from the outer surface of the brick wall through the fibrous insulation in the walls and to the environment (52318 Btu/hr),
Qhr = equilibrium heat transfer from the roof liner through the fibrous insulation in the roof and to the environment (7285 Btu/hr),
Tamb = ambient temperature (28 °F),
To = outside brick temperature (527 °F),
Th = hot salt temperature (957 °F).

Substitution of these values into the above equations yields values for Uhins and Uhr of 0.166 and 0.0659 Btu/hr F ft*2, respectively.

The overall heat-transfer coefficient for the cold tank was estimated with data collected from the cooldown test of the cold tank conducted in September 1986. The original Martin Marietta test data were not used because during that test the tank insulation was observed to be wet; the wet insulation severely degraded the thermal performance of the tank. During the September 1986 test, the insulation was dry and the thermal performance was significantly better. The overall heat-transfer coefficient for the cold tank, Ucwr, was estimated using the following equation and experimental data:

$$Ucwr = \frac{Mc*Cs*(dTc/dt)}{Acwr*(Tc - Tamb)} \quad , \quad (5\text{-}4)$$

where,

Acwr = approximate area of the cold tank walls and ceiling (728 ft**2),
Cs = specific heat of salt (0.365 Btu/(lbm °F)),
dTc/dt = the rate of temperature decay of the cold salt (0.75 °F/hr),
Mc = mass of cold salt in the tank (53797 lbm),
Tamb = average ambient temperature (70 °F),
Tc = cold salt temperature (550 °F).

40

The experimental values listed above were presented in Chapters 2 and 4. Substitution of these values into the above equation yields a value for Ucwr of 0.042 Btu/(hr ft**2 °F).

5.3 Comparison of Analytical Model with Experimental Results

In this section we compare the predictions of the analytical model described in Chapter 3 with experimental results. Two separate experiments were performed; one for the hot tank and one for the cold tank. These comparisons are presented in Sections 5.3.1 and 5.3.2, respectively.

5.3.1 Validation of the Analytical Model for the Hot Tank

The hot-tank model was validated with experimental data collected during the charging and subsequent stagnation of the hot tank. These data were discussed in Chapter 4. The model can be considered valid if it can predict a reasonable estimate of the actual thermal response of the tank given known input disturbances. The most important input disturbances are listed and discussed below:

1) inlet salt flow rate,
2) ambient temperature, and
3) inlet salt temperature.

The thermal response of the model and the actual system can be compared by a comparison of the following variables:

1) level of salt in the tank,
2) salt temperature in the tank, and
3) temperature at the outside surface of the brick.

A comparison of these variables follows the discussion of the input disturbances.

Estimation of inlet salt flow rate

As discussed in Chapter 4, at the start of the experiment the hot tank level was 30 inches. The tank was then completely drained in a stepwise fashion over a period of approximately 5000 seconds. The tank remained empty for about 3500 seconds and was then charged at a constant flow rate of 12.33 lbm/sec to a level of 127 inches. The charging phase lasted about 7000 seconds. The charging pump was then turned off and remained off for approximately 11 days. After 11 days the pump was restarted and the tank was emptied.

The simulation model utilized essentially the same flow rate that was measured during the test. The only approximation made was during the initial drain of the tank. Rather than model a stepwise drain, a drain at a constant flowrate was assumed. The constant flow rate of 4.9 lbm/sec was estimated by a curve fit of the data.

Estimation of ambient temperature

The ambient temperature ranged from 55 to 85 °F during the 11-day test. These data are plotted in Figure 4-9. Rather than using a curve fit of these data, a constant ambient temperature of 70 °F was used in the simulation model. The importance of this assumption is believed to be small compared with other assumptions employed in the model.

Estimation of inlet salt temperature

An accurate measurement of the hot-tank salt inlet temperature cannot be made at the CRTF; a thermocouple does not exist that measures this temperature directly. Indirect measurements can be made, but they only provide an approximation of the true temperature. There are three methods of indirect measurement.

The first method employs a thermocouple attached to the exterior of the tank inlet valve (FCV-242). As discussed previously in Section 4.3, this measurement is lower than the actual temperature during the charging phase due to the temperature gradient across the valve body. We have estimated the temperature gradient to be approximately 70 °F during charging. On the other hand, the valve temperature is expected to be higher than the actual salt temperature in the early phases of a transient caused by a large temperature decrease in the salt inlet temperature; this is due to the thermal lag of the valve body. (Following achievement of equilibrium heat transfer, the measurement would again be lower than the actual temperature.) This latter phenomenon was believed to occur after the propane heater was turned off at the end of the charging phase.

The second and third methods use thermocouples located toward the bottom of the hot tank. Thermocouple HRW-3 is located on the liner at an elevation of 19.75 inches, and TE-291 is located in the center of the tank at an elevation of 12 inches. These thermocouples are believed to give a reasonable measure of inlet temperature because they are located near the inlet stream. Inaccuracies in their measurements are caused by mixing the inlet salt with salt already present in the tank. Thermocouples are also inaccurate before they are covered by the salt because they measure the temperature of the air.

Given the inaccuracies discussed above, we were only capable of postulating an inlet temperature scenario that was consistent with the data obtained from the three thermocouples. This temperature scenario is labeled THTI in Figure 5-1. It should be compared to the thermocouple readings labeled HRW-3 and FCV-242 in Figure 5-1, and the thermocouple reading labeled TE-291 in Figure 5-2.

Comparison of salt levels in the hot tank

Figure 5-3 displays the experimentally measured salt tank level

and the analytical prediction. Agreement is generally good. The curve-fit approximation to the stepwise drain can be noted in the 0- to 5000-second time interval.

Comparison of salt temperature in the hot tank

As discussed in Chapter 3, the analytical model does not include temperature stratification within the tank, i.e., the salt is assumed to be at a single, homogenous temperature. The experimental data indicate that this is a good assumption when the charging pump is not operating. With the pump operating, the data indicate that some temperature stratification does occur. These phenomena are displayed in Figure 5-4. In that figure, the measured temperatures of the tank liner at three elevations are plotted. (The tank-liner temperature is typically 10 °F lower than the salt temperature.) During charging, the salt closest to the bottom of the tank was the hottest because it was closest to the hot inlet stream. The salt in the higher elevations was at a lower temperature because cooler salt was pumped into the tank earlier in the charging phase, and this cooler salt had not yet mixed with the hotter salt at the bottom. After the pump was turned off at 15600 seconds, the salt temperature throughout the tank approached a single value.

In Figure 5-2, we compare the salt temperatures during the charging phase of the test. The homogenous salt temperature of the analytical model is compared with the measured salt temperature at the 12-inch elevation and the measured liner temperature at the 180-inch elevation. The homogenous temperature is seen to lie between the stratified salt temperatures while the charging pump is on. After the charging pump is turned off, the model and the experimental data approximately converge after the tank becomes fully mixed.

In Figure 5-5, we compare the salt temperatures during the 11 days in which the charging pump was turned off and during final tank drain at the end of the test. The homogenous salt temperature of the analytical model is compared with the measured liner temperatures at locations of 19.75 inches and 180 inches. The model is seen to produce a good estimate of the actual salt temperature.

Comparison of the temperature at the outside surface of the hot tank brick wall

Displayed in Figure 5-6 is a comparison of the measured outside temperature of the brick wall at the 55.75-inch location with the analytical prediction. The analytical model is seen to produce a reasonable temperature response. The differences between data and the model are due to modeling approximations and experimental uncertainties.

5.3.2 Validation of Cold-Tank Analytical Model

The cold-tank model was validated with experimental data

collected during a cooling test. These data were discussed in Chapter 4. Since the tank walls lack significant thermal mass, unlike the hot tank, the cold tank quickly achieves equilibrium heat transfer. The thermal performance of the cold tank should therefore not be significantly different during a charging or cooling test. For this reason, only a cooling test was performed.

Displayed in Figure 5-7 is a comparison of the analytical prediction of the cold tank's salt temperature with the experimental temperatures measured inside the tank. The level of tank was maintained at approximately 46 inches during the test. It can be noted that the model accurately predicted the actual salt temperature measured by TE-281. The other two thermocouples, TE-282 and TE-283, indicated a lower temperature because they were not in contact with the salt; they were located in the air space above the salt at locations of 84 inches and 132 inches, respectively.
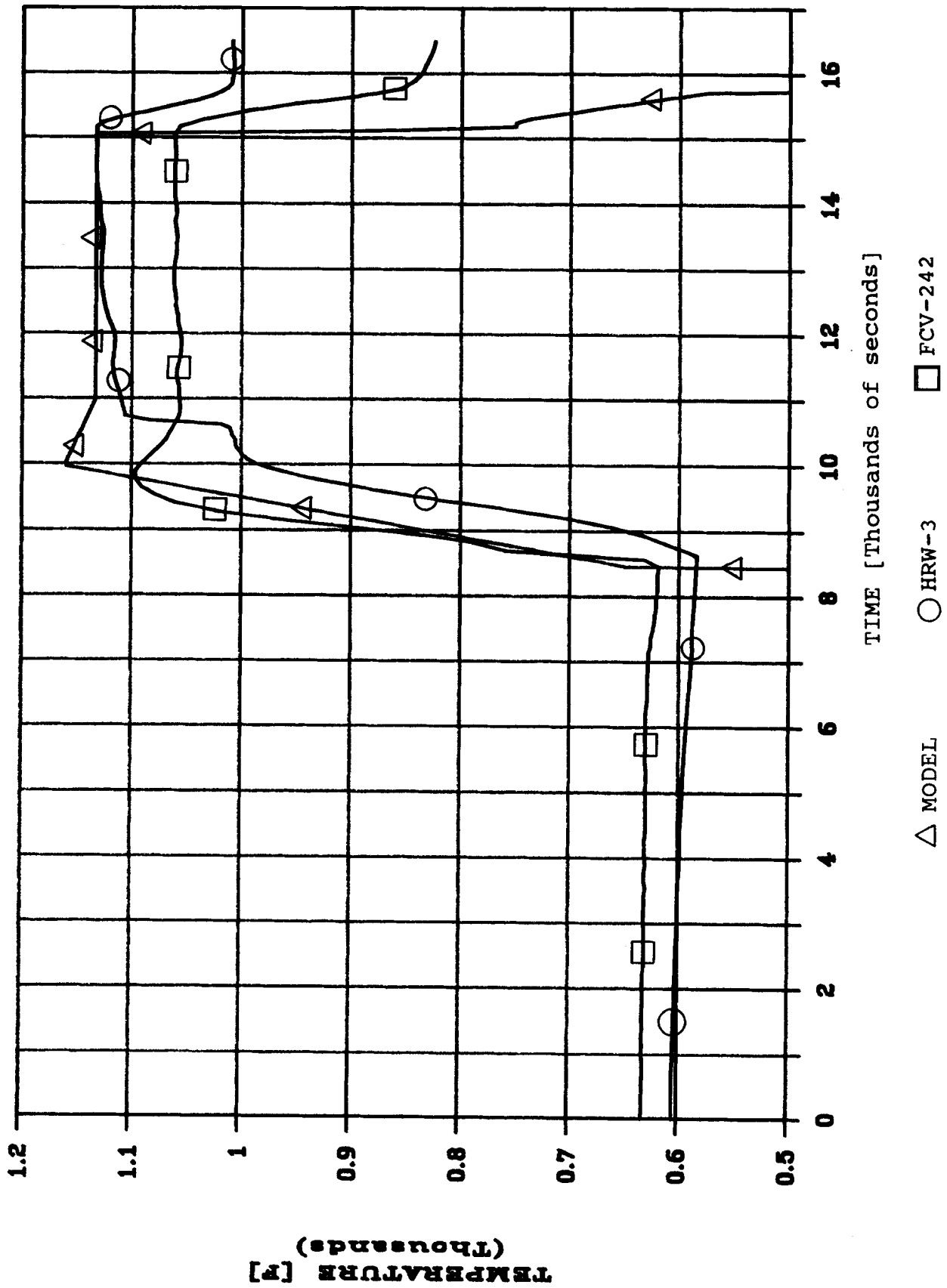
Figure 5-1 Comparison of Estimated Inlet Salt Temperature to the Hot Tank During the Charging Test

45
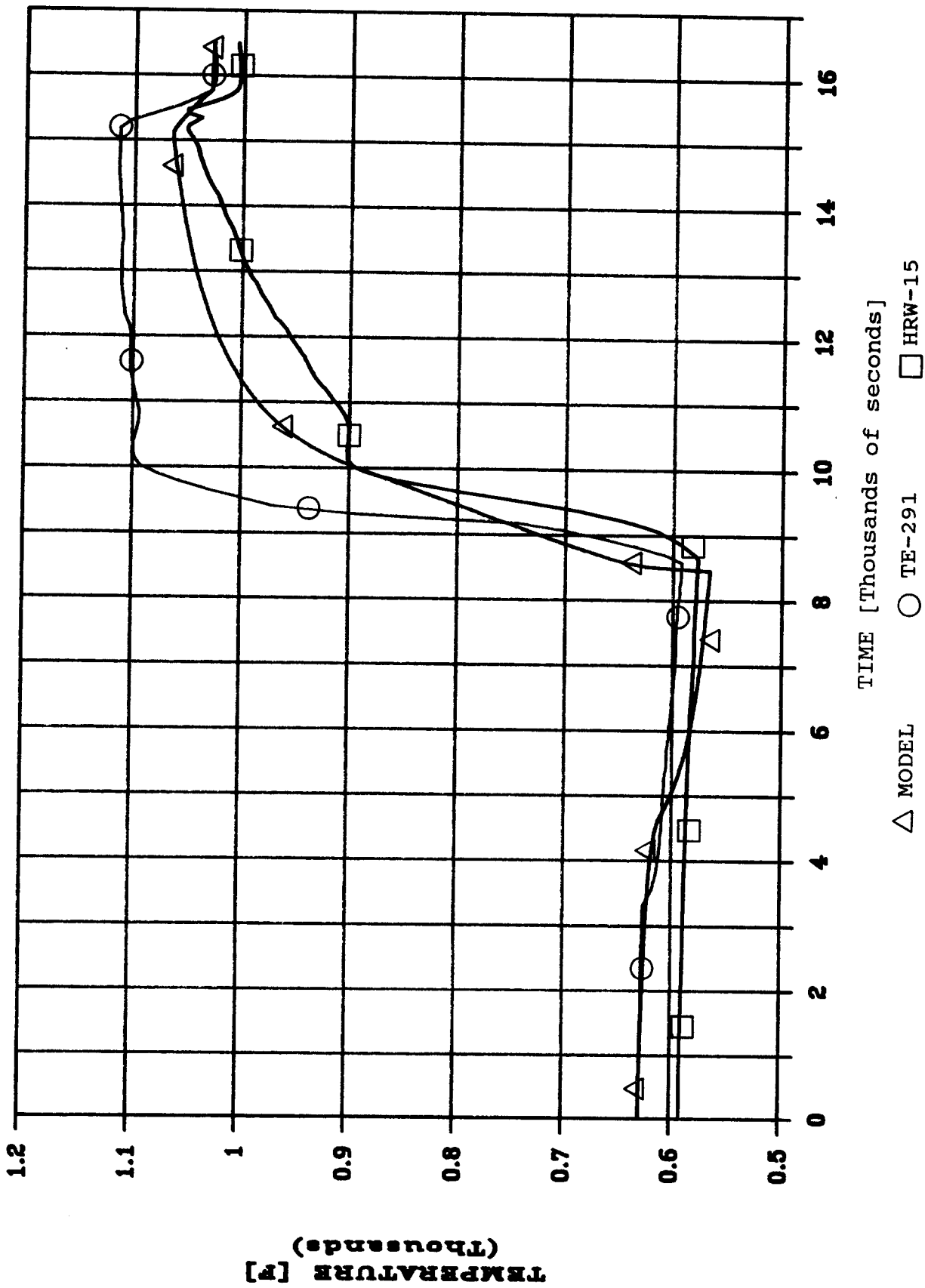
Figure 5-2 Comparison of Salt Temperatures During the Charging Test
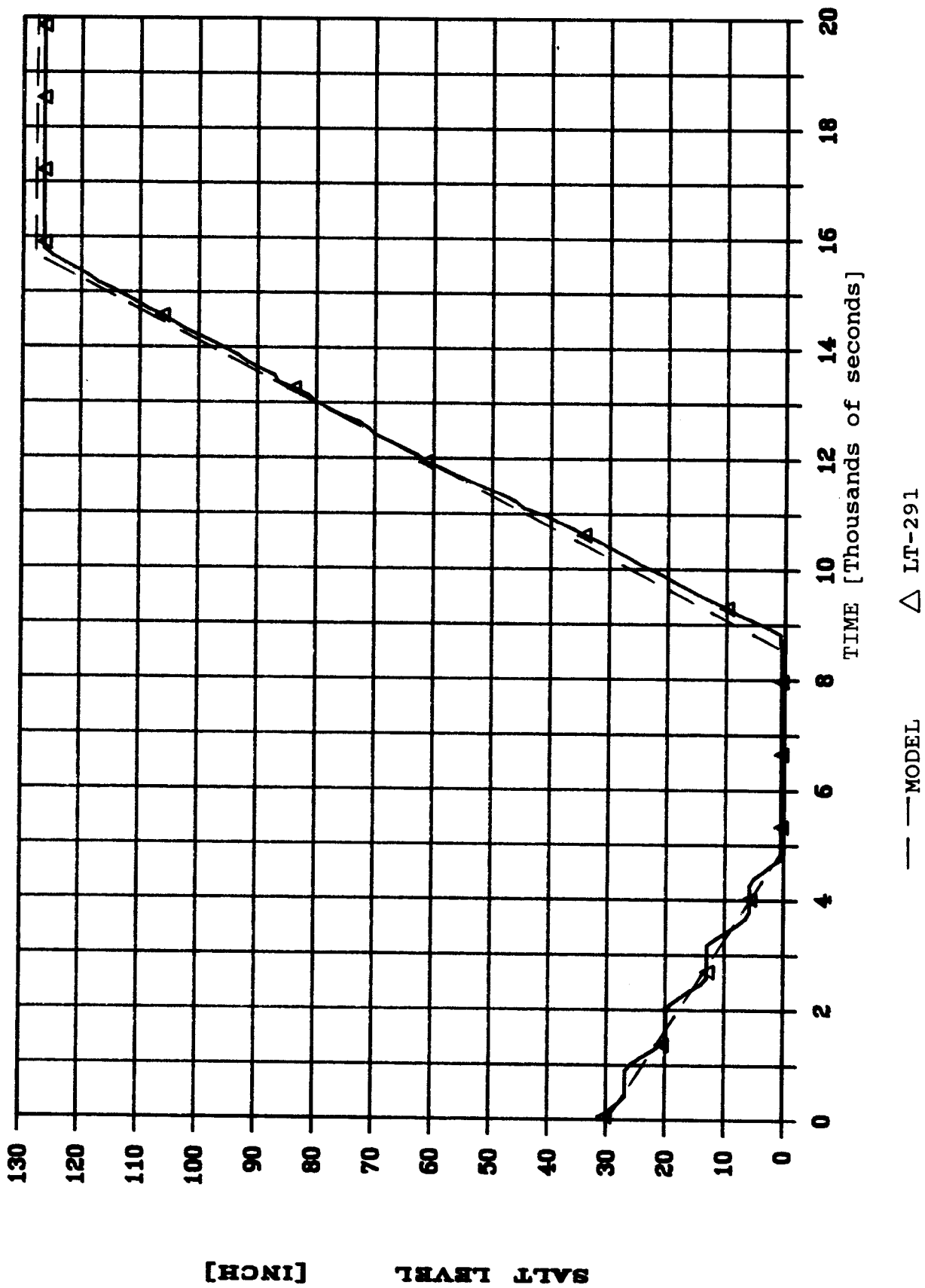
Figure 5-3   Comparison of Hot Tank Salt Levels During the Charging
Test
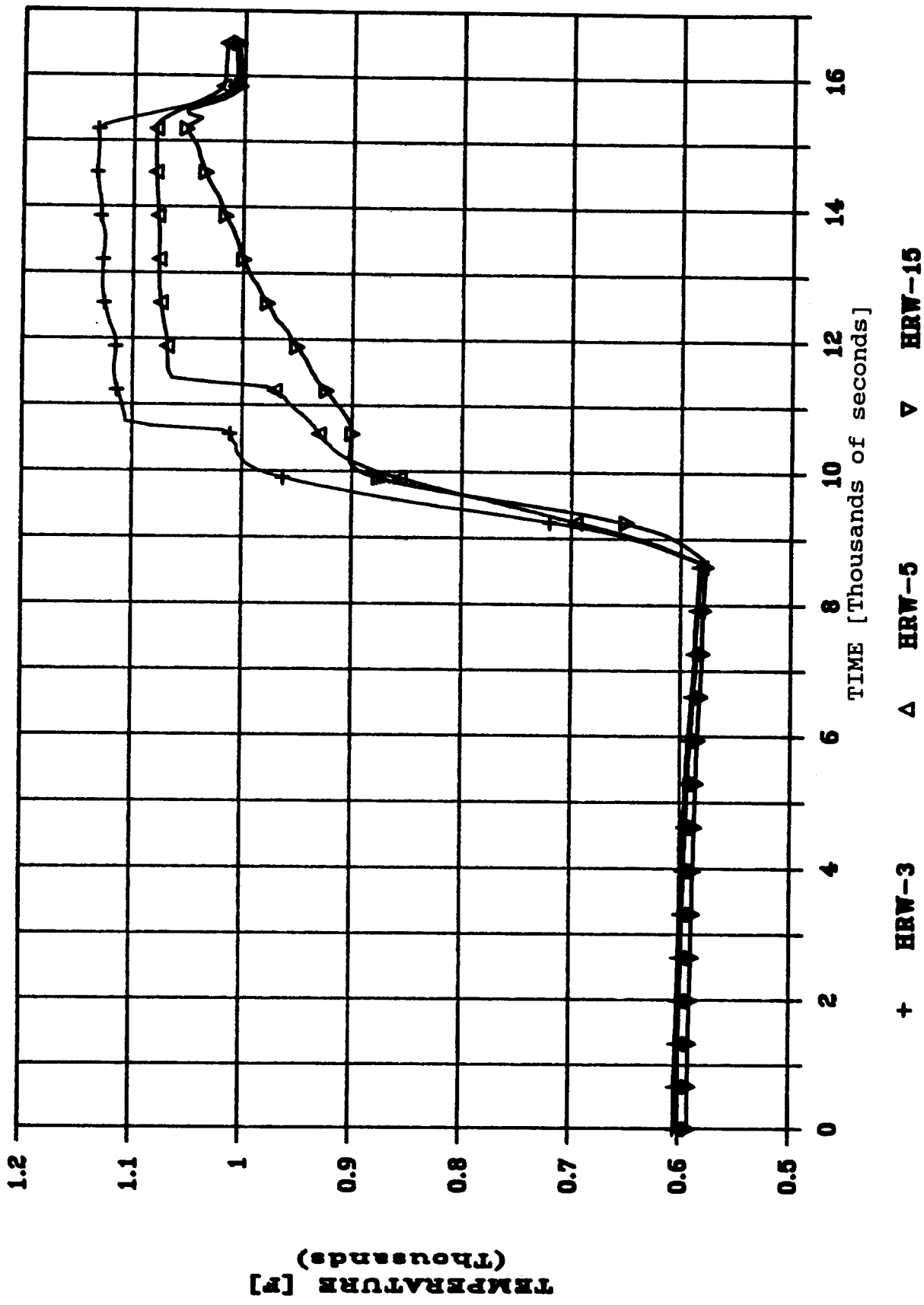
Figure 5-4 Hot Tank Liner Temperatures at Three Locations During the Charging Test
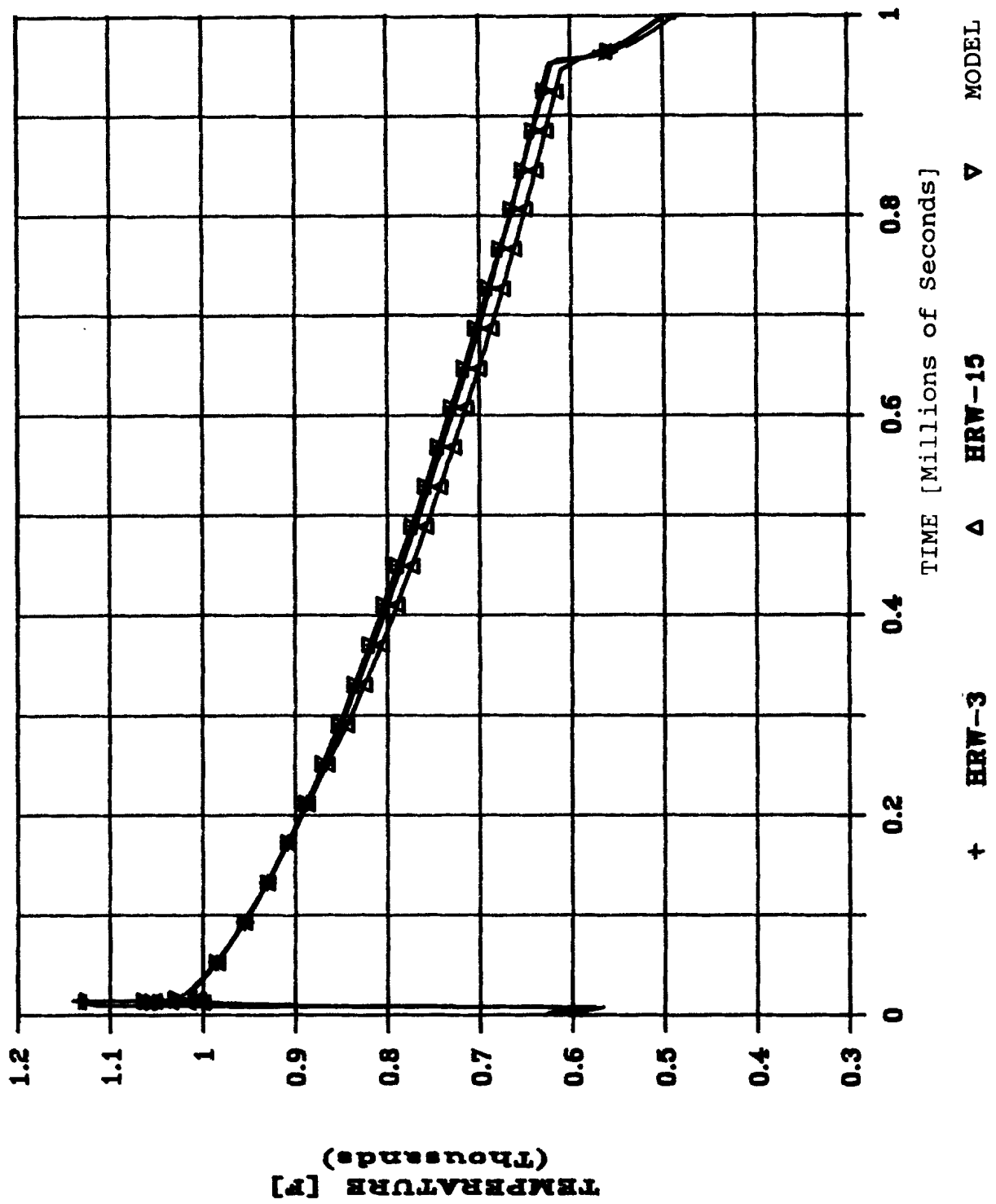
Figure 5-5   Comparison of Salt Temperatures in the Hot Tank During
the Cooling Test Conducted from June 1, 1987 to
June 11, 1987
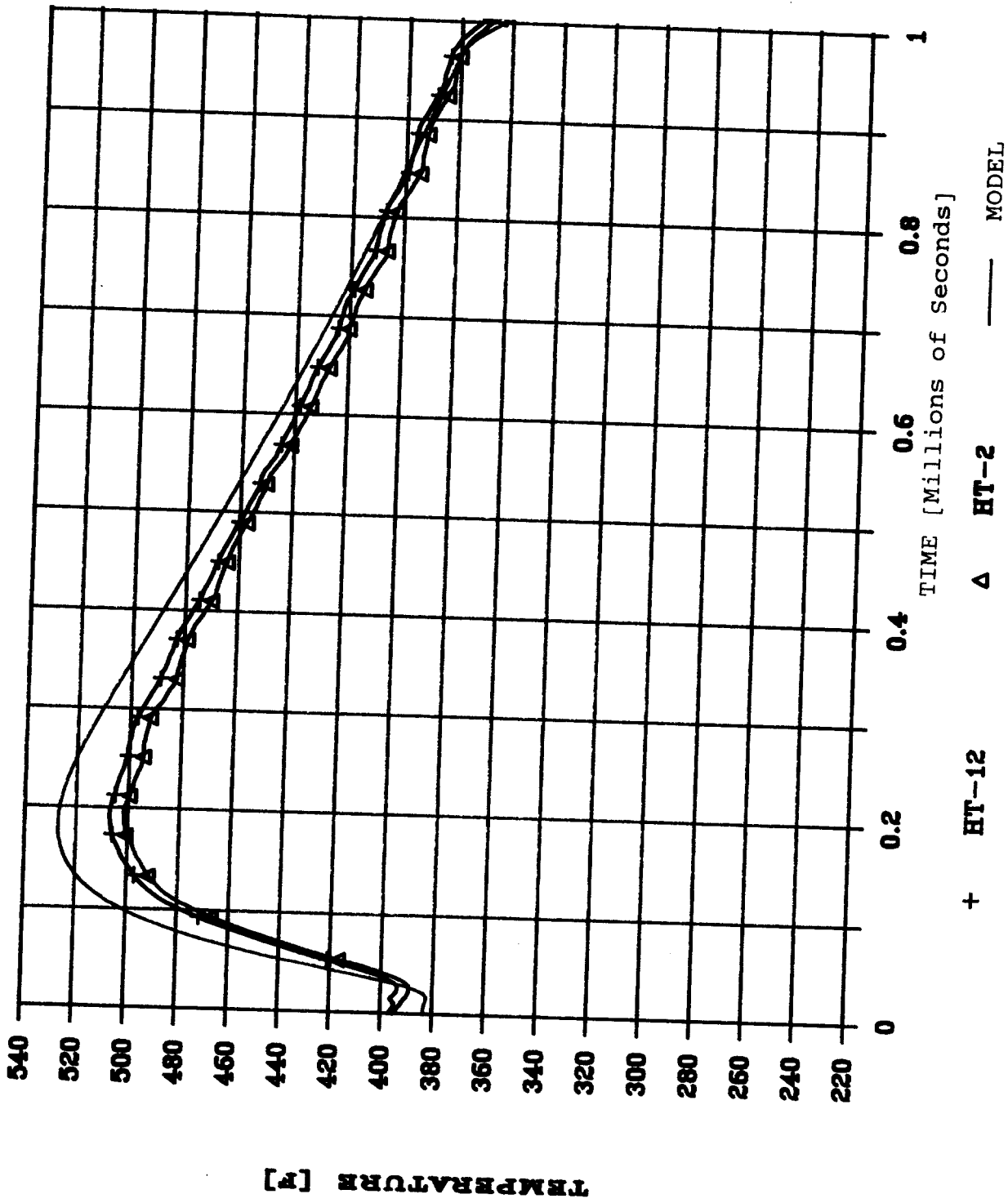
Figure 5-6   Comparison of Temperatures at the Outer Surface of the
Hot Tank Brick Insulator

+   HT-12   Δ   HT-2   ——   MODEL

TIME [Millions of Seconds]
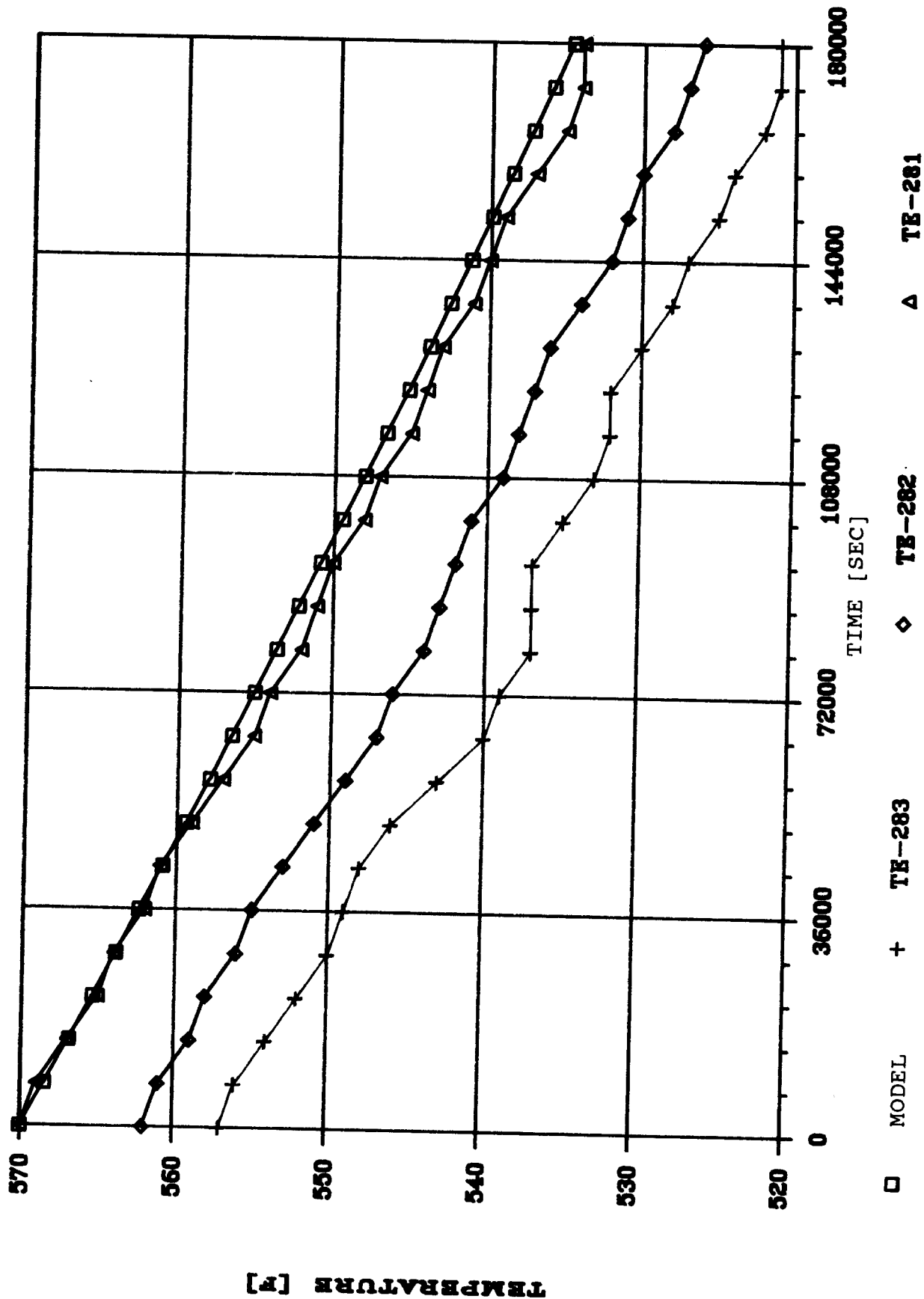
TEMPERATURE [F]

Figure 5-7   Comparison of Salt Temperatures in the Cold Tank During the Cooling Test Conducted from September 27, 1987 to September 29, 1987

□ MODEL   + TB-283   ◇ TB-282   △ TB-281

Table 5-1
Parameters Employed in CRTF Storage System Model

Name	Description	Value
Cb	Specific heat of brick	.24 Btu/lb °F
Ccf	Specific heat of castable	.20 Btu/lb °F
Cs	Specific heat of salt	.365 Btu/lb °F
Kb	Thermal Conductivity of brick wall	.25 Btu/hr ft °F
Kc	Thermal Conductivity of castable	.20 Btu/hr ft °F
Ucwr	Overall heat transfer coefficient between the cold salt and the environment via the walls and roof	.042 Btu/hr ft*2 °F
Uhins	Overall heat transfer coefficient between the outer surface of the hot tank brick wall and the environment	.17 Btu/hr ft*2 °F
Uhr	Overall heat transfer coefficient between the hot salt and the environment via the roof	.066 Btu/hr ft*2 °F
ρ_b	Density of the brick	47. lb/ft**3
ρ_c	Density of the castable	120. lb/ft**3
ρ_s	Density of the salt	(132. − .023T) lb/ft**3

All parameter values are handbook values except those that are underlined. The underlined values were determined from the CRTF storage system experimental results.

Chapter 6

Calculations of Charge and Discharge Cycle Efficiencies for the CRTF Hot Tank

6.1 Overview

In this chapter we use the validated simulation model described in Chapters 3 and 5 to calculate the thermal efficiency of the CRTF hot tank during charge and discharge cycles. The thermal efficiency of the tank is bounded by performing worst case and best case calculations. These type of calculations are of interest to an analyst who wants to compare the thermal efficiency of a wide variety of thermal storage systems. For example, similar calculations have been performed for the Dual Medium Storage System located in Almeria, Spain (7). Oil is the heat carrier in this system, rather than molten salt, and iron plates are used to store the thermal energy.

The thermal efficiency of the CRTF hot tank during the charging phase (EFFc) can be defined as:

$$EFFc = \frac{Ecin - Elc}{Ecin} , \qquad (6-1)$$

where

Ecin = the energy contained within the salt that entered the hot tank during the charging phase,
Elc = the energy lost from the salt to the tank materials and to the environment during the charging phase.

The efficiency during the discharge phase (EFFd) can be defined as:

$$EFFd = \frac{Eh - Eld}{Eh} = \frac{Edout}{Eh} \qquad (6-2)$$

where

Eh = the energy contained within the hot tank's salt immediately prior to discharge of the tank
Eld = the energy lost from the salt to the tank materials and to the environment during the discharging phase,
Edout = the salt energy pumped out of storage during the discharging phase.

The efficiency of the total charge/discharge cycle (EFFtot) for the hot salt storage tank can be expressed as:

$$EFFtot = \frac{Edout}{Ecin + Eo} , \qquad (6-3)$$

where

Eo = energy contained within the hot tank salt prior to start of
     charging phase,
Ecin, Edout = defined previously.

6.2 Worst-Case Calculation of Charge and Discharge Cycle
     Efficiency

In the worst-case calculation, we assume the tank is at the
lowest operating temperature allowed by procedures prior to the
start of the tank charge; i.e., the salt in the tank is at 600
°F just before the start of the charging cycle, and the brick
walls and floor have cooled and are experiencing equilibrium
heat transfer with the salt. This assumption will cause the
maximum amount of heat loss from the salt during the charge and
discharge cycle.

The following assumptions were made:

- the tank was empty just prior to charging;
- the tank was in thermal equilibrium before charging;
- the interior tank temperature was 600 °F before charging;
- the salt inlet temperature was held constant at 1050 °F during
  charging;
- the salt inlet mass flow was held constant at 12.33 lb/s
  during charging;
- the charging ended when the level in the tank reached 128
  inches;
- no discharging occurred while charging or vice versa;
- discharging occurred immediately after charging; and
- the salt outlet mass flow was held constant at 12.33 lb/s
  during discharging.

The efficiency during the charging phase is depicted in Figure
6-1. Equation 6-1 was used to generate the curve. The
efficiency dropped initially and increased slowly to a final
value of 0.968. The drop resulted from the large temperature
gradient between the salt and the brick insulator during the
early period of the charging phase; a large temperature drop
implies relatively higher energy losses and thus a lower
efficiency. Later, as the temperature of the brick increased,
the temperature gradient lessened. This caused relatively lower
energy losses and thus a higher efficiency.

The efficiency during the discharging phase, as well as the
total cycle efficiency, are displayed in Figure 6-2. Equations
(6-2) and (6-3) were used to generate these curves.

Depicted in Figure 6-3 is the time-dependent energy contained
within the hot tank, as well as the total energy entering and
leaving the tank during the entire charge and discharge cycle.
At the completion of the charging phase (t=15700 seconds) the
energy input remained constant because no further salt entered
the tank. At this point it can be seen that the total energy

54

contained within the tank was less than the total energy that entered. The difference can be attributed to the energy lost to the tank insulator materials and the environment during the charging phase. Insertion of the energy values at t=15700 seconds into Equation (6-1) yields the same charging efficiency (i.e., 0.968) described in the previous paragraph. At the end of the discharge phase (t=23000 seconds) the total energy that exited the tank was less than the total energy entering. The difference can be attributed to the energy lost to the tank insulator materials and the environment during the entire charge and discharge cycle. Insertion of these final energy values into Equation (6-3) yields a total charge/discharge efficiency of 0.93. This is the same value displayed in Figure 6-2 at t=23000 seconds.

6.3   Best-Case Calculation of Charge and Discharge Cycle Efficiency

In the best-case calculation, we assume the tank is at the highest operating temperature allowed by procedures prior to the start of the tank charge; i.e., the salt in the tank is at 1050 °F just before the start of the charging cycle and the temperature of the brick walls and floor are at their highest values and are experiencing equilibrium heat transfer with the salt. This assumption will cause the minimum amount of heat loss from the salt during the charge and discharge cycle.

The assumptions made in this calculation were the same as listed in the previous section except for the initial starting temperature. This calculation resulted in a total charge and discharge cycle efficiency of 0.967.
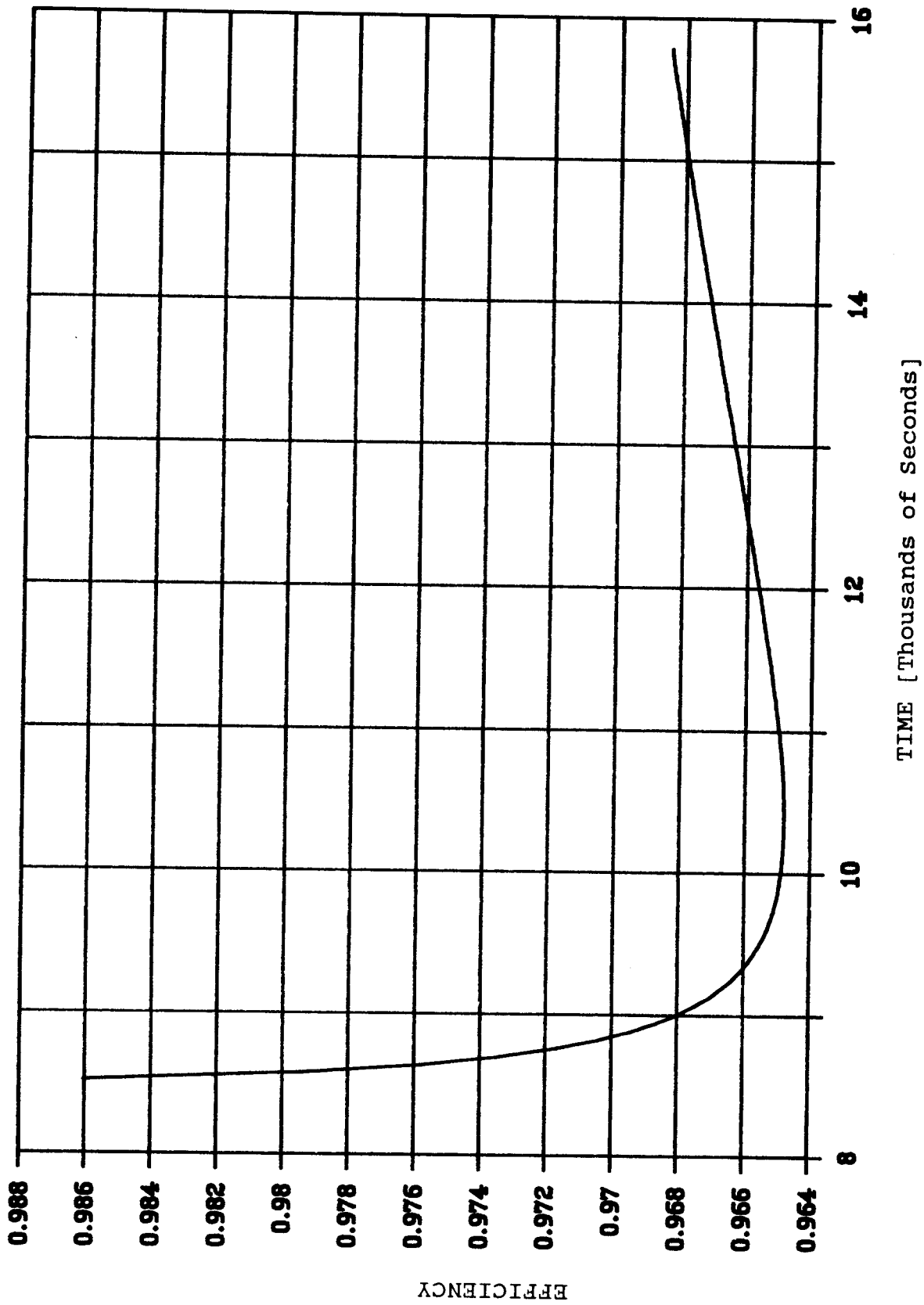
Figure 6-1   Calculated Efficiency of the CRTF Hot Tank During
the Charging Phase
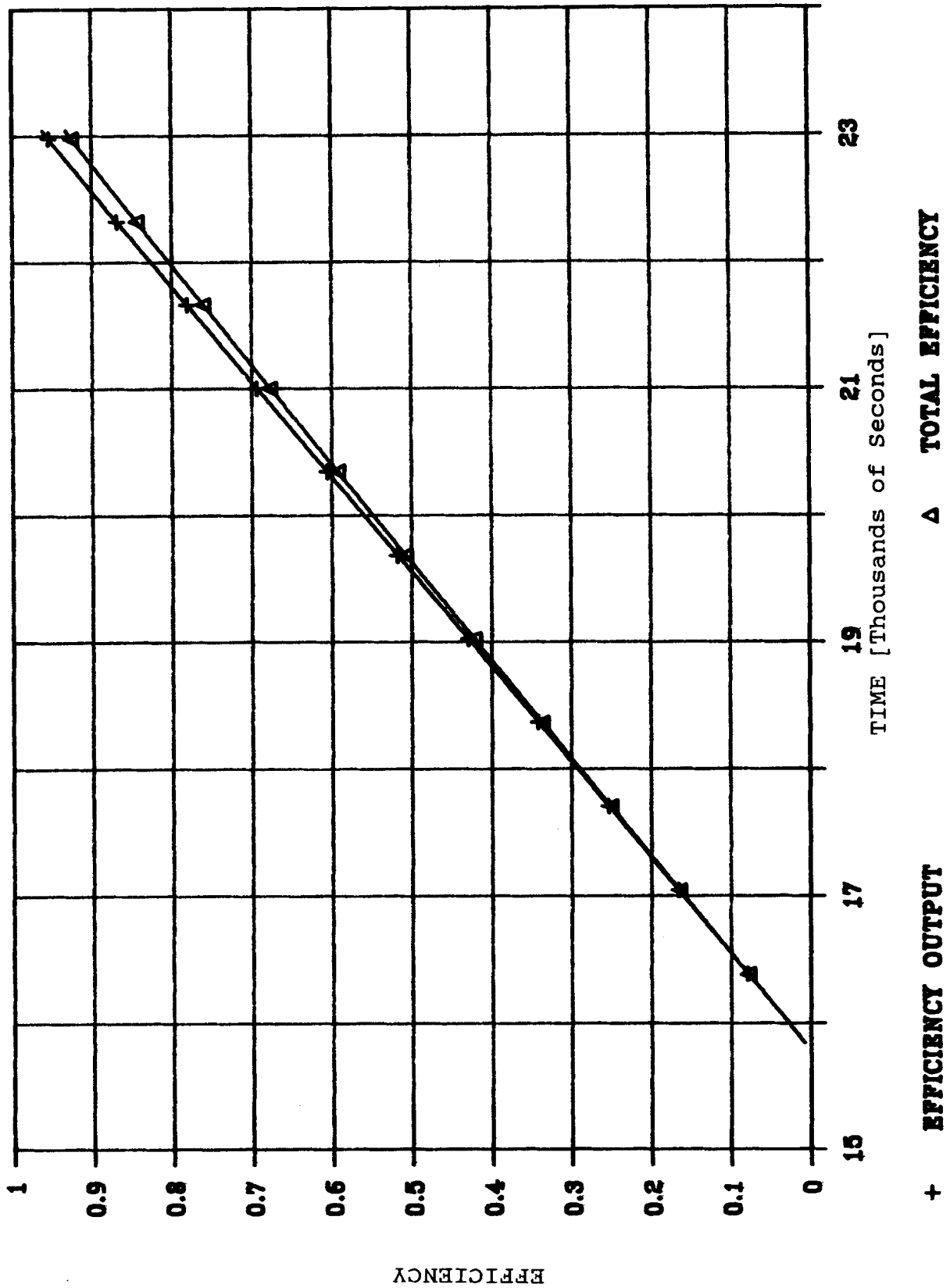
Figure 6-2   Calculated Efficiency of the CRTF Hot Tank During
the Discharge Phase as well as the Total Charge/Discharge
Cycle Efficiency

KWh
(Thousands)

TIME [Thousands of Seconds]
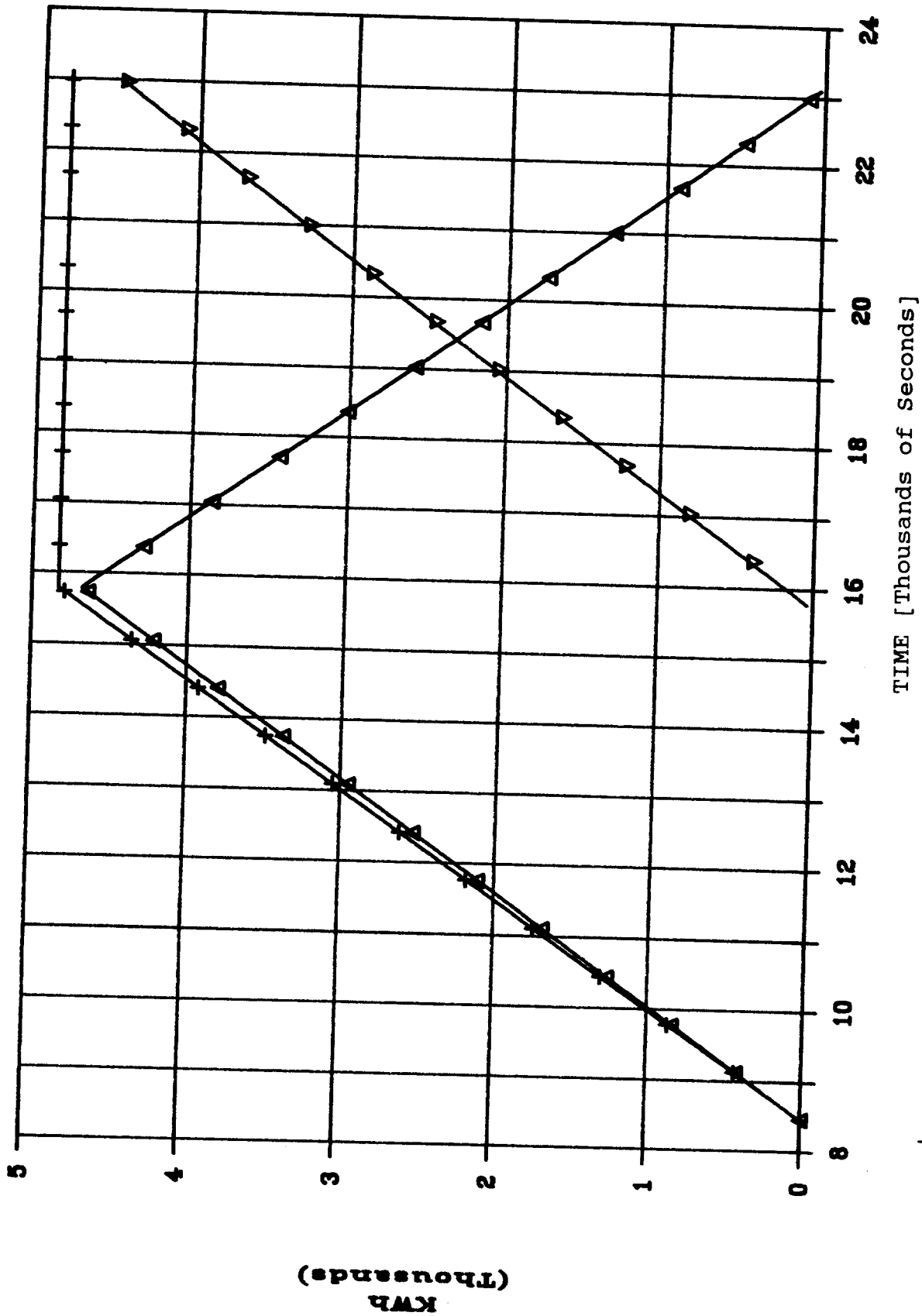
+ TOTAL ENERGY ENTERING HOT TANK DURING CHARGING PHASE
△ TOTAL ENERGY CONTAINED IN THE HOT TANK SALT
▽ TOTAL ENERGY EXITING HOT TANK DURING DISCHARGING PHASE

Figure 6-3   Calculated Energy Flows During a Charge/Discharge
Cycle of the CRTF Hot Tank

58

Chapter 7

Comparison of the CRTF Thermal Storage System
With European Molten Salt Thermal Storage Systems

7.1 Overview

A cost-effective thermal storage system should possess the
following qualities:

1) the storage medium should have a high thermal storage
   capacity per unit volume,
2) the thermal losses from the system should be minimal, and
3) system costs should be low.

Salt storage systems are believed to possess these qualities.
Three salt storage systems have been used at solar plants:

1) Central Receiver Test Facility (United States)
2) CESA-1 (Spain)
3) Themis (France)

The designs and thermal performance of these three systems are
compared in Section 7.2.

7.2 Comparison of the Themis and CESA-1 Storage Systems with
     the CRTF Storage System

Design and Operation of the CESA-1 and Themis Storage Systems

Figure 7-1 is a simplified process diagram of the CESA-1
receiver and salt storage systems. Superheated steam produced
by the receiver heats up molten salt in the desuperheater,
condenser, and overcooler heat exchangers. The temperature of
the salt is increased from 428 °F to 644 °F. The maximum
storage capacity of the hot salt tank is 16 MWh. The heat
energy can be used to produce steam by pumping hot salt through
the overheater and evaporator heat exchangers.

Figure 7-2 is a simplified process diagram of the Themis
receiver and salt storage systems. Salt from the cold storage
tank is pumped through the receiver, heated up, and stored in
the hot storage tank. The temperature of the salt is increased
from 392 °F to 482 °F. The maximum storage capacity of the hot
tank is 40 MWh. The heat energy is used for steam generation.

Detailed descriptions of the CESA-1 and Themis systems can be
found in Andujar and Rosa (5) and in Etievant et al. (6),
respectively.

Design and Operation of the CRTF Storage System

The design and operation of the CRTF storage system are

described in Chapter 2.

Results of the Comparative Investigations

The salt data and the design points of the three solar plants
are summarized in Table 7-1. The first row lists the
composition of the salt. While CESA-1 and Themis use a mixture
of sodium and potassium nitrates and nitrites (HiTec) as
coolant, the CRTF plant uses a salt consisting of 40 percent
KNO_3 and 60 percent $NaNO_3$.

The operating temperatures and thermal storage capacities of the
three systems are different. Themis has the highest heat
storage capacity and operates at the lowest temperature. Due to
these differences, a direct comparison is difficult.

The hot tanks of all three systems were subjected to cooling
tests; the tanks were filled with hot salt, all pumps were shut
down, and the tanks were allowed to cool down over a period of
one to several days. Tank losses were estimated by measuring
the slope (dT/dt) of the salt temperature's decay at the
evaluation temperature and inserting this value into the
following equation:

$$Q_{loss} = (m*c_p*dT/dt)_{salt}. \qquad (7-1)$$

The overall heat-transfer coefficients, also known as U-values,
were then estimated by the following equation:

$$U = \frac{Q_{loss}}{A*(T_{salt} - T_{ambient})}. \qquad (7-2)$$

Cylindrical geometries were assumed for all three tanks when
calculating the heat-transfer surface area (A).

CESA-1 Cooling Tests

Two cooling tests were performed at CESA-1 on December 21-22,
1986, and June 6-7, 1987. The hot tank's salt-temperature
decays for these two tests are displayed in Figure 7-3. The
cooling down rate was 5.4 - 10.8 °F/day during the June test and
reached 7.2 - 14.4 °F/day during the December test. Since both
tests were performed with an equal salt mass (approximately
518,000 pounds), the higher cool-down rate during the December
test can be attributed to the higher salt temperature, i.e., the
initial salt temperature of the December test was 294 °C (561
°F) and the initial temperature of the June test was 260 °C (500
°F). It can be noted that a temperature gradient of
approximately 12 °C (22 °F) existed within the salt. The
gradient was apparently caused by flaws in the insulator
materials at various tank elevations (these flaws were called
"temperature bridges" in Andujar and Rosa, 5).

Themis Cooling Tests

On November 16, 1984, and January 11, 1985, two cooling tests were performed at Themis. The salt temperatures versus time are shown in Figures 7-4 and 7-5, respectively. The November test had a start temperature of 328 °C (622 °F) and the January test had a start temperature of 305 °C (581 °F). The cooling down rates were 10.5 °F per day and 66.1 °F per day, respectively. The January test had a low salt level (approximately 34,500 pounds); this explains the high cool-down rate. During the November test the tank was filled with 628,000 pounds of salt. It can be noted that the Themis November test and the CESA-1 tests show similar cooldown rates.

CRTF Cooling Tests

The results of the cooling tests at the CRTF are described in Section 4.1 and 4.3. The reader should refer to these sections for a detailed discussion of the test results.

Comparison of the CESA-1, Themis, and CRTF Cooling Test Results

Table 7-2 summarizes the measured data collected during the cooling tests for all three hot storage tanks. Row one shows the amount of salt mass during the cooling tests. These quantities fill the tanks to the levels indicated in row two. The specific heat is listed in row three and assumed to be independent of the salt's temperature. The size of each of the three hot tanks was considerably different, evident by comparing surface areas listed in row four. A wide range of cooling rates is displayed in row five. The highest cooling rate was reached during the test held at Themis during January; the lowest was reached at CESA-1 during the December test. Cooling rates for a particular tank are constantly decreasing as the tank cools down. The cooling rates listed in the fifth row were measured at the salt temperature listed in the sixth row. Available data did not allow us to compare the measured cooling rates of the three tanks at the same temperature.

Depicted in row seven are the overall heat-transfer coefficients (U-values) calculated with Equation (7-2). This parameter represents the thermal conductance of the tank's insulation materials and is the parameter one should use to compare the thermal performance of the three hot tanks. The Themis tank generally exhibited the best thermal performance (i.e., lowest thermal conductance) during tests in which the tanks were greater than 50% full.

The U-values calculated for the two CESA-1 tests were approximately the same; the variation is believed to be within the experimental uncertainty. The values listed in the table also compare favorably with values calculated by the Spanish experimental team [U-values in the range of 0.30 to 0.36 $W/(m^2$ °C) (0.053 to 0.063 Btu/(hr ft^2 °F)) were calculated in Andujar and Rosa (5)].

By comparing the CRTF and Themis U-values it can be noted that there appears to be a dependence between the U-value and the level of salt in the tank. For both CRTF and Themis the U-values decrease at very low tank levels. The thermal performance of these tanks therefore improves at very low levels. The reason for this dependence is not completely understood but a plausible explanation is the following:

At very low levels in the tanks a large air gap exists between the surface of the salt and the tank ceiling. This air gap acts as an additional thermal resistance to heat flow between the salt and the upper portions of the tank. This additional resistance therefore decreases the thermal conductance (U-value) of the tank.

We did not have experimental data for the CESA-1 tank at a low level and were therefore not able to determine if a dependence existed between U-value and tank level. However, a statement was made in Andujar and Rosa (5) that suggests the opposite dependence exists, i.e., the U-value appears to increase at low level. The explanation given was that known temperature bridges (i.e., tank supports) in the bottom portion of the tank decrease the average thermal resistance of the tank when the salt level is low.
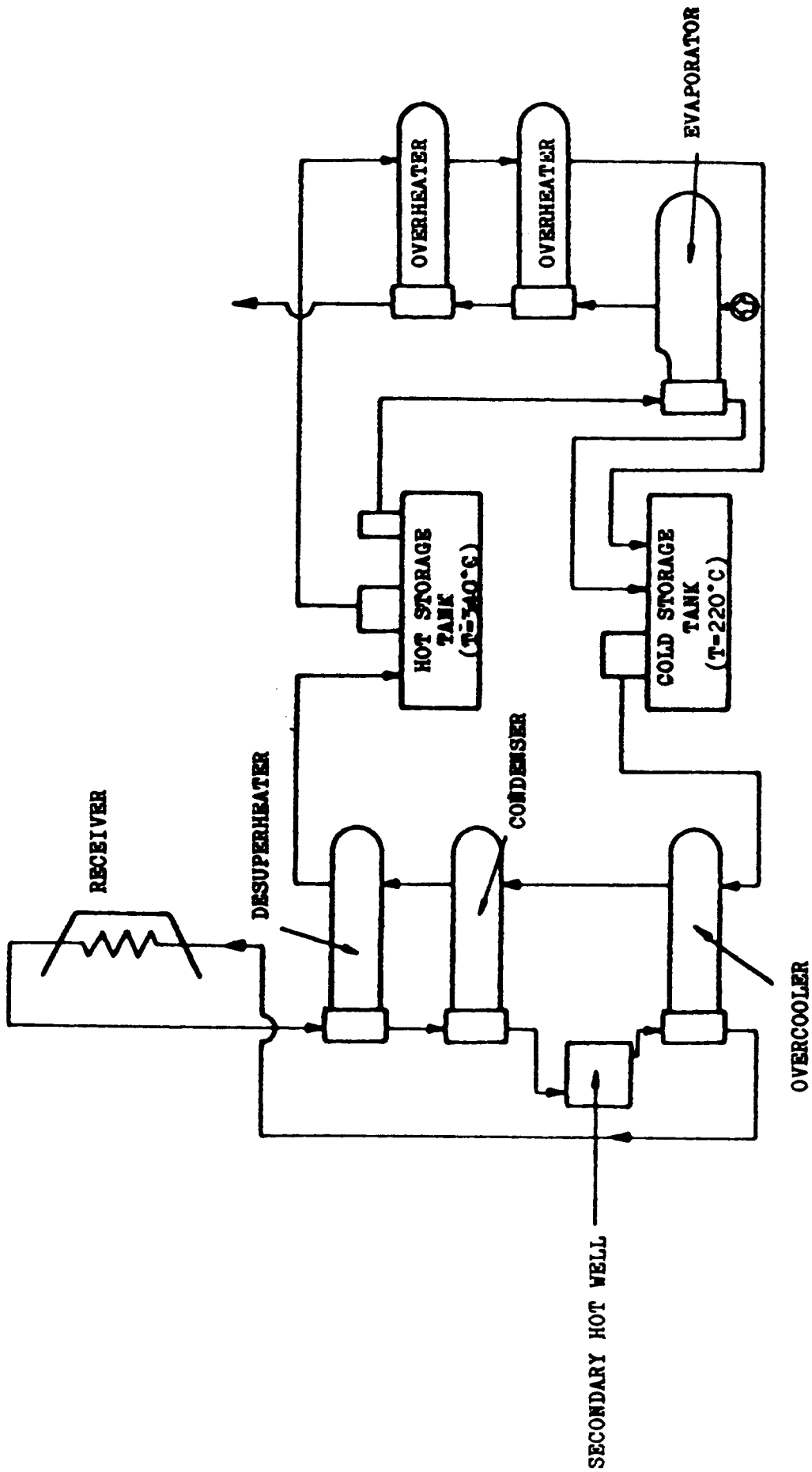
Figure 7-1 Simplified Process Diagram of the CESA-1 Molten
Salt Storage System

63
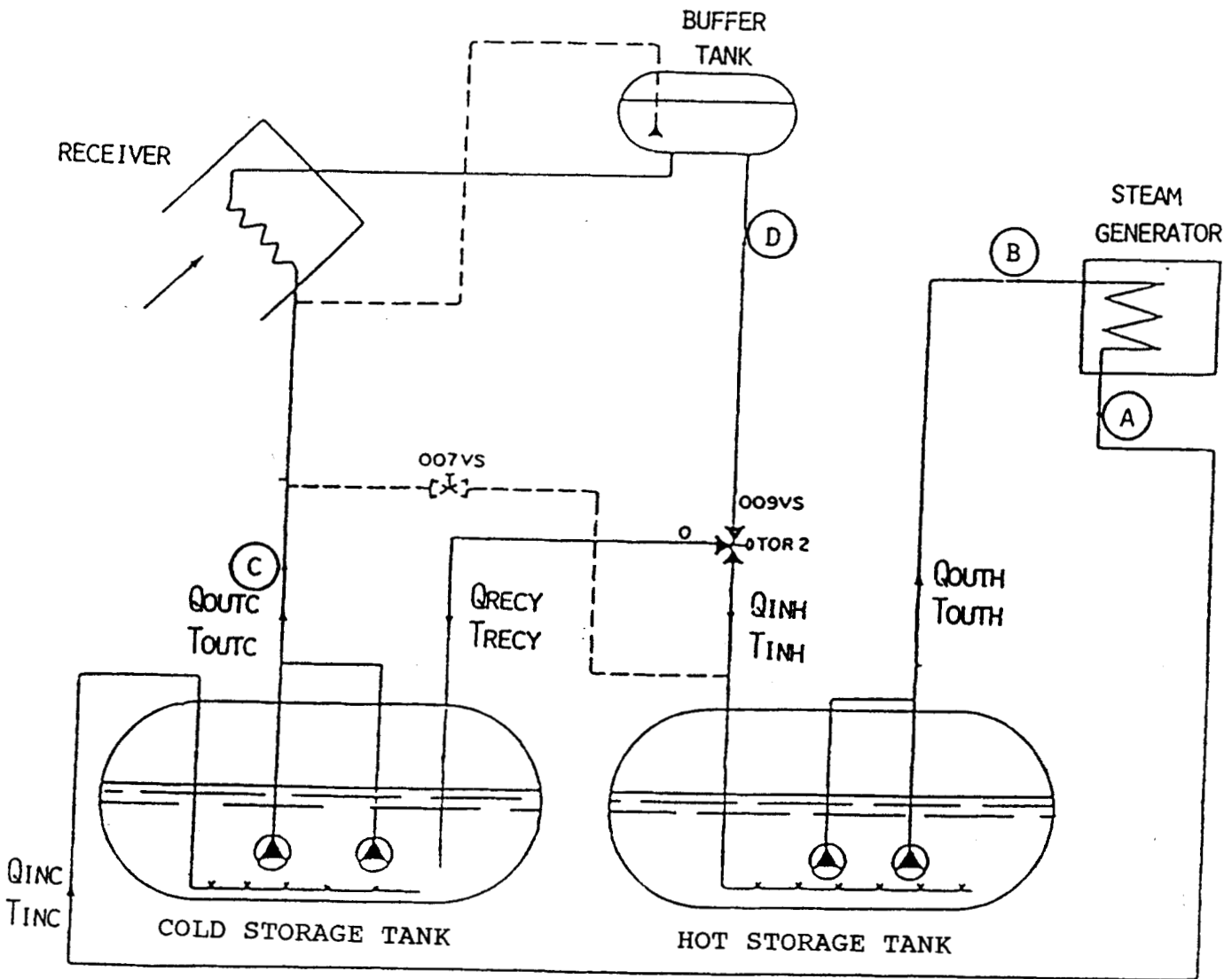
Figure 7-2   Simplified Process Diagram of the Themis Molten
              Salt Storage System
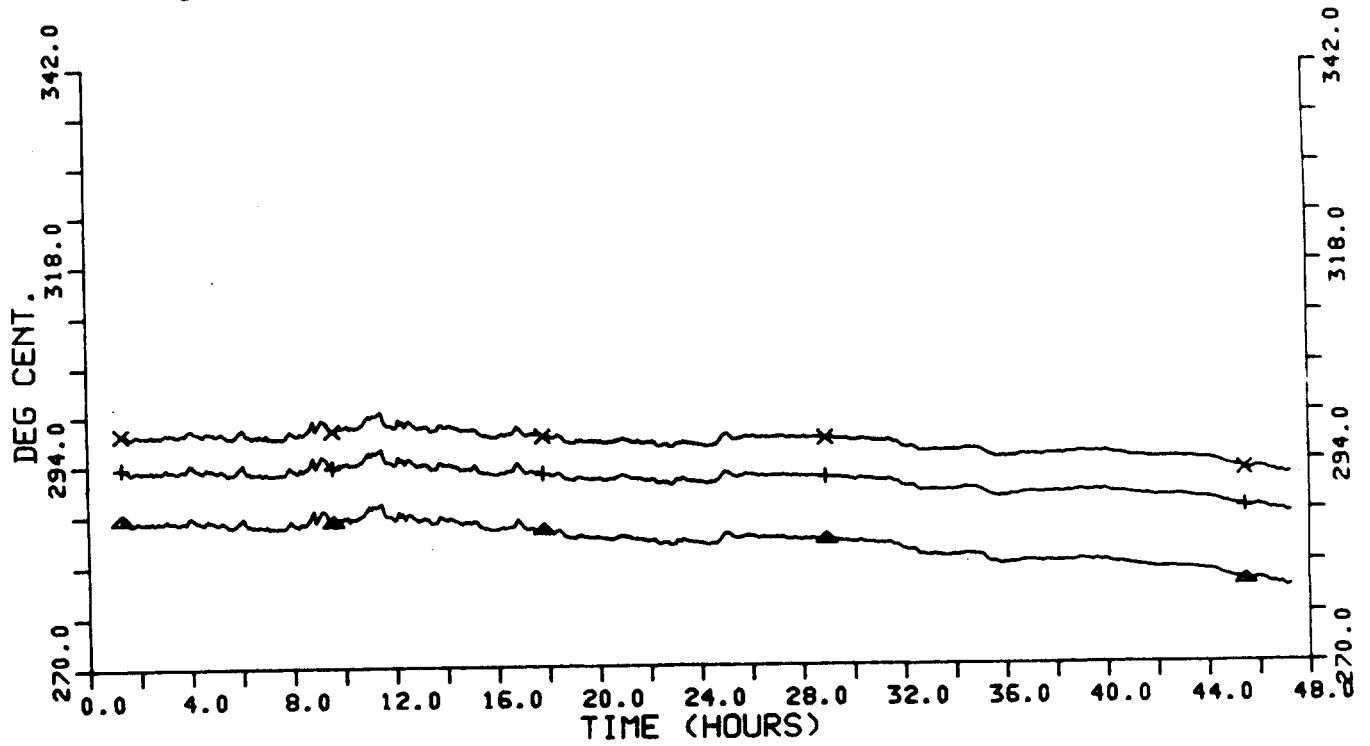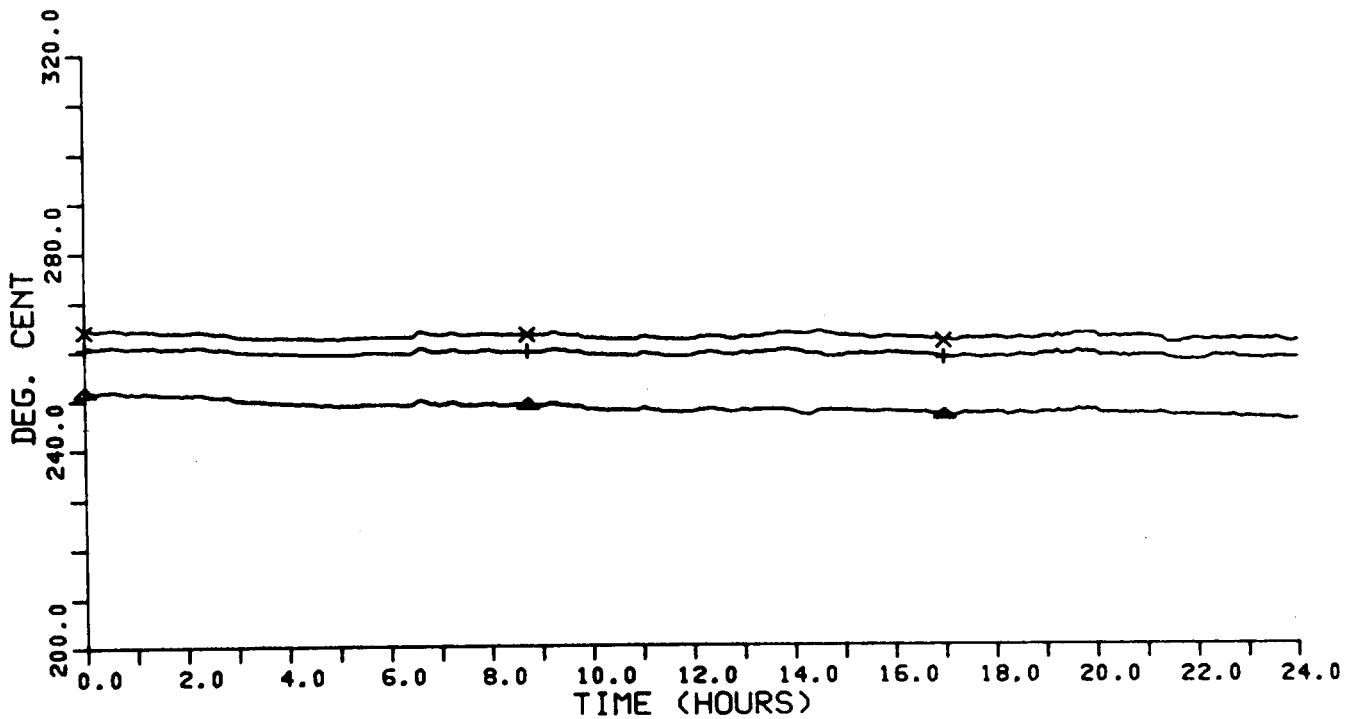
Figure **7-3** Hot Tank Cooling Data Collected From CESA-1 Tests

65
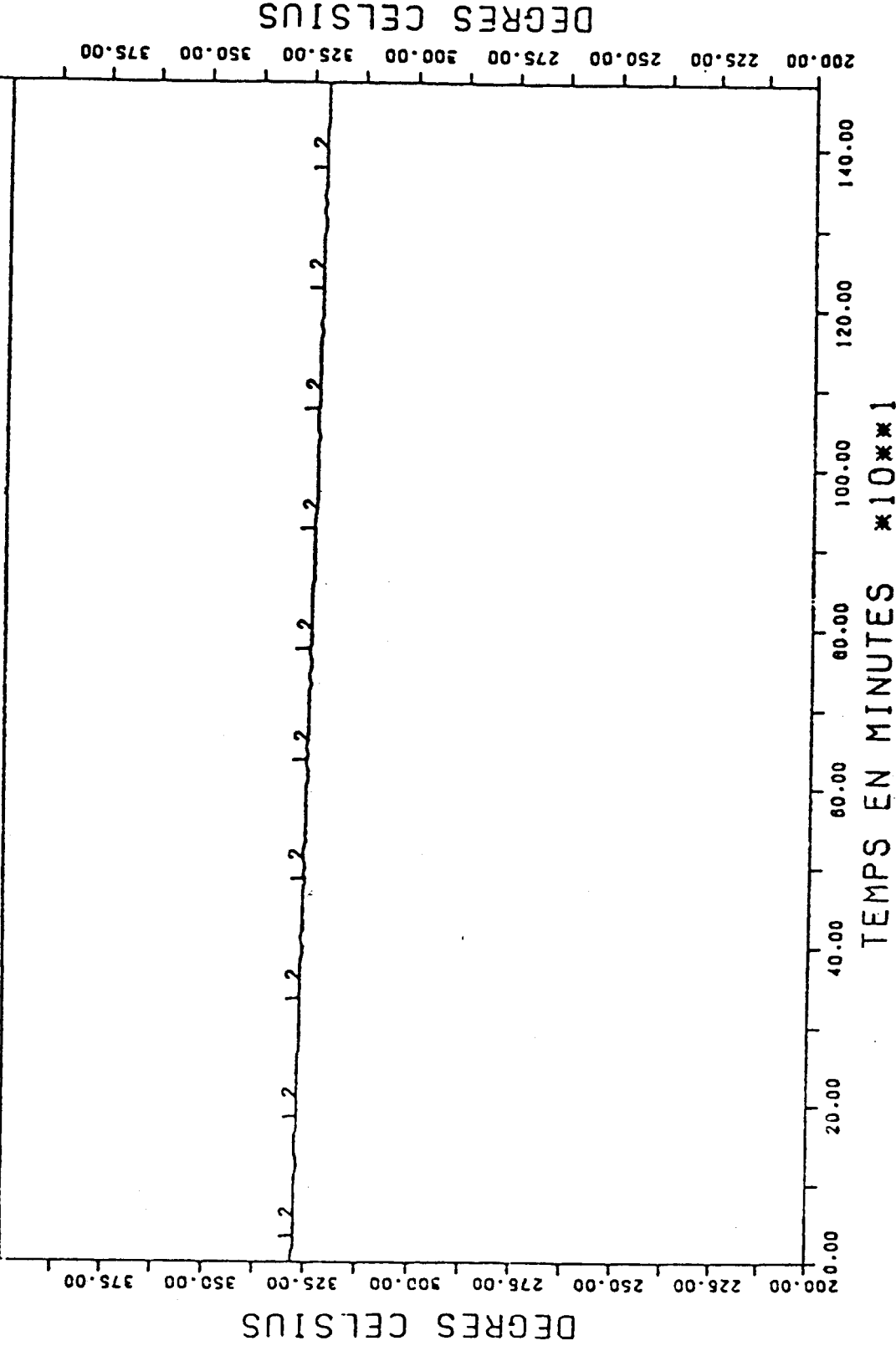
Figure 7-4 Hot Tank Cooling Data Collected From Themis Test
Conducted on November 16, 1984
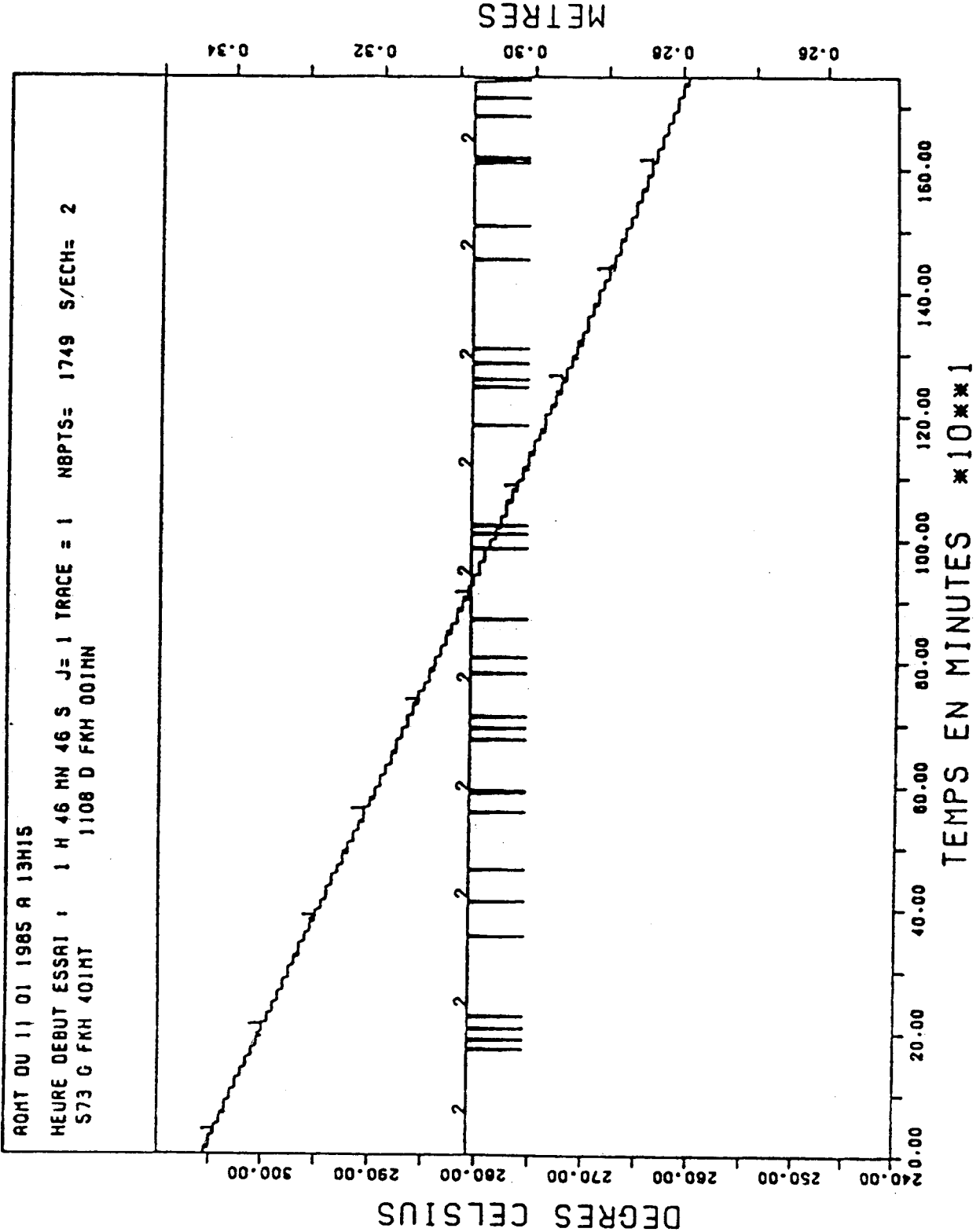
Figure 7-5 Hot Tank Cooling Data Collected From Themis Test Conducted on January 11, 1985

Table 7-1
Comparison of Design Parameters
for Three Molten Salt Thermal Storage Systems

	CRTF	CESA-1	Themis
Salt Composition	40% KNO_3, 60% $NaNO_3$	7% $NaNO_3$, 40% $NaNO_2$ 53% KNO_3	7% $NaNO_3$, 40% $NaNO_2$ 53% KNO_3
Melting Point (°F)	430.	294.	294.
Density (lb/ft^3) (T in °F)	132 − 0.0232T	128 − 0.01097T	128 − 0.01097T
Specific Heat Btu/(lb °F)	0.365	0.373	0.373
Maximum Salt Temperature (°F)	1200.	850.	850.
Storage Capacity (MWhrs)	7.1	16.	40.1
Low Reference Temperature (°F)	550.	428.	392.
Charging Temperature (°F)	1050.	644.	482.
Maximum Salt Mass in Hot Tank (lb)	117,000	518,000	1,018,000

Table 7-2

Summary of Salt Storage System Test Data

	CRTF 5/28/87	CRTF 6/1/87	CESA-1 12/21/86	CESA-1 6/6/87	Themis 11/16/84	Themis 1/11/85
Salt Mass (lb)	23700.	97900.	518000.	518000.	566000.	31000.
Percent Full (%)	20.	83.	100.	100.	56.	3.
Heat Transfer Area (ft^2)	815.	815.	2434.	2434.	3285.	3285.
Cooling Rate (°F/day)	60.2	25.2	10.8	8.1	10.5	66.1
Start Temperature (°F)	670.	670.	561.	500.	622.	581.
U Value $\frac{Btu}{hr\ ft^2\ °F}$	0.044	0.077	0.062	0.070	0.051	0.019
(W/m^2 °C)	0.25	0.44	0.35	0.40	0.29	0.11

Chapter 8

Annual Performance Calculation for a
Commercial-Scale Molten Salt Thermal Storage System

8.1 Introduction

The CRTF 7-MWht storage system is a prototype for a proposed
commercial-scale system rated at 1200 MWht. In this chapter we
extend the validated CRTF model described in Chapters 3 and 5 to
allow simulation of the commercial-scale system. Rather than
simulate system performance during a single charge and discharge
cycle, as was done in Chapter 6, we have extended the
calculations to cover an entire calendar year. The reason we
performed an annual simulation was to gain additional insights
regarding system operation and performance that could not be
obtained from performance calculations for a single
charge/discharge cycle. In particular, we were interested in
answering the following questions:

1) What is the annual efficiency for a proposed commercial
    scale storage system?
2) How much energy from auxiliary heating is required to
    prevent salt freezing during the year?
3) Can an operating strategy be developed that minimizes the
    dependency on auxiliary heating?

The importance of obtaining answers to these questions is
discussed in the following paragraphs.

The Department of Energy has established an annual efficiency
goal of 99% for central receiver thermal storage systems (2).
The answer to the first question will indicate whether the
proposed commercial-scale system can achieve that goal.

An annual efficiency estimate is also important to economic
analyses aimed at determining the most cost-effective storage
system design. Heat losses from the storage system result in
less annual energy produced by the turbine/generator and thus
less revenue. The most cost-effective design would be chosen by
a trade study that compared the cost of reducing heat loss
versus the additional revenue generated by the
turbine/generator. Obtaining answers to the first two questions
will aid in performing a trade study. (In the analysis
presented here, we assumed the storage system will be coupled
with a turbine-generator to produce electricity. It is
recognized that storage could also be coupled with other,
non-electrical, heat loads. Given this arrangement, the trade
study would compare the cost of reducing the heat loss versus
the additional revenue saved by not burning additional fossil
fuels.)

Current conceptual designs for commercial molten salt thermal
storage systems employ electrical trace heating to protect
against salt freezing but electrical trace heating at the CRTF

is expensive and unreliable. Answers to the second and third questions listed above will help us determine whether a plant can reduce its dependence on trace heating or other methods of preventing freezing.

In the next section we describe the annual simulation model. In Sections 8.3 and 8.4 we discuss the results of the simulation, and in Section 8.5 we attempt to answer the three questions posed above.

8.2 Description of the Annual Simulation Model

The validated CRTF model described in Chapter 3 and 5 was extended to model the proposed commercial scale system. The changes made to the model are listed below:

1)   The overall tank dimensions were enlarged to those in Table 8-1.
2)   Power flows to and from the storage system throughout the year were estimated by scaling Solar 1 experience during 1985.
3)   The ambient temperatures were allowed to vary throughout the year and were based upon data collected at Solar 1 during 1985.
4)   The hot and cold tank's salt temperatures were not allowed to drop below 475 °F during the year. (The salt freezes below 450 °F.) The salt was maintained above this temperature by energy supplied by auxiliary tank heaters.
5)   An annual efficiency measure was defined, which includes the effect of storage temperature on turbine-generator efficiency.
Each of these changes is discussed below.

Tank Dimensions

The tank dimensions listed in Table 8-1 are the design values presented in Tracey (1) for the proposed 1200-MWht commercial system. The CRTF and commercial systems employ the same insulating materials and material thicknesses within the hot and cold storage tanks. This fact made it possible for us to use the experimentally determined overall heat-transfer coefficients and thermal conductivities in the commercial model. (These parameters are listed in Table 5-1.) This fact also adds credence to the validity of the model extrapolation.

Power Flows To and From Storage

Solar plants do not operate every day; outages are caused by cloudy weather, nighttime, and equipment problems. Thermal storage would therefore not be charged or discharged every day.

In order to obtain realistic estimates of the duration and frequency of storage charging for a 110-MWe commercial plant, the power flows leaving the receiver at the 10-MWe Solar 1 plant

throughout 1985 were multiplied by a factor of 11. The Solar 1 power flows were calculated at 15-minute intervals by a SOLERGY (10) computer model of the plant. [The SOLERGY model was validated with Solar 1 data and it produces a very good estimate of the daily and hourly plant performance (8).] As an example, depicted in Figure 8-1 are the energy flows from the receiver to the hot tank (i.e., charging flow) for the period of January 1 through 4, 1985.

The charging energy flow is represented by the term "Whin*Cs*Thin" in Equation 3-5. The charging temperature of the salt (Thin) was assumed to be 1050 °F. The charging flow rate (Whin) was calculated based on knowledge of the charging energy flow and the inlet temperature.

The discharging energy flow is represented by the term "Whout*Cs*Thout" in Equation 3-5. Discharge of the hot tank was assumed to occur when it was 40% full (19 feet). The discharge flow rate (Whout) was assumed to be constant during the entire discharge period and was set at a value required by a 110 MWe power conversion system (4.8×10^6 lbm/hr). Discharge of the hot tank was terminated when the level reached the 6-inch mark. All flow leaving the hot tank was sent to the cold tank after passing through the power conversion system (PCS). (The temperature of salt entering the cold tank was assumed to be 550 °F.) This discharge strategy is a plausible one, but it should be recognized that many other strategies are also possible.

Ambient Temperature

The ambient temperature affects the heat loss from the storage tanks. The ambient temperatures employed in the annual simulation were those recorded at the Solar 1 plant during 1985. As an example, the ambient temperatures recorded at the plant during January 1 through 4, 1985, are plotted in Figure 8-1.

Auxiliary (Parasitic) Heating

If the storage system sits idle for an extended period, the salt temperatures in the hot and cold tank may approach the freezing point (approximately 450 °F). The plant would activate an auxiliary heater at a temperature above the freezing point. (In this analysis we assumed that either an electrical or fossil tank heater would be activated at a temperature of 475 °F). We calculated that a power flow from the auxiliary heater of 160 KW would adequately maintain the salt temperature above 475 °F in either tank. A term representing this trace heating power flow was added to the hot and cold tank's conservation-of-energy equations [Equations (3-5) and (3-14), respectively]. This term was activated when the salt temperature dropped below 475 °F and was deactivated when it exceeded 475 °F.

Annual Efficiency Measure

The second law of thermodynamics tells us the efficiency of a thermodynamic cycle depends on the maximum temperature of the cycle. In a solar plant the maximum temperature is determined by the hot tank's salt temperature. If this temperature degrades below the design value (1050 °F), the thermal-to-electric efficiency of the PCS will also degrade. For example, displayed in Figure 8-2 is a curve showing how the turbine-generator efficiency is affected by variations in main steam temperature (11). (The curve shows the effect on turbine-generator heat rate. Heat rate is the inverse of efficiency and is expressed in units of Btus/KWhr).

We have taken the viewpoint that degradation of the efficiency of the PCS, caused by an off-design hot tank temperature, should be classified as an inefficiency of the storage system; if the storage system sustained no losses, the PCS would always operate at full efficiency.

To accurately model the degradation of the efficiency of the PCS given a lower than design point salt temperature is a non-trivial task. Complex simulation models of the various components within the PCS are required (12). To facilitate our calculation of annual efficiency, we made a simplifying assumption that allowed us to perform a simple calculation. This simple calculation was done after performing the annual simulation described in Section 8.3. The annual efficiency calculation is described in Section 8.4.

8.3 Results of the Annual Simulation

The dynamic model of the commercial-scale storage system was constructed by making the changes described in the previous section to the SYSL simulation model described in Chapter 3. Experimentation revealed that an integration time step of 20 seconds provided sufficient solution accuracy and simulation speed. The model ran approximately 800 times faster than real time on an IBM AT microcomputer.

Displayed in Figure 8-3 is the predicted response of the hot storage tank during the period January 1 through 4, 1985. The hot tank was assumed to be in equilibrium with a salt temperature of 550 °F and a level of 6 inches at midnight on January 1. On January 1 the solar plant did not operate. Since hot salt was not made that day, the salt in the tank cooled down and reached a temperature of 475 °F (curve A). At this point, the auxiliary heaters were activated to prevent salt freezing. The temperature was maintained at 475 °F until charging of the hot tank commenced at 7:30 a.m. on January 2 (31.5 hours). The charging flow rate into the tank (curve D) varied throughout the day according to the intensity of the insolation. During charging, the level in the tank initially increased. At a tank level of 19 feet, the turbine/generator was activated, and the tank began to be discharged. From this point until sundown the

tank was undergoing a simultaneous charge and discharge. The rate of the charge was greater than the rate of the discharge until approximately 38 hours. At 38 hours the tank reached a maximum level of 32 feet. Beyond this time, the rate of discharge was greater than the rate of charge. The tank level thus decreased. Sundown occurred near the 40-hour mark. The tank operated in only discharge mode from 40 to 44 hours. At the 44-hour mark the level of salt in the hot tank was 6 inches, and the discharge phase was terminated. The solar plant did not operate on January 3 due to a weather outage. The salt in the tank therefore cooled until charging was again commenced at approximately 7:30 a.m. on January 4. The charge/discharge cycle on January 4th was similar to the one on January 2nd; only slight differences in the peaks and shapes of the curves can be noted. This can be attributed to the similarity of the weather on both days.

Displayed in Figure 8-4 is the temperature of the hot and cold tanks during the entire year. The points of the curve are plotted at 4.5-day intervals. The first temperatures plotted are at midnight on January 1, and the succeeding points are at noon, midnight, noon, etc. The tank temperatures can undergo a significant change between noon and midnight; this explains the jagged appearance of the curves. Starting near days 40 and 310 the plant experienced two extended outages. During both outages the salt in the hot tank cooled down a significant amount. (The plant operated briefly during the 310 outage; this explains the peak near day 332.) Twice during the outage starting on day 310 the auxiliary heaters were activated to maintain the salt temperature above 475 °F and prevent salt freezing. During the 310 outage, the temperature of the hot salt decreased much more rapidly than the 40 outage. This can be explained by the difference in salt levels. The level in the hot tank was 11.1 feet and 0.4 feet during the outages commencing on days 40 and 332, respectively.

The results of our annual simulation of the 1200-MWht storage system are summarized in Table 8-2. It can be noted that very little auxiliary heating energy was required to prevent salt freezing in the storage tanks. Also listed are thermal and electrical energy values that were calculated during the simulation. These values will be used in the annual efficiency calculation described below.

8.4   Calculation of Annual Efficiency for the Commercial Scale
       System

As mentioned in Section 8.2, our annual efficiency calcuation involved a simplifying assumption. This assumption was made in order to avoid a complex calculation of turbine performance during off-design conditions.

Let us assume that auxiliary heaters operate continuously throughout the year to exactly replace the hot and cold tank's heat losses and maintain the salt in the tanks at their design

temperatures, i.e., 1050 °F in the hot tank, 550 °F in the cold
tank. The tanks steady-state heat losses at these temperatures
can be calculated by substituting the 1200-MWht system
parameters into the equations presented in Chapter 3 and setting
all derivatives equal to zero. This calculation predicts the
hot and cold tank losses to be 448 KW and 99 KW, respectively.
(In this calculation we have used an ambient temperature of 66
°F; this is the mean annual temperature for Daggett,
California.) By maintaining the salt temperatures at their
design values, the turbine/generator will always operate at
maximum efficiency and it will produce the maximum amount of
annual electrical energy.

Given the information and assumption presented in the previous
paragraph, the annual efficiency (EFF_a) can be calculated with
the following equation:

$$EFF_a = \frac{EE_m - EE_p}{EE_m} \quad , \qquad\qquad (8\text{-}1)$$

where

E_p = the annual amount of parasitic energy required by the
auxiliary heaters to maintain the hot tank at 1050 °F
(8760 hrs * 0.448 MW = 3925 MWhrs) and the cold tank
at 550 °F (8760 hrs * 0.099 MW = 867 MWhrs).

EE_m = the maximum amount of thermal energy delivered to
the PCS given no tank heat loss (602,004 MWhrs from
Table 8-2), or
the maximum amount of electrical energy produced by the
PCS given no tank heat loss (255,023 MWhrs from Table
8-2).

If a fossil auxiliary heater is used to maintain the temperature
of the tanks, we base our calculation on thermal energies and
calculate the efficiency to be 0.992 = (602004 - 4792)/602004.
If an electric auxiliary heater is used, we base our calculation
on electric energies and calculate 0.981 = (255023 -
4792)/255023. These annual efficiencies are listed in Table
8-3.

8.5 Conclusions Drawn from the Annual Simulation

The annual efficiency of the 1200-MWht commercial-scale system
will be high and close to 0.99 goal established by the
Department of Energy.

The detailed simulation revealed that only a small amount of
auxiliary energy is needed to prevent salt freezing during the
year. The tanks cool down very slowly and thus an extended
plant shutdown must occur before auxiliary heating is required.
The time at which heating is needed during the shutdown depends
on the salt levels and temperatures in both tanks at the start
of the shutdown period. The simulation results indicate that
auxiliary heating would not be required for approximately two

months if the hot tank were filled to approximately the 20% level with 566 °C (1050 °F) salt prior to the shutdown. (This conclusion was drawn by extrapolating the day 40 cooldown curves, described in Section 8.3, to the salt freezing temperature). This insight indicates it may be possible to reduce the dependence on auxiliary heating at a commercial scale central receiver plant by raising the minimum level in the hot tank. The minimum level would be chosen so that the freezing point would not be reached during the majority (say 99%) of the expected plant shutdowns. Auxiliary heaters can be a significant source of costs and unavailability at a central receiver plant. (For example, electrical heaters at the CRTF fail often.) It would be very desirable to eliminate them.
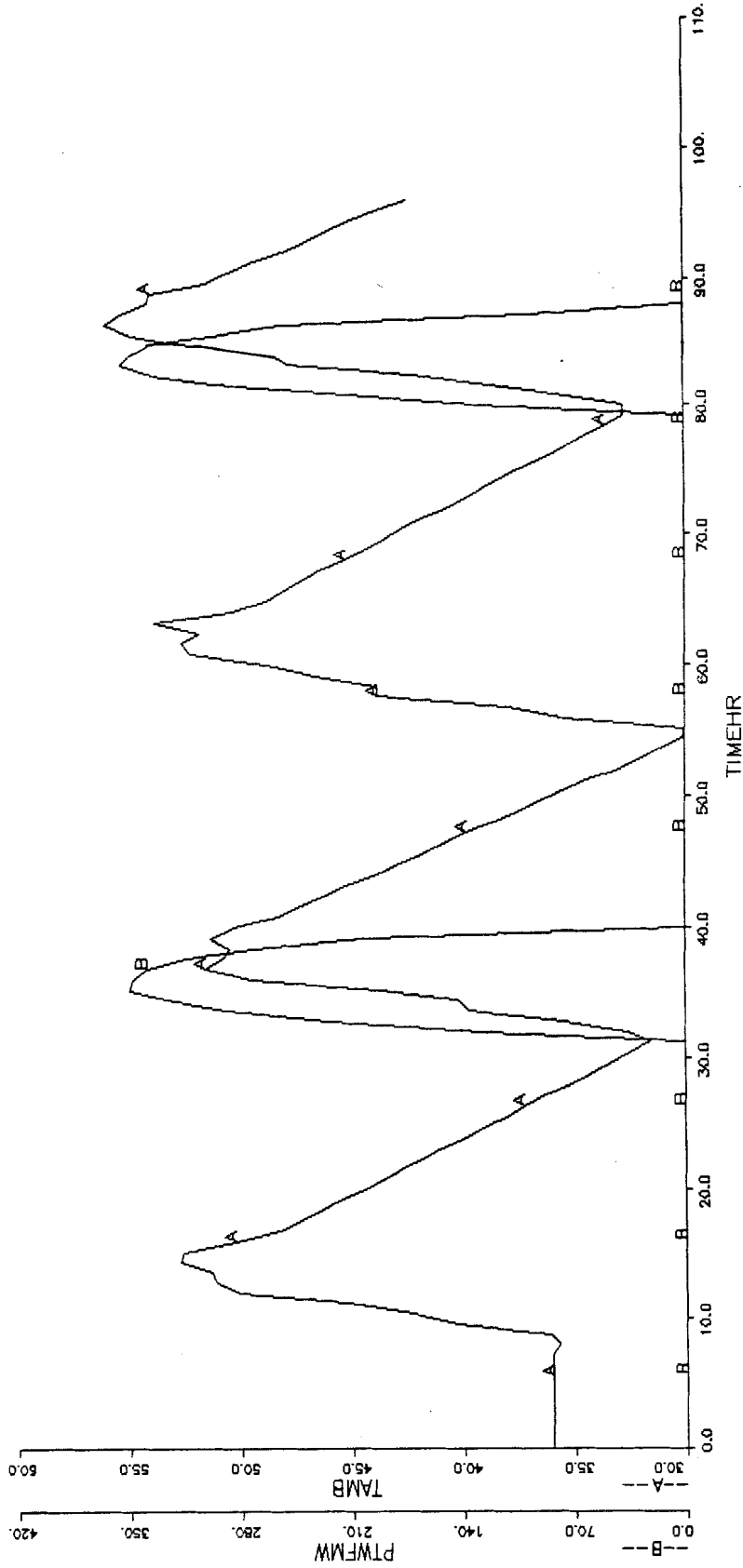
Figure 8-1 Energy Flows From the Receiver to the Hot Tank (PTWFMW) and Ambient Temperature (TAMB) During the Period January 1 to 4, 1985

% CHANGE IN HEAT RATE
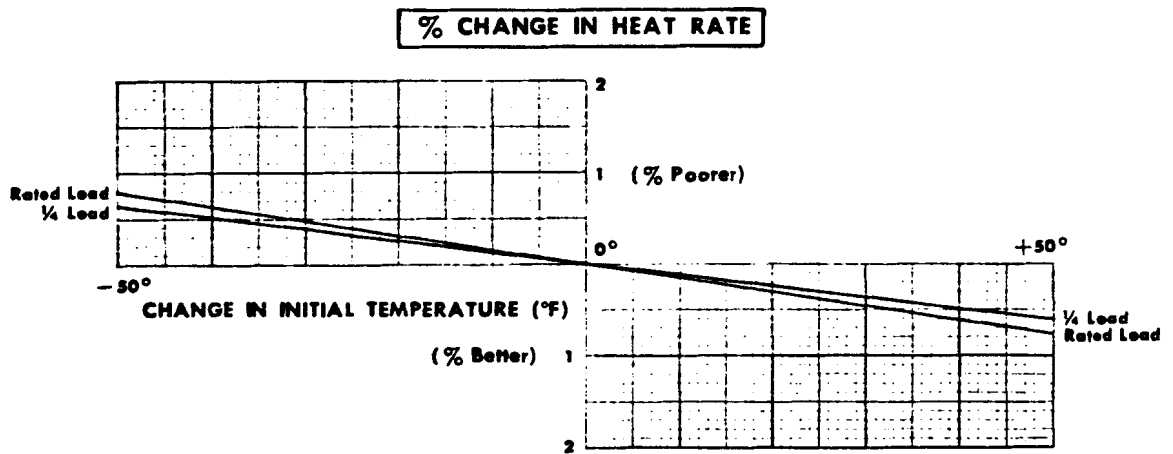
Figure 8-2 Effect of Turbine Inlet Temperature on Turbine/Generator
Gross Heat Rate

THT – Salt Temperature (F)
LHT – Salt Level (ft)
WHTX – Exit Flowrate (lb/sec)
WCTX – Inlet Flowrate (lb/sec)
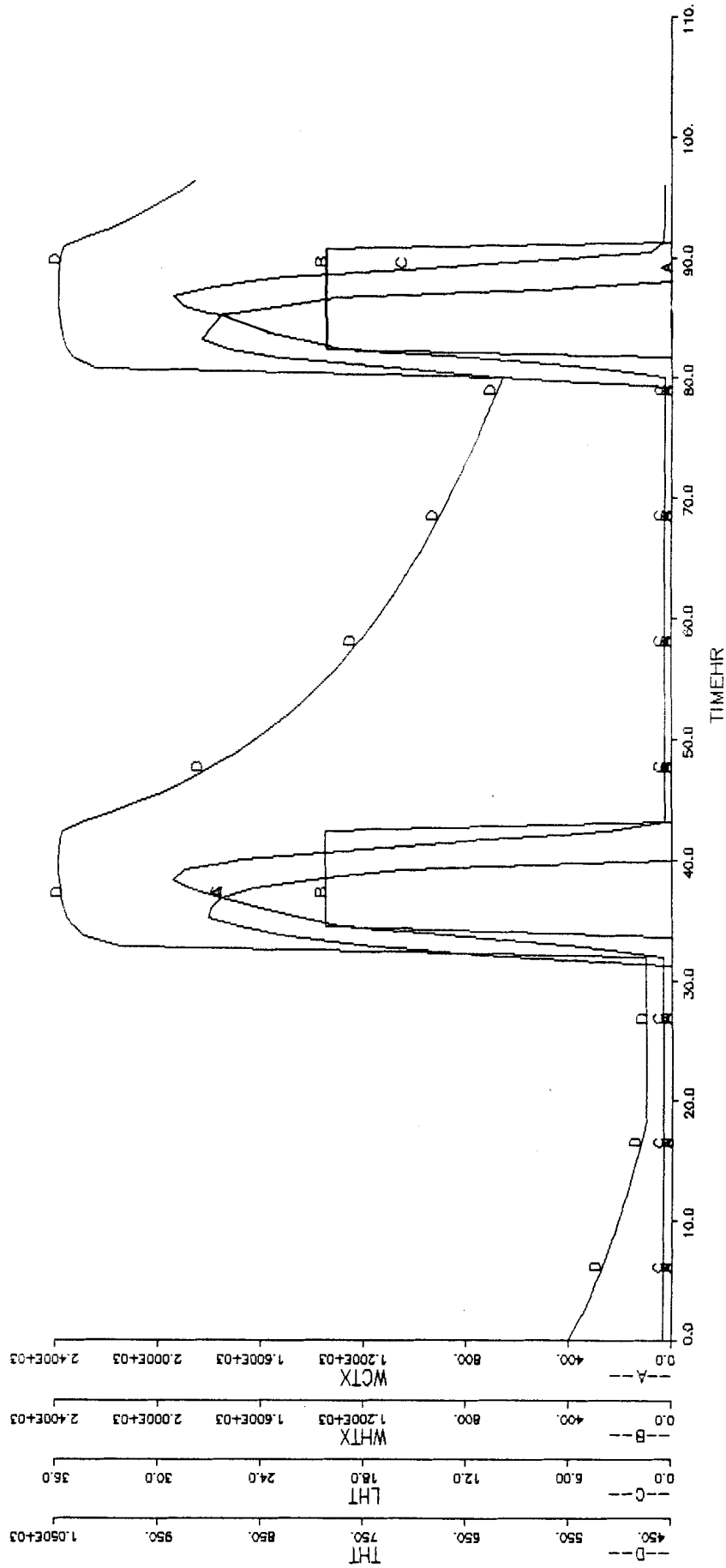
Figure 8-3 Response of Hot Tank During the Period January 1 to 4, 1985

82
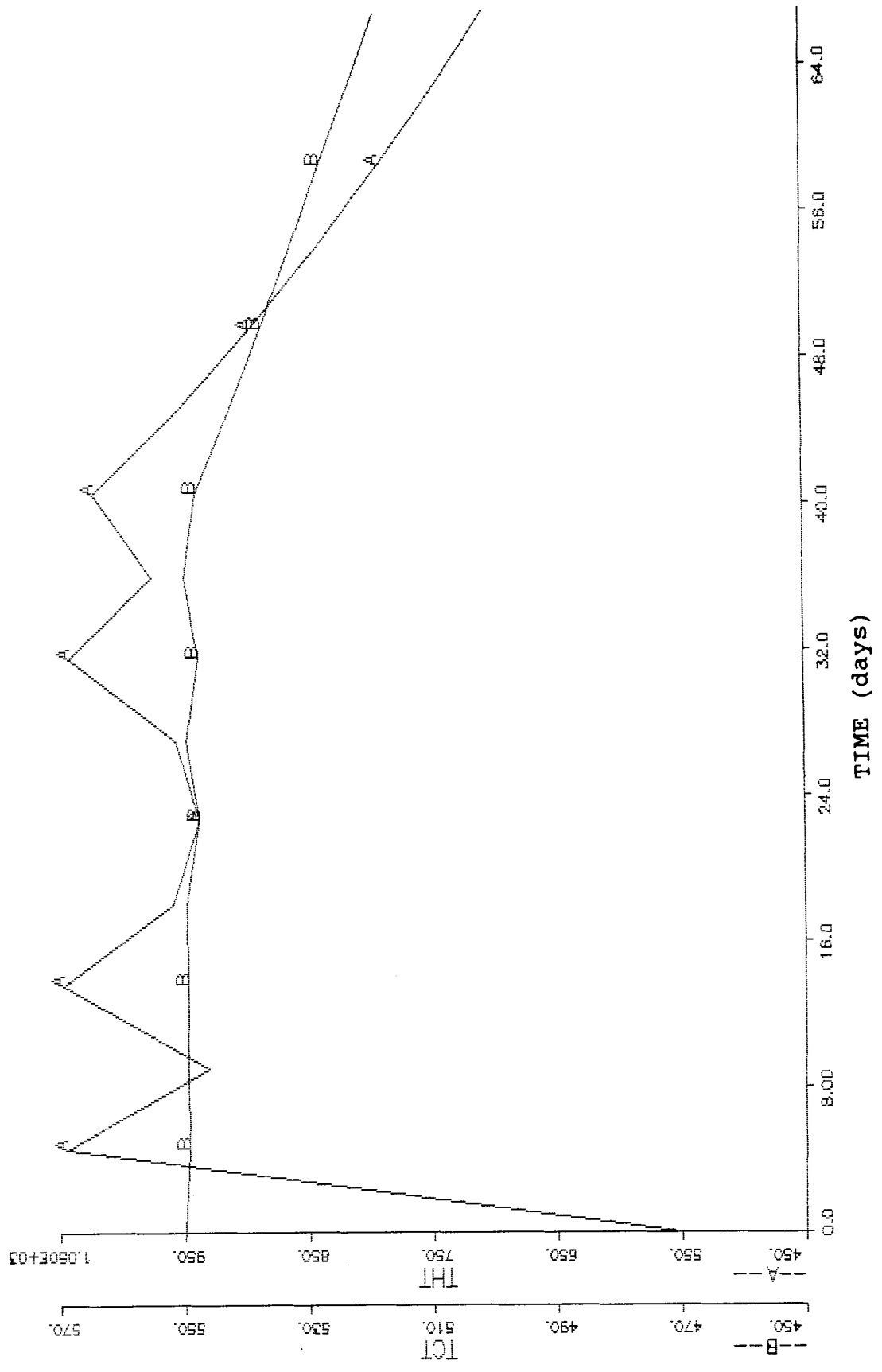
Figure 8-4 Hot Tank Temperature (THT) and Cold Tank Temperature (TCT) Plotted at 4.5 Day Intervals
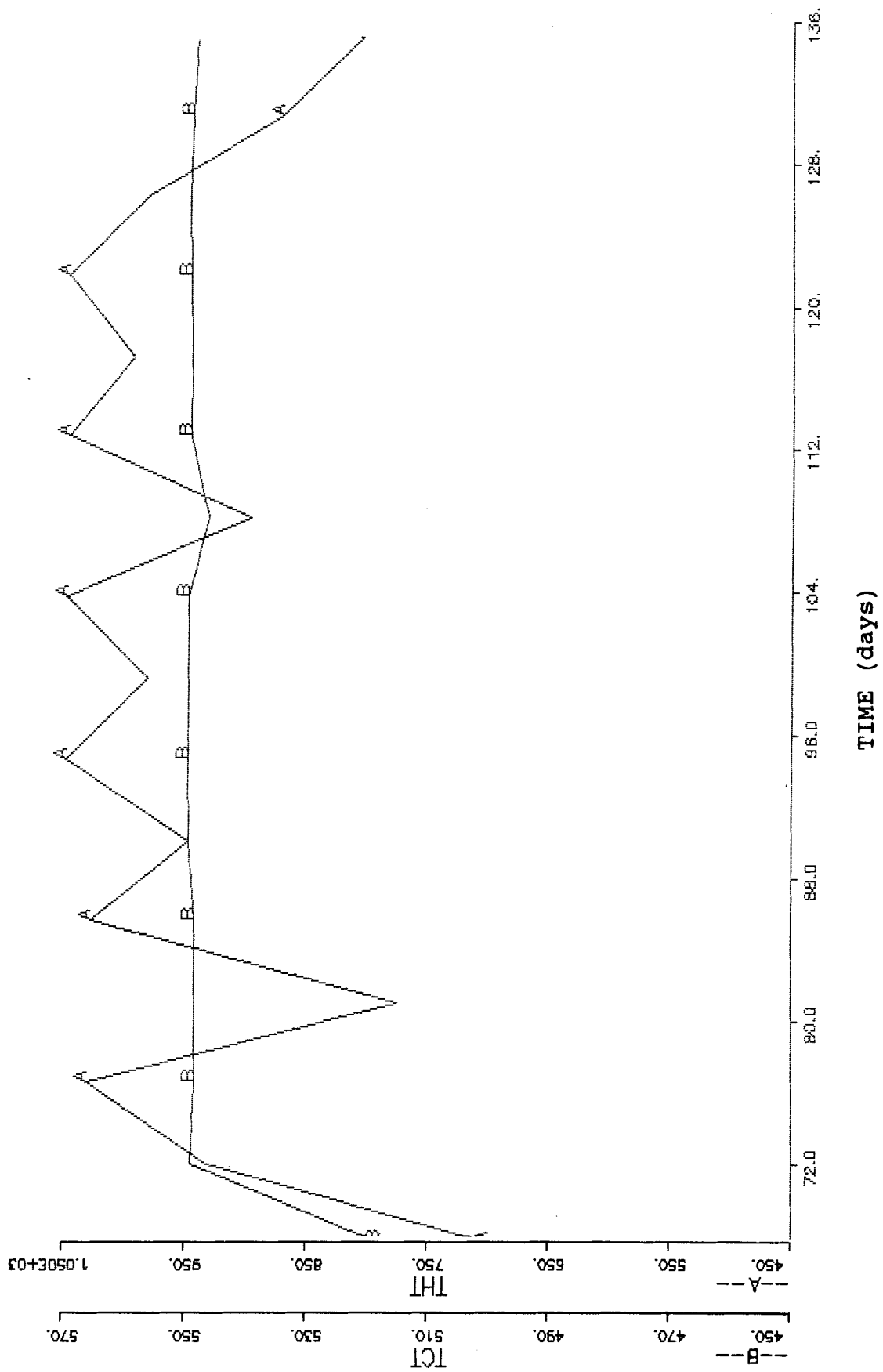
83

TIME (days)

Figure 8-4 (continued)

84

Figure 8-4 (continued)

85

Figure 8-4 (continued)

86

Figure 8-4 (continued)

87
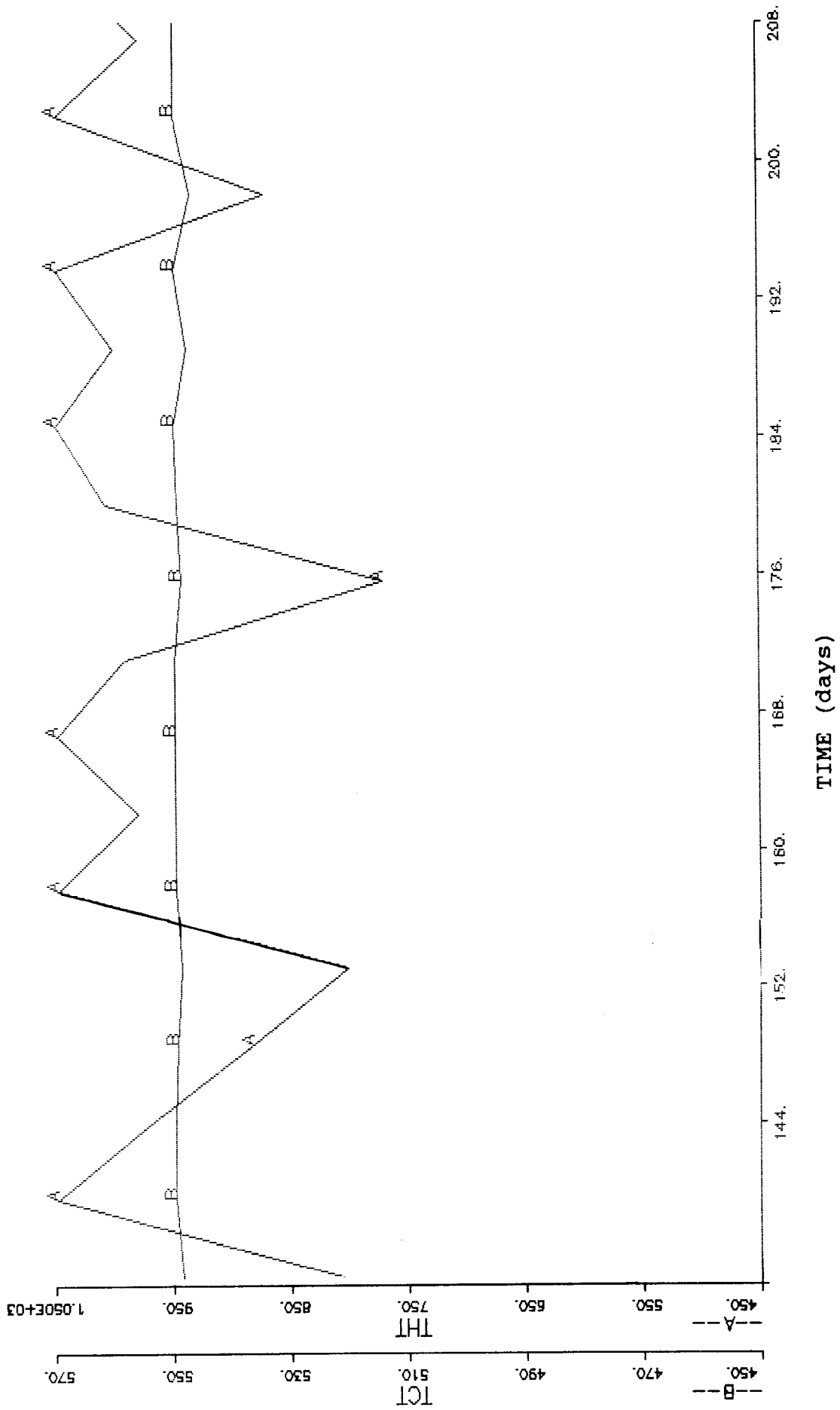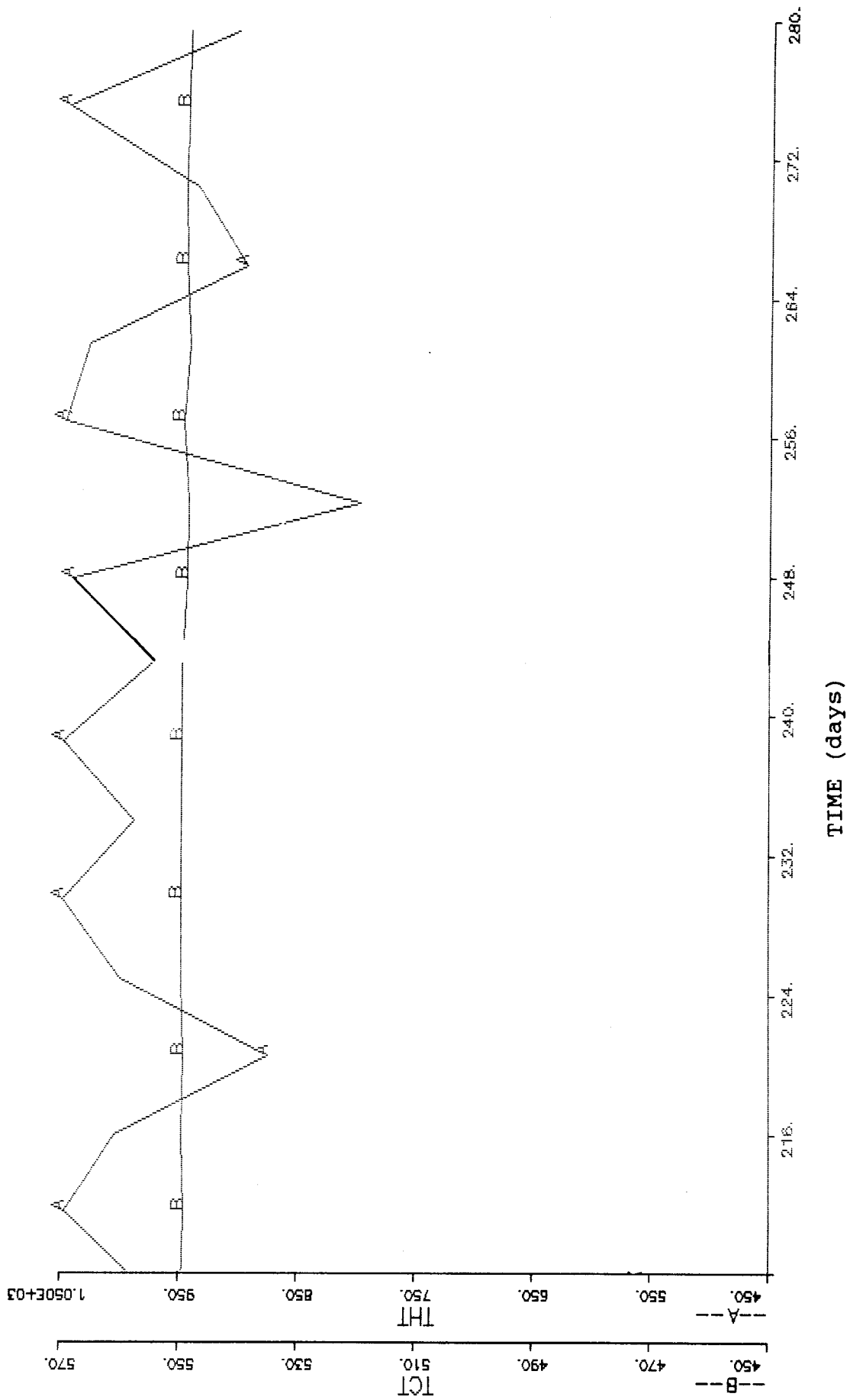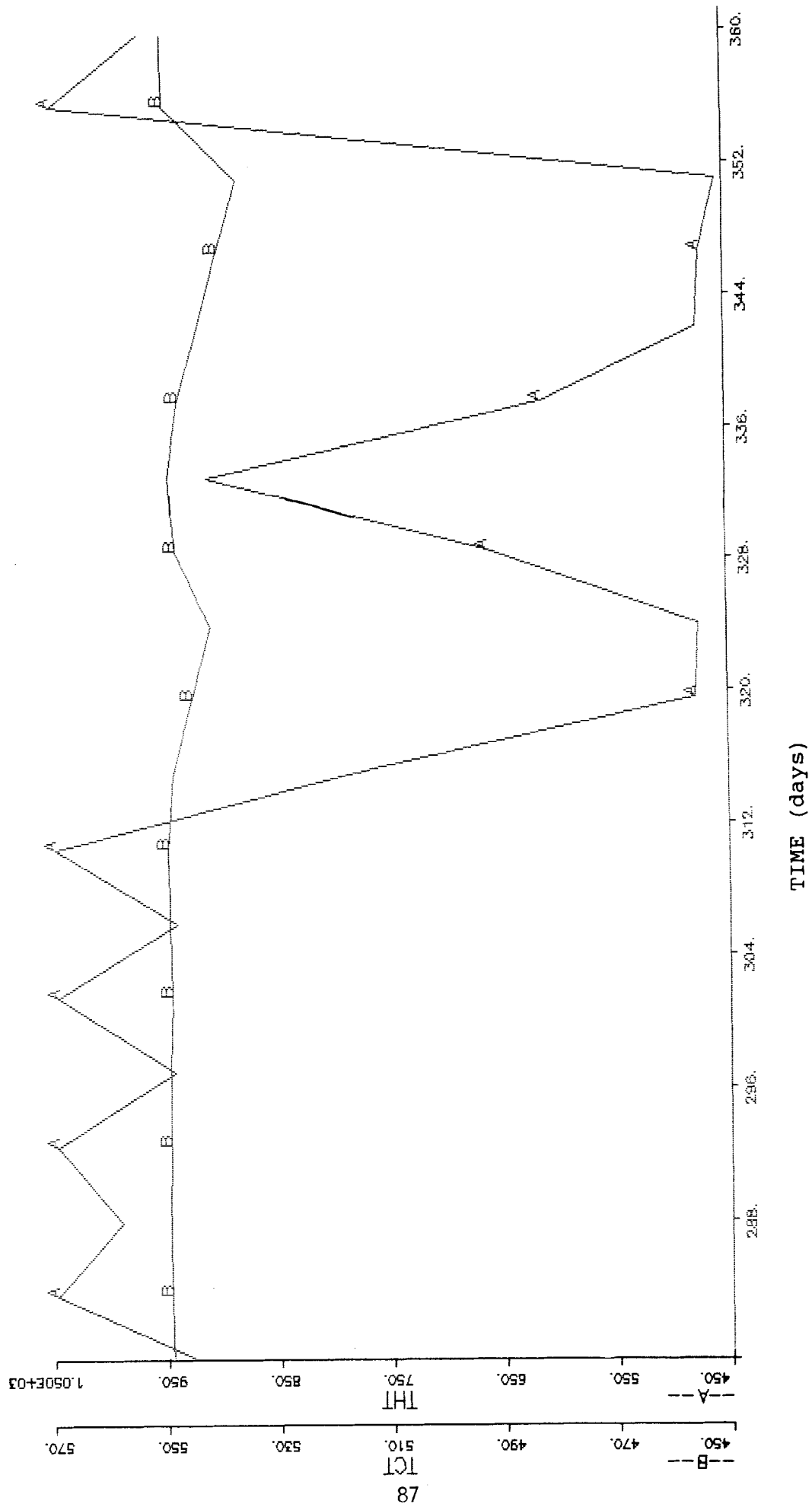
Table 8-1

Dimensions of 1200-MWht Commercial Scale
Thermal Storage System

	Hot Tank	Cold Tank
Diameter	46.6 ft (14.2 m)	42.4 ft (12.9 m)
Height	45.0 ft (13.7 m)	43.0 ft (13,1 m)

Table 8-2

Results of Annual Performance Calculations

Energy Required to Prevent Freezing of Salt in Cold Tank	0 MWhrs
Energy Required to Prevent Freezing of Salt in Hot Tank	56 MWhrs
Thermal Energy Delivered to PCS from Storage System Given No Losses from Storage Tanks	602004 MWhrs
Electrical Energy Produced by PCS Given No Losses from Storage Tanks	255023 MWhrs

Table 8-3

Results of Annual Efficiency Calculation

Annual Efficiency (fossil heater)   .992

Annual Efficiency (electric heater)   .981

Chapter 9

Conclusions and Recommendations

9.1 Conclusions

Several conclusions can be drawn based on the analysis presented in this report.

1) The current tests at the CRTF indicate that the hot tank's thermal losses are similar to those previously measured by Martin Marietta in 1982. The cold tank, however, appears to have considerably fewer losses today than were measured in 1982. During the Martin tests the cold tank's insulation was wet; however, the insulation is dry today and therefore performs much more effectively.

2) The dynamic computer model we constructed of the CRTF storage system provides a very reasonable estimate of the actual time-dependent temperature response of the system, as well as the system's thermal losses during charging and discharging scenarios. The model predictions are very good at high tank levels; at very low levels the model tends to overpredict thermal losses.

3) The use of brick as an insulator in the walls and floor of the CRTF hot tank cause additional thermal losses during tank heat-up. Losses during tank heat-up could be lessened if, rather than brick, a less massive insulator was used.

4) The experimental results obtained from the test of the 7MWht CRTF system appear to be directly applicable to the proposed 1200-MWht commercial system. Both systems employ the same insulation materials and thicknesses; the overall heat-transfer coefficients and thermal conductivities should therefore be similar.

5) The annual efficiency of the proposed commercial scale storage system is predicted to be high (greater than 98%) and close to the goal set forth by the Department of Energy.

6) Salt freezing does not appear to be a major problem for the commercial size (1200-MWht) system, and auxiliary heating can be minimized. If the minimum level in the tanks is maintained above 20%, salt freezing would not occur during an extended shutdown for at least two months.

7) The thermal performance of the CRTF, Themis, and CESA-1 molten salt storage systems appears to be similar. All three systems have similar overall heat-transfer coefficients.

8) Thermal storage tanks with higher volumes of salt have a lower cooling rate.

9) Detailed simulations of the annual performance of molten salt storage systems are particularly useful in understanding the daily temperature histories of the system. Daily temperature histories vary throughout the year and depend on the duration of nighttime, weather, and plant outages; the duration of the charge and discharge cycle; the ambient temperature; and the levels of salt in the tanks. This information was useful in this study in understanding how often auxiliary heating will be needed within the thermal storage system to prevent salt freezing. Future studies that investigate other issues, such as thermal cycling of the tanks, should find the information provided by a detailed annual simulation to be very useful.

9.2 Recommendations for Future Work

1) Studies have recently been completed by two U. S. utilities (9) that proposed two new commercial-scale molten salt thermal storage system designs. The costs and thermal performance of these new systems should be compared with the 1200-MWht system analyzed in this report. The analysis would identify the most cost-effective system.

2) The frequency and severity of storage-tank thermal cycling should be studied. This analysis could determine the tank level operating bounds that minimize thermal cycling problems.

3) The analysis of the commercial-scale storage system presented in this report was based on a single, plausible, dispatch strategy. Alternate strategies should be investigated with the simulation model to determine the most cost-effective approach.

4) The annual efficiency calculation employed in this report assumed that auxiliary heating was used to maintain the inlet steam temperature to the power conversion system at the design point. This assumption was made to facilitate the calculation and may not be the preferred mode of operation. An alternate mode of operation would be to operate the power conversion at a lower than design point temperature. A trade study should be performed to determine the most cost-effective mode of operation.

REFERENCES

1. T. R. Tracey, <u>Molten Salt Thermal Storage Subsystem Research Experiment</u>, sponsored by Sandia National Laboratories Livermore, MCR-82-1722 (Martin Marietta Corporation, 1982).

2. <u>National Solar Thermal Technology Program Five Year Reasearch and Development Plan 1986-1990</u>, Department of Energy, December 1985.

3. "Solar Central Receiver Utility Study Guidlines, Ground Rules, and Trade Study Input Specifications - Revision 1", Arizona Public Service Company, Pacific Gas and Electric Comyany, and Southern California Edison Company, July 22, 1986.

4. <u>System Simulation Language Users Guide, SYSL/M Version 1.0</u>, E^2 Consulting, September 1985.

5. J. M. Andujar, F. Rosa, <u>CESA-1 Thermal Storage System Evaluation</u>, Plataforma Solar de Almeria, Draft Report, Summer 1987.

6. C. Etievant, et. al., <u>Central Receiver Plant Evaluation -- IV) Themis Thermal Storage Subsytem Evaluation</u>, prepared for Sandia National Laboratories under contract n 90-1575, Draft Report.

7. W. Bitterlich, M. Geyer, K. Werner, <u>Messungen Und Berechnungen Am Thermischen Rippenplatten-Zweistoffspeicher Im IEA-SSPS Sonnenkraftwerk Almeria</u>, VDI-Verlag GmbH, Dusseldorf, 1986.

8. D. J. Alpert and G. J. Kolb, "Annual Energy Improvement Study," <u>Proceedings of the Solar Thermal Technology Conference</u>, Albuquerque, NM (August 1987).

9. T. Hillesland Jr. (PG&E), E. R. Weber (APS), et. al., Solar Central Receiver Technology Advancement for Electric Utility Application, Pacific Gas and Electric Company, Arizona Public Service Company, in preparation.

10. M. C. Stoddard, S. E. Faas, C. J. Chiang, J. A. Dirks, <u>SOLERGY - A Computer Code for Calculating the Annual Energy from Central Receiver Plants</u>, SAND86-8060 (Livermore, CA: Sandia National Laboratories, 1987).

11. Letter from L. Stoddard, Black and Veatch Corp., to T. Hillesland, Pacific Gas & Electric Co., Subject: Heat Balance Data for a 110 MWe Turbine Generator, May 20, 1987.

12. M. R. Erbes and R. H. Eustis, "A Computer Methodology for Predicting the Design and Off-Design Performance of Utility Steam Turbine-Generators", Stanford University, Stanford, California, 1985.

U.S. Department of Energy (5)
Forrestal Building
Code CE-314
1000 Independence Avenue, S.W.
Washington, D.C. 20585
Attn: H. Coleman
       S. Gronich
       F. Morse
       M. Scheve
       R. Shivers

U.S. Department of Energy
Forrestal Building, Room 5H021C
Code CE-33
1000 Independence Avenue, S.W.
Washington, D.C. 20585
Attn: C. Carwile

U.S. Department of Energy
Albuquerque Operations Office
P.O. Box 5400
Albuquerque, NM 87115
Attn: D. Graves

U.S. Department of Energy
San Francisco Operations Office
1333 Broadway
Oakland, CA 94612
Attn: R. Hughey

University of California
Environmental Science and Engineering
Los Angeles, CA 90024
Attn: R. G. Lindberg

University of Houston (2)
Solar Energy Laboratory
4800 Calhoun
Houston, TX 77704
Attn: A. F. Hildebrandt
       L. Vant-Hull

Analysis Review & Critique
6503 81st Street
Cabin John, MD 20818
Attn: C. LaPorta

94

Arizona Public Service Company
P.O. Box 21666
Phoenix, AZ 85036
Attn: E. Weber

Babcock and Wilcox
91 Stirling Avenue
Barberton, OH 44203
Attn: D. Young

Bechtel Group, Inc. (2)
P.O. Box 3965
San Francisco, CA 94119
Attn: P. DeLaquil
       S. Fleming

Black & Veatch Consulting Engineers (2)
P.O. Box 8405
Kansas City, MO 64114
Attn: J. C. Grosskreutz
       J. E. Harder

Boeing Aerospace
Mailstop JA-83
P.O. Box 1470
Huntsville, AL 35807
Attn: W. D. Beverly

California Energy Commission
1516 Ninth St., M/S 40
Sacramento, CA 95814
Attn: A. Jenkins

California Public Utilities Com.
Resource Branch, Room 5198
455 Golden Gate Ave.
San Francisco, CA 94102
Attn: T. Thompson

Centro Investigations Energetica (2)
Medroansental Technologie (CIEMAT)
Avda. Complutense, 22
28040 Madrid
Spain
Attn: J. M. Andujar
      F. Sanchez

DFVLR RF-ET (6)
Linder Hohe
D - 5000 Koln 90
West Germany
Attn: Ulrich Nikolai (5)
       Michael Geyer

El Paso Electric Company
P.O. Box 982
El Paso, TX 79946
Attn: J. E. Brown

Electric Power Research Institute (2)
P.O. Box 10412
Palo Alto, CA 94303
Attn: J. Bigger
       E. DeMeo

Foster Wheeler Solar Development Corp.
12 Peach Tree Hill Road
Livingston, NJ 07039
Attn: S. F. Wu

Georgia Institute of Technology
GTRI/EMSL Solar Site
Atlanta, GA 30332

D. Gorman
5031 W. Red Rock Drive
Larkspur, CO 80118

Jet Propulsion Laboratory
4800 Oak Grove Drive
Pasadena, CA 91103
Attn: M. Alper

Los Angeles Department of Water and Power
Alternate Energy Systems
Room 661A
111 North Hope St.
Los Angeles, CA 90012
Attn: Hung Ben Chu

Martin Marietta Aerospace
P.O. Box 179, MS L0450
Denver, CO 80201
Attn: H. Wroton

McDonnell Douglas (2)
MS 49-2
5301 Bolsa Avenue
Huntington Beach, CA 92647
Attn: R. L. Gervais
       J. E. Raetz

Meridian Corporation
5113 Leesburg Pike
Falls Church, VA 22041
Attn: D. Kumar

Public Service Company of New Mexico (2)
M/S 0160
Alvarado Square
Albuquerque, NM 87158
Attn: T. Ussery
       A. Martinez

Olin Chemicals Group (2)
120 Long Ridge Road
Stamford, CT 06904
Attn: J. Floyd
       D. A. Csejka

Pacific Gas and Electric Company
77 Beale Street
San Francisco, CA 94106
Attn: J. Laszlo

Pacific Gas and Electric Company (4)
3400 Crow Canyon Road
San Ramon, CA 94526
Attn: G. Braun
       T. Hillesland, Jr.
       B. Norris
       C. Weinberg

Public Service Company of Colorado
System Planning
5909 E. 38th Avenue
Denver, CO 80207
Attn: D. Smith

Rockwell International
Rocketdyne Division
6633 Canoga Avenue
Canoga Park, CA 91304
Attn: J. Friefeld

Sandia Solar One Office
P.O. Box 366
Daggett, CA 92327
Attn: A. Snedeker

Science Applications International Corp.
10401 Roselle Street
San Diego, CA 92121
Attn: B. Butler

Solar Energy Research Institute (3)
1617 Cole Boulevard
Golden, CO 80401
Attn: B. Gupta
       M. Bohn
       L. M. Murphy

Solar Kinetics Inc.
P.O. Box 47045
Dallas, TX 75247
Attn: J. A. Hutchison

Southern California Edison
P.O. Box 325
Daggett, CA 92327
Attn: C. Lopez

Stearns Catalytic Corp.
P.O. Box 5888
Denver, CO 80217
Attn: T. E. Olson

Stone and Webster Engineering Corporation
P.O. Box 1214
Boston, MA 02107
Attn: R. W. Kuhr

G. Bertha
Pitt - Des Moines Inc.
3400 Grand Avenue
Pittsburg, PA 15225

T. Brumleve
1512 N. Gate Road
Walnut Creek, CA 94598

T. Gallagher
CBI Industries
1501 N. Division Street
Plainfield, Illinois 60544

L. Gutierrez
434 School Street
Livermore, CA 94550

R. Holl
23011 Moulton Parkway
Suite C-13
Laguna Hills, CA 92653

D. Kearney
Luz Engineering Corporation
15720 Ventura Boulevard
Suite 504
Encino, CA 91436

T. R. Tracey
6922 S. Adams Way
Littleton, CO 80122

3141	S. A. Landenberger (5)	
3151	W. L. Garner (3)	
3154-1	C. H. Dalin - DOE/OSTI (8)	
6000	D. L. Hartley; Attn: V. L. Dugan, 6200	
6220	D. G. Schueler	
6221	E. C. Boes	
6222	J. V. Otts	
6223	G. J. Jones	
6224	D. E. Arvizu	
6226	J. T. Holmes	
6226	G. J. Kolb (10)	
6226	D. J. Alpert	
6226	J. M. Chavez	
6226	J. W. Grossman	
6226	D. F. Menicucci	
6226	C. E. Tyner	
6227	J. A. Leonard	
8133	A. C. Skinrood	
8133	L. G. Radosevich	
8471	S. E. Faas	
8524	P. W. Dean	